

Egan
221

O .GAN

ENGINEERING
LIBRARY

The Canadian Journal of Chemical Engineering

formerly

CANADIAN JOURNAL OF TECHNOLOGY

CONTENTS

Effect of Packing Configuration on Mass and Heat Transfer in Beds of Stacked Spheres	<i>L. R. Galloway</i> <i>W. Komarnicky</i> <i>N. Epstein</i>	139
The Carbon Dioxide-Hydrogen Sulphide-Methane System Part I—Phase Behaviour at 100°F.	<i>D. B. Robinson</i> <i>J. A. Bailey</i>	151
Recent Developments in the Extrusion of Plastics	<i>G. L. Bata</i>	159
The Velocity of Fall of Circulating and Oscillating Liquid Drops Through Quiescent Liquid Phases	<i>A. I. Johnson</i> <i>L. Braida</i>	165
Principles of Aeration as Applied to Waste Treatment	<i>W. Wesley Eckenfelder</i>	173

Published by

THE CHEMICAL INSTITUTE OF CANADA
OTTAWA

CANADA

The Canadian Journal of Chemical Engineering

formerly

Canadian Journal of Technology

VOLUME 35

DECEMBER, 1957

NUMBER 4

EDITOR:

W. M. CAMPBELL

Chemistry and Metallurgy Division, Atomic Energy of Canada Limited,
Chalk River, Ont.

Assistant Editor: R. N. CALLAGHAN

Editorial Assistant:
R. G. WATSON

Circulation Manager:
M. M. HOLDEN

EDITORIAL BOARD:

Chairman

J. R. DONALD, Montreal, Que.

A. CHOLETTE, Quebec, Que.

E. B. LUSBY, Toronto, Ont.

W. H. GAUVIN, Montreal, Que.

LÉO MARION, Ottawa, Ont.

GLEN GAY, Ottawa, Ont.

R. R. McLAUGHLIN, Toronto, Ont.

G. W. GOVIER, Edmonton, Alta.

E. R. ROWZEE, Sarnia, Ont.

A. I. JOHNSON, Toronto, Ont.

H. R. L. STREIGHT, Montreal, Que.

G. A. LEDINGHAM, Saskatoon, Sask.

EX-OFFICIO:

O. J. WALKER, Edmonton, Alta.

H. P. GODARD, Kingston, Ont.

L. PICHE, Montreal, Que.

H. S. SUTHERLAND, Montreal, Que.

Authorized as second class mail, Post Office Department, Ottawa. Printed in Canada

Manuscripts for publication should be submitted to the Editor: Dr. W. M. Campbell, Chemistry and Metallurgy Division, Atomic Energy of Canada Limited, Chalk River, Ontario. (Instruction to authors are on inside back cover)

Proofs, correspondence concerning proofs, and orders for reprints should be sent to: The Chemical Institute of Canada, 18 Rideau Street, Ottawa 2, Ont.

Subscriptions, renewals, requests for single or back numbers and all remittances should be sent to: The Chemical Institute of Canada, 18 Rideau Street, Ottawa 2, Ont.

C.J.Ch.E. is published by The Chemical Institute of Canada every two months. Subscription rate is \$3.00 per year and .75c per single copy; U.S. and U.K.—\$4.00; and Foreign—\$4.50 per year.

Unless it is specifically stated to the contrary, the Institute assumes no responsibility for the statements and opinions expressed in *The Canadian Journal of Chemical Engineering*. Views expressed in the editorials do not necessarily represent the official position of the Institute.

Editorial Offices: Dr. W. M. Campbell, Chemistry and Metallurgy Division, Atomic Energy of Canada Limited, Chalk River, Ont.

Production and circulation offices: 18 Rideau Street, Ottawa 2, Ont.

Change of Address: Advise the Circulation Department, The Chemical Institute of Canada, 18 Rideau Street, Ottawa 2, Ont. in advance of any change of address, providing old as well as new address. Enclose address label if possible.

of n
from
blag
300-
cons

four
sligh
Reyn
desi
rela
as w

for
faile
abili
prop

the
mea

T
s
heat
a pa
face
cern
encle

Im
ation
heati
as w
desi
nearl
exch
fluid
twee

.....
Note:
Vanco
1 Man
2 Texti
3 Poly
4 Assis
Vanc
Contri

The

Effect of Packing Configuration on Mass and Heat Transfer in Beds of Stacked Spheres¹

L. R. GALLOWAY², W. KOMARNICKY³ and N. EPSTEIN⁴

Experimental measurements are reported on the simultaneous rates of mass and heat transfer for the surface evaporation of water into air from two orthorhombic, a rhombohedral, and two simple cubic assemblages of uniform celite spheres, in the particle Reynolds number range 300-1200. The measurements were confined to the pre-determined constant rate drying period of the spheres.

No appreciable differences in mass or heat transfer factors were found for the various assemblages, except for the cubics, which exhibited slightly lower transfer factors than the other assemblages at the higher Reynolds numbers. The negative slope of the $\log j$ vs. $\log Re$ curves was designated the "index of turbulence inhibition". This index was correlated with the projected fractional free area of the packings, as well as with the wall effect.

Various methods proposed by investigators of randomly packed beds for modifying the mass transfer factor and/or the Reynolds number failed to improve the overall correlation of the results. The inapplicability of a simple analogy between momentum and mass transfer, as proposed by Ergun, is demonstrated.

Based on the model of McHenry and Wilhelm, the magnitude of the axial mixing factor required to correct for the use of logarithmic mean potentials is indicated.

This study is concerned with the simultaneous transfer of mass and heat between a fluid flowing through a packed bed of spheres and the surface of these spheres. It does not concern transfer to or from the walls enclosing the bed.

Important as they are in such operations as drying, leaching, pebble heating, adsorption and ion exchange, as well as in heterogeneous reactor design, packed beds of perfect or nearly perfect spheres undergoing an exchange of mass and/or heat with fluid permeating the void spaces between the spheres have been exper-

imentally investigated before⁽¹⁻¹⁸⁾. The studies which have been reported, however, all deal with randomly packed and hence inherently unrepeatable packing assemblages. In the present investigation a new variable has been introduced, namely, the geometric configuration of the packing. This was done by dealing with carefully stacked, rather than randomly packed, assemblages.

Fluid Friction

A precedent for this type of study was set by Martin et al.⁽¹⁹⁾ who investigated the fluid friction characteristics of nine different orderly

configurations of brass balls, stacked according to the arrangements elaborated by Graton and Fraser⁽²⁰⁾. Four of these arrangements, illustrated schematically in Figure 1, were studied in the present work. The simple cubic represents the loosest, while the rhombohedral (hexagonal close-packed) represents one of the two densest, stable arrangements of uniformly sized spheres. The two orthorhombics have identical lattices, but differ by 90° in their orientation with respect to the major flow axis. Thus the plan of No. 2 Clear Passage is equivalent to the elevation of No. 4, while the elevation of No. 2 Clear Passage is equivalent to the plan of No. 4. Orthorhombic No. 2 Blocked Passage was not constructed in the present work.

Martin's results on the four assemblages, in the particle Reynolds number range of the present investigation, are shown in Figure 2. While the large differences in friction factor between the cubic, orthorhombic and rhombohedral packings can be explained in part at least by the large fractional void volume differences between these three arrangements, the four-fold difference in friction factor between the two orthorhombics is a surprising result in view of the identical lattice of the two packings. This result was confirmed in the present work by making longitudinal pressure profiles on the two orthorhombic assemblages in conjunction with a number of the mass and heat transfer measurements subsequently reported. The data obtained for air flow through celite spheres are plotted in Figure 2, where they show good agreement with Martin's best lines for liquid flow through metal spheres.

Note: Presented in part at the 40th Annual Conference of The Chemical Institute of Canada, Vancouver, B.C., June 4, 1957.

¹Manuscript received October 2, 1957.

²Textile Fibres Division, Du Pont of Canada (1956) Limited, Kingston, Ont.

³Polymer Corporation, Sarnia, Ont.

⁴Assistant Professor, Department of Chemical Engineering, University of British Columbia, Vancouver, B.C.

Contribution from the Department of Chemical Engineering, University of British Columbia; based in part on the M.A.Sc. Theses of L. R. Galloway, 1955, and W. Komarnicky, 1956.

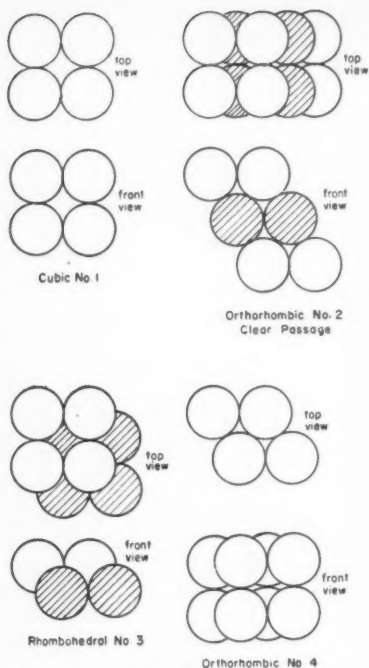


Figure 1—Arrangements of spheres studied.

Whether the inordinate increase in friction factor from Orthorhombic No. 2 to Orthorhombic No. 4, which represents a corresponding increase in rate of momentum transfer, would reflect itself, in part at least, in an increase in rates of heat and mass transfer between the spheres and the fluid, was one of the questions which spurred the present study. It should be noted that this large percentage increase in friction factor cannot simply be attributed to form drag, since it was shown by Martin to be even larger in the viscous flow range, where skin friction alone prevails. This is in contradistinction to the case of No. 2 Clear Passage versus No. 2 Blocked Passage, where a considerably smaller difference in friction factor occurs only at particle Reynolds numbers exceeding 20 and the difference increases with Reynolds number.

Experimental Method

The spheres used to construct the packings were composed of 50% celite, 37.5% alundum cement and

12.5% colloidal kaolin, by weight. The method developed for fabricating them has already been reported (21). They had a mean diameter of 0.673 in., with a standard deviation of less than 1% from this mean. Their high internal porosity allowed them to retain about two-thirds their own volume of water, which was transferred to an air stream during the course of an experimental run. The spheres also fulfilled the requirements of being tough, machineable, and subject to negligible attrition in handling.

The assemblages were built by individually drilling small holes in each sphere and pinning each to its tangent neighbour with 0.022 in. stainless steel fishing wire. The wire was secured in each hole with Araldite cement. The tendency of the spheres to bridge and cause extra porosity at the wall was eliminated by using fractional spheres at the walls and corners, in the manner of Martin et al. (19). The bundles of spheres were enclosed on all sides except the top and bottom by 1/16-in. brass plate cemented to the faces of the fractional spheres. Photographs of the assembled packings are shown in Figure 3.

Packing Nos. 1, 2, and 3, based as they are on square horizontal layers (see Figure 1), were housed in square containers with half-spheres at the walls and quarter-spheres in the corners, while Orthorhombic No. 4, composed of rhombic layers, could only be adapted to a hexagonal container, using half-spheres at the walls and one-third spheres in the corners. A fifth stacked assemblage, Cubic No. 1A, was also constructed and studied. This was similar in all respects to Cubic No. 1 except that no fractional spheres were used at the walls. The effect of exposing the additional wall area to the air flow could thus be ascertained.

Dimensions of the various assemblages are shown in Table 1. Eight layers of spheres were used for each stacked assemblage, a compromise between too few layers which could make for end effects and too many layers which would cause thermal and diffusion equilibrium to occur part way through the packing, thus rendering the determination of heat and mass transfer coefficients by integral methods impossible. The variation in fractional void volume was more than double that which can normally be obtained in randomly packed beds of uniform-size spheres (22). Measurements were also made

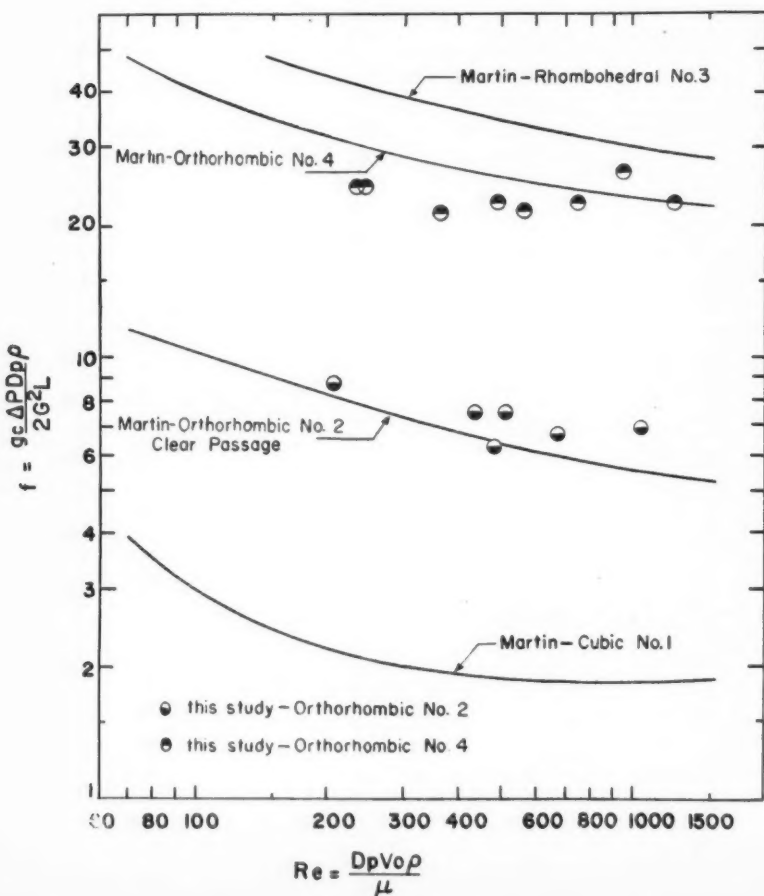


Figure 2—Fluid friction characteristics of packings.

on the spheres randomly packed, to ensure that the methods used give results in reasonable agreement with other investigators of transfer in randomly packed beds.

The apparatus in which the packings were housed is illustrated schematically in Figure 4. After removing any entrained moisture from the pressure-regulated building compressor air, this air was throttled to reduce its relative humidity to below 40%, orifice-metered into the test column, and finally exhausted to the atmosphere. Both the square and the hexagonal test columns were made from $\frac{1}{2}$ -in. aluminum plate, with $\frac{1}{4}$ -in. aluminum flanges. The inside cross-sectional dimensions of these columns were such as to make a snug fit when the assemblages of spheres with brass side plates were placed inside the columns. Empty calming zones on either side of the assemblages, and about twice their depth, were lined with $\frac{1}{16}$ -in. brass plates in order to maintain a constant cross-section throughout the entire column. Five equally spaced pressure taps (see Figure 3f) from each assemblage were brought through a flange of the column via a brass plate attached to the wall containing the pressure taps. These were connected to open and differential draft gauge manometers, in order to measure in conjunction with barometer readings, the absolute pressure and its variation throughout the depth of packing. The columns were insulated with two inches of glass wool.

The dew point of the entrance air and of the air after it had picked up moisture from the wet spheres, was measured to within 0.3 Fahrenheit degrees by passing samples of these streams through a Foxboro "dewcel" linked to a continuous recorder. Temperatures immediately below and immediately above the packing were measured with carefully calibrated thermometers, reading to the nearest 0.1 Fahrenheit degree.

Before making a run the entire packing assemblage was soaked in a water bath held within 2 Fahrenheit degrees of the adiabatic saturation temperature of the inlet air, for at least three hours. After shaking off excess water, the wet assemblage was inserted into the column and the run started. All the relevant measurements were made during the constant rate period of drying. This was predetermined at several air velocities through two layers of randomly packed spheres, a typical drying curve of which is illustrated in Figure 5. Even at the highest particle Rey-

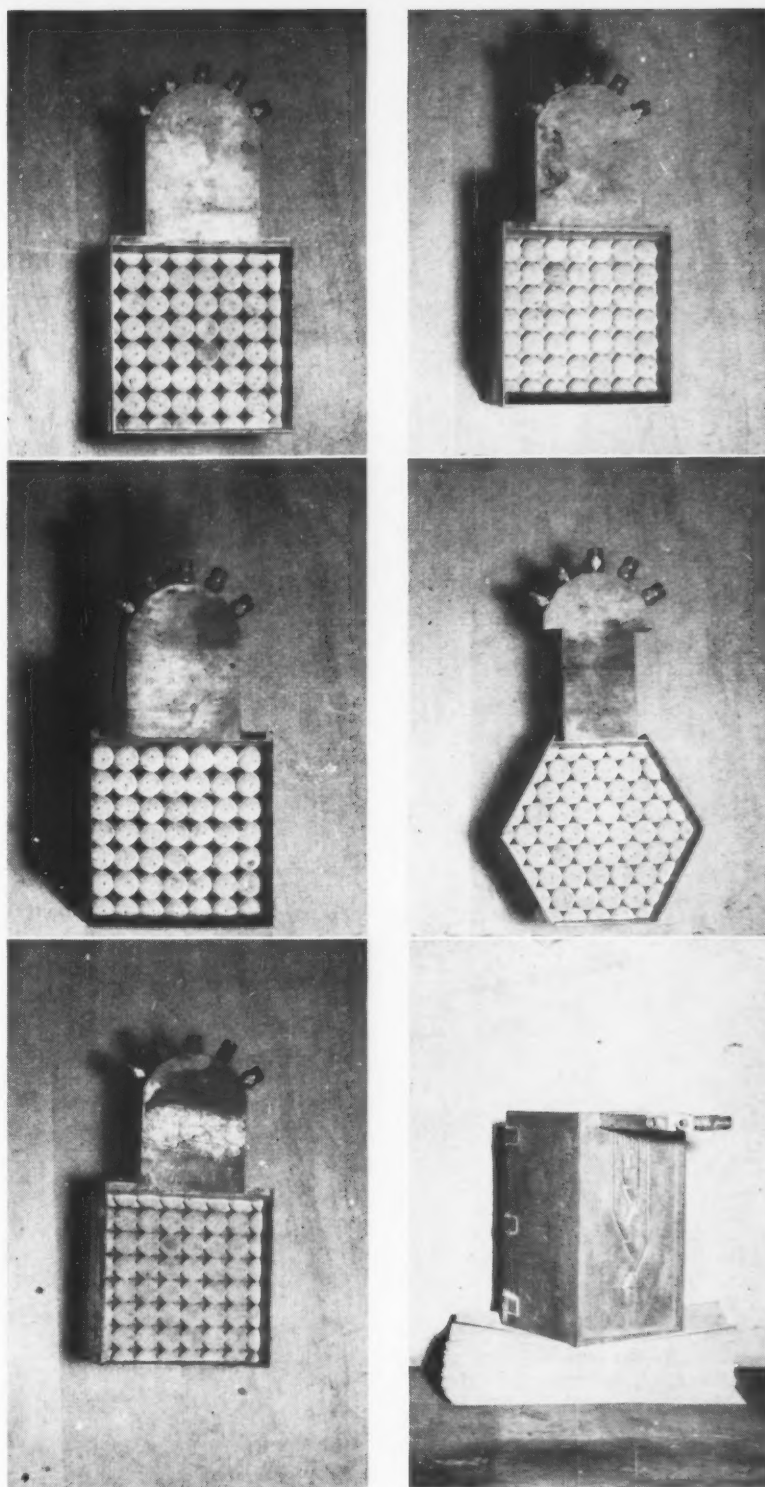


Figure 3—Photographs of assemblages

- | | |
|--------------------------------------|------------------------|
| (a) cubic no. 1 | (d) rhombohedral no. 3 |
| (b) cubic no. 1A | (e) orthorhombic no. 4 |
| (c) orthorhombic no. 2 clear passage | (f) pressure taps |

TABLE I
CHARACTERISTICS OF PACKINGS

Packing Arrangement	Shape of Column	Side or Diameter of Column inches	Cross-Sectional Area sq. ft.	No. of Spheres	Surface Area of Spheres sq. ft.	Depth inches	Fractional Void Volume	Largest Fractional Free Area	Smallest Fractional Free Area	Projected Fractional Free Area
Cubic No. 1 & 1A	Square	4 11/16	0.1526	392	3.873	5.38	0.4764	1.0	0.215	0.215
Orthorhombic No. 2 clear passage	Square	4 11/16	0.1526	392	3.873	4.66	0.3954	0.635	0.215	0.043
Rhombohedral No. 3	Square	4 11/16	0.1526	392	3.873	3.81	0.2595	0.349	0.215	0
Orthorhombic No. 4	Hexagonal	2 11/16	0.1303	384	3.795	5.38	0.3954	1.0	0.093	0.093
Random	Circular	3.00	0.0491	142	1.404					
Random	Square	4 11/16	0.1526	142	1.404					

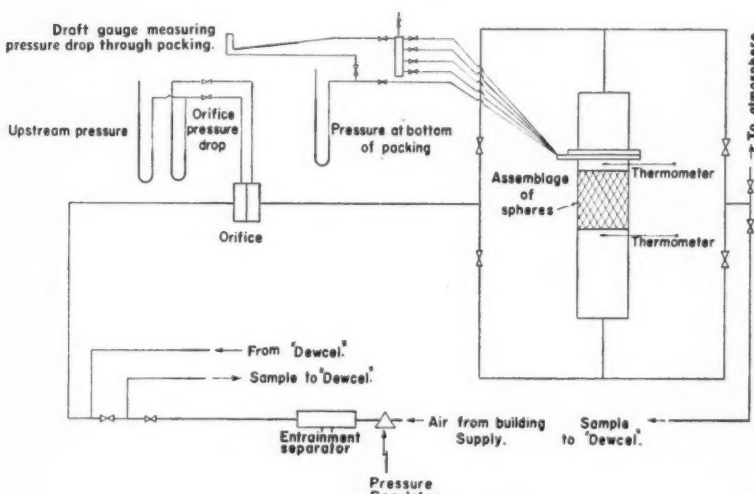


Figure 4—Schematic of apparatus.

nolds number studied, about 1,200, this period lasted more than one-half hour, giving ample time for reliable measurements.

Most of the runs performed were with unheated air, but for a few runs the inlet air had to be pre-heated in order to reduce its relative humidity. The outlet air was thus kept at a relative humidity below 94%, usually in the range of 80-90%.

Data Processing

The following rate equations were used to calculate the coefficients of mass and heat transfer respectively:

$$N = k_A(p^* - p)_{l.m.} \quad (1)$$

$$q = hA(t - t^*)_{l.m.} \quad (2)$$

The quantity p^* was taken as the vapor pressure of water at the temperature t^* . The mean partial pressure difference derived by Gamson et al.⁽⁴⁾ simplifies to the logarithmic mean used in equation 1 when p^* , p_1

and p_2 are small compared to the total pressure P as in the present work, where the two means never differed by more than 0.4%. The partial pressures of the water vapor in the inlet and outlet streams were taken as the saturated vapor pressures corresponding to the respective dew points. In conjunction with the measured absolute pressures of these streams, the partial pressures were used to establish the humidities. The mass transfer rate N was evaluated from the measured air rate and the change in humidity, while the heat transfer rate q was evaluated from the corresponding thermal data.

The transfer area A was taken as the geometric surface area of the spheres. No correction was applied for the area lost due to insertion of the connection wires, since this loss amounted to only 1%.

The quantity t^* , the surface temperature of the spheres during the constant rate drying period, was assumed constant throughout the depth

of packing and equal to the adiabatic saturation temperature of the outlet air. This was calculated from the measured temperature, dew point, and absolute pressure of the exit air and fell within 0.5 Fahrenheit degrees of the adiabatic saturation temperature calculated from the inlet air data. It also fell within 0.5 Fahrenheit degrees of the values measured, for several trials, by baking thermocouples into the spheres with junctions located at the surfaces opposite to the entrance points of the insulated thermocouple wires. The same assumption was made by Gamson, Thodos and Hougen⁽⁴⁾ in their similar measurements on randomly packed celite spheres and cylinders in a particle Reynolds number range encompassing and exceeding that of the present study, as well as by Wilke and Hougen⁽²³⁾ on celite cylinders at lower Reynolds numbers. The latter investigators resorted to this assumption because of difficulties in making accurate measurements of surface temperature by means of attached thermocouples. In the discussion of the Gamson-Thodos-Hougen paper it was noted by Chilton that Hurt's experimental check of t^* "with the temperature of adiabatic saturation, or the wet bulb temperature, was as good as the agreement is between these two temperatures". Although Hobson and Thodos⁽¹⁰⁾ subsequently criticized this assumption for very low Reynolds numbers, they found that it was increasingly applicable for the air-water system as the Reynolds number approached the lower values of the present investigation, even under non-adiabatic drying conditions. More recently Heertjes and Ringens⁽²⁴⁾ have shown experimentally that for the constant rate evaporation of four different liquids from earthenware blocks into an air stream, cover-

ing a wide range of air velocity, the solid temperature was equal to the wet-bulb temperature. It should be noted that in the present study the wet-bulb temperature is interchangeable with the adiabatic saturation temperature. This follows from the fact that thermal radiation to the packing surface was almost wholly absent, since most of the spheres could "see" nothing but other spheres at the same surface temperature. If the value of the air-water psychrometric ratio is taken as 0.236, recently reported as the most reliable value of this ratio in the absence of radiation effects (25), then for the low humidity range of the present study the wet-bulb temperature falls within 0.1 Fahrenheit degree of the adiabatic saturation temperature.

The data for each packing were correlated by means of the particle Reynolds number and the j -factors of Colburn (26) and Chilton (27). Physical properties of air-water vapor mixtures were obtained from the most reliable sources available (4, 28, 29, 30). For all the runs performed the Schmidt and Prandtl numbers were within 1% of their average values of 0.609 and 0.718 respectively.

Experimental Results and Their Interpretation

The results for 57 runs on Assemblage Nos. 1, 2, 3, and 4 are summarized in Figures 6 and 7. Except for the lower than average points of Cubic No. 1 at the higher Reynolds numbers, the points for the four assemblages largely overlap. The straight lines drawn in Figures 6 and 7 have been obtained by fitting the data for each assemblage, using the method of least squares, by equations of the form

$$\text{and } j_d = aRe^{-m} \quad (3)$$

$$j_b = bRe^{-n} \quad (4)$$

The empirical equations for each assemblage along with the corresponding standard errors are recorded in Table 2. Even for Assemblage Nos. 1-4 taken together the standard errors in j_d and j_b were $\pm 15\%$ and $\pm 18\%$ respectively. It is therefore concluded that packing configuration plays a much smaller role in mass and heat transfer than it does in fluid friction.

The negative slopes of the $\log j$ vs. $\log Re$ curves, m and n in equations 3 and 4 respectively, are an inverse measure of the development of transfer-effective turbulence in a flow system, varying as they do from

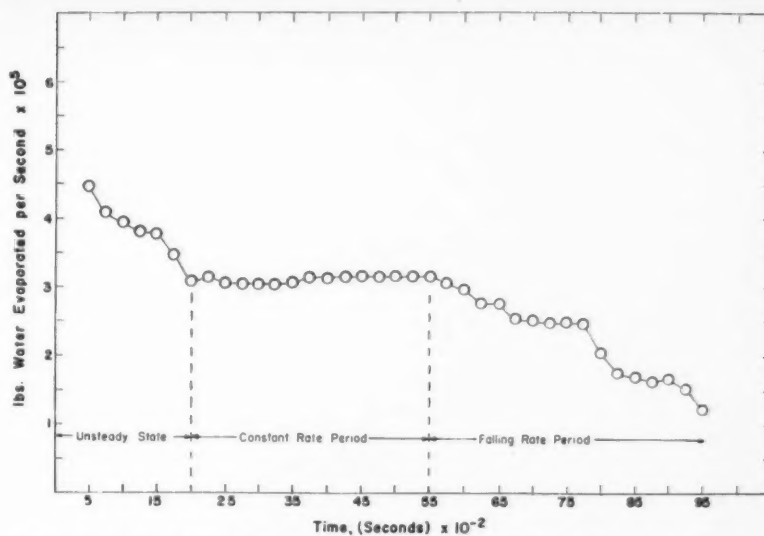


Figure 5—Drying curve for two layers of randomly packed spheres at $Re = 443$.

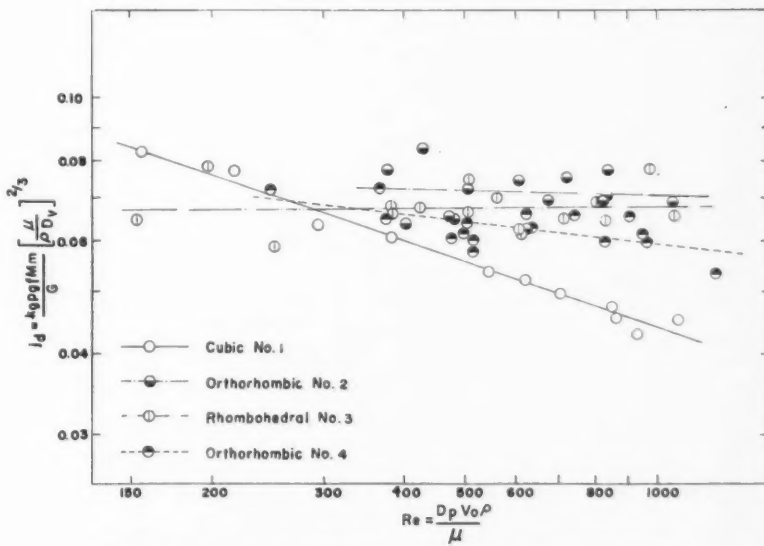


Figure 6—Effect of packing arrangement on mass transfer.

unity for viscous flow to zero for the rare case in packed beds of fully developed turbulence. Coppage and London (16) were able to correlate n with ϵ for screen matrices, broken solids, and random beds of spheres. In the present experiments, however, of the interstitial properties listed in the last four columns of Table 1, the projected fractional free area gave the best correlation with these slopes. This correlation is shown in Figure 8, where the arithmetic mean of m and n is plotted against the projected fractional free area for Assemblage Nos. 1 and 4, and the corresponding point for an isolated sphere is also included. The average slope for an isolated sphere was calculated for

$Re = 300-1200$, $Sc = 0.609$, from the Frössling-Ranz equation (31). The ordinate of Figure 8 may be considered an "index of turbulence inhibition". Its steady increase with the area of unobstructed passageways in the net direction of fluid flow suggests that channeling occurs through these passageways at the expense of cross-flow. The rhombohedral arrangement with its completely blocked off "view" represents one extreme with a maximum of tortuosity and therefore a maximum development of turbulence, while the isolated sphere with its surrounding infinite flow area represents the other extreme with a minimum development of turbulence, for the given

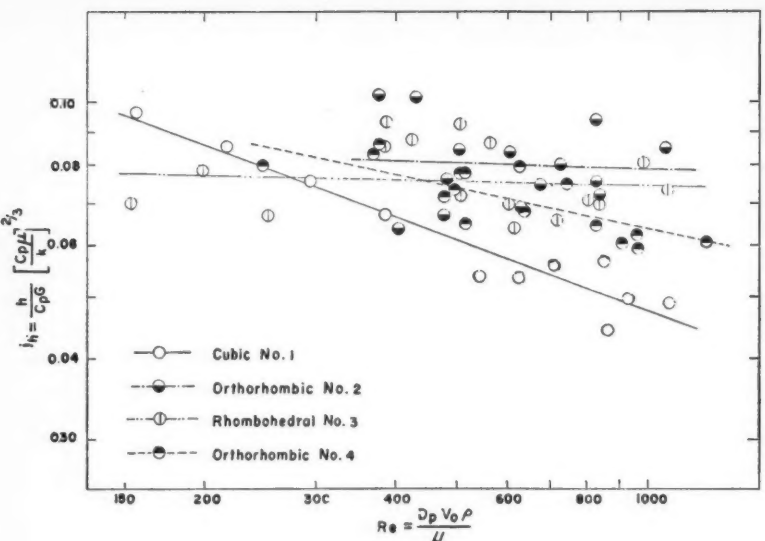


Figure 7—Effect of packing arrangement on heat transfer.

TABLE 2
EMPIRICAL EQUATIONS FOR PACKINGS

Packing Arrangement	Mass Transfer	Standard Error	Heat Transfer	Standard Error
Cubic No. 1	$j_a = 0.460 \text{ Re}^{-0.340}$	$\pm 3.6\%$	$j_h = 0.612 \text{ Re}^{-0.370}$	$\pm 7.9\%$
Orthorhombic No. 2 clear passage	$j_a = 0.084 \text{ Re}^{-0.025}$	$\pm 9.0\%$	$j_h = 0.097 \text{ Re}^{-0.030}$	$\pm 12.7\%$
Rhombohedral No. 3	$j_a = 0.064 \text{ Re}^{+0.008}$	$\pm 8.6\%$	$j_h = 0.088 \text{ Re}^{-0.023}$	$\pm 14.0\%$
Orthorhombic No. 4	$j_a = 0.130 \text{ Re}^{-0.114}$	$\pm 6.5\%$	$j_h = 0.279 \text{ Re}^{-0.213}$	$\pm 7.9\%$
Combined No. 1, 2, 3, 4	$j_a = 0.135 \text{ Re}^{-0.117}$	$\pm 14.6\%$	$j_h = 0.197 \text{ Re}^{-0.159}$	$\pm 18.3\%$
Cubic No. 1 A	$j_a = 2.963 \text{ Re}^{-0.038}$	$\pm 9.2\%$	$j_h = 5.423 \text{ Re}^{-0.722}$	$\pm 8.9\%$

particle Reynolds number range and in the absence of wall effect.

The "turbulence inhibition index" of deep randomly packed beds of spheres in the particle Reynolds number range of the present study is 0.30 or very close to this value, according to several investigations (5, 6, 7, 9, 11, 12, 16, 32). This value is bracketed by those for Orthorhombic No. 4 and Cubic No. 1. Since the void fraction of random beds of uniformly sized spheres is usually between that for the orthorhombic arrangement and that for the cubic (22), it can be surmised that a heat and mass transfer model for such beds is a mixture of local cubics and local orthorhombics.

Because slightly better correlation was obtained for j_a than for j_h , subsequent discussion will be largely restricted to mass transfer, though it should be realized that similar statements can be made about heat trans-

fer. Sherwood (33), in fact, has pointed out that taking the particle surface temperature as the adiabatic saturation temperature is in effect saying that the ratio of j_h to j_a is given by $(Pr/Sc)^{2/3}$. This is borne out by the fact that while $(Pr/Sc)^{2/3}$ for the present study is $(0.718/0.609)^{2/3}$ or 1.120, the average value of j_h/j_a for the 57 runs discussed was 1.128.

Figure 9 compares the best straight line for the combined results of Assemblage Nos. 1-4 with corresponding results on randomly packed beds. As representative of the latter, the line based on the empirical equation of Gamson, Thodos and Hougen (4) for particle Reynolds numbers exceeding 350 was chosen, since these investigators also dealt with celite spheres and the air-water system. The two lines cross each other and deviate on the average by only about 10% over the range involved. Moreover, the relatively low

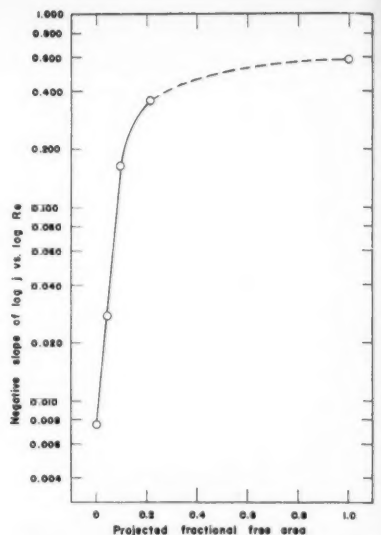


Figure 8—Dependence of turbulence inhibition on passageways open to unobstructed through-flow.

negative slope of the line for the 57 runs on the four assemblages can be explained by the non-selective averaging method used. If, for instance, more weight had been given to the cubic assemblage, the fractional void volume of which is very close to that of "random-loose" beds (22), and less to the rhombohedral, the void fraction of which is more than 0.11 below that of even "random-dense" beds (22), then this slope would have markedly increased. On the other hand, the slope of the Gamson-Thodos-Hougen line is somewhat higher than that obtained by investigators of other systems involving randomly packed spheres in the same or even lower particle Reynolds number range (5, 6, 7, 9, 11, 12, 13, 16). This has been explained (7, 11) by the shallowness of the packed beds used by Gamson et al.—as low as three layers of spheres in some cases—an effect which prevents the maximal development of turbulence.

The dozen runs on randomly packed beds made in the present study are also summarized in Figure 9. The upper six points, obtained in the square column, are in good agreement with the best line of Gamson et al. The six points obtained in the 3-in. diameter round column fall somewhat lower, though they are still above the line for an isolated sphere by a factor of two. The low points are readily explained by the small ratio of column diameter to sphere diameter for this case, that is, by the large wall effect. The marked tendency of the spheres to bridge at

the wall causes excessive voids and hence the channeling of an undue proportion of the air near the wall (8, 84, 85). This channeling air cannot in large measure participate in the exchange of mass and heat with the spheres, thus lowering the integral coefficients of mass and heat transfer. The same effect has been found for heat transfer in the absence of mass transfer (7, 11).

Figure 10 compares the results on Cubic No. 1A, which makes only point contact at the walls, with those for Cubic No. 1, which contains the flat side of half-spheres in contact with the walls and thus removes $\pi/4$ or 78.5% of the wall area. An even greater negative slope is obtained for No. 1A than for No. 1. This can be explained by the turbulence-inhibiting action of the added wall area, which is in the direction of the net air flow and therefore adds to the skin friction. The two lines intersect at a particle Reynolds number close to that at which Rose and Rizk (85) found that the wall-effect factor for fluid friction switched from positive to negative. A similar intersection due to wall effect on j_a , though at a higher value of Re , was found by Denton, Robinson, and Tibbs in their differential measurements on steady state heat transfer from electrically heated copper spheres in packed beds (7, 11). A positive deviation from the case where wall effects are absent denotes the predominance of the wall surface resistance over channeling effects, while a negative deviation is attributable to the predominance of channeling. Although such channeling occurs along the wall in the case of a randomly packed bed with a small value of D_c/D_p , it probably occurs through the centre of the bed in the case of Cubic No. 1A, in which the void fraction near the wall is no larger than in the core of the bed (86).

Correlating Functions

An attempt was made to narrow the spread of the points in Figure 6 by means of modifications to Re and j_a which have achieved some success in the case of randomly packed beds. These are listed chronologically in Table 3. Most of the modifications were derived on the assumption that the effective velocity to be used in Re and sometimes also in j_a is the average interstitial velocity V_o/ϵ rather than the superficial velocity V_o . In some of these cases six times the hydraulic diameter, $D_p\epsilon/(1-\epsilon)$, also replaces the particle diameter D_p in the Reynolds number. Ranz (81) used the maximum

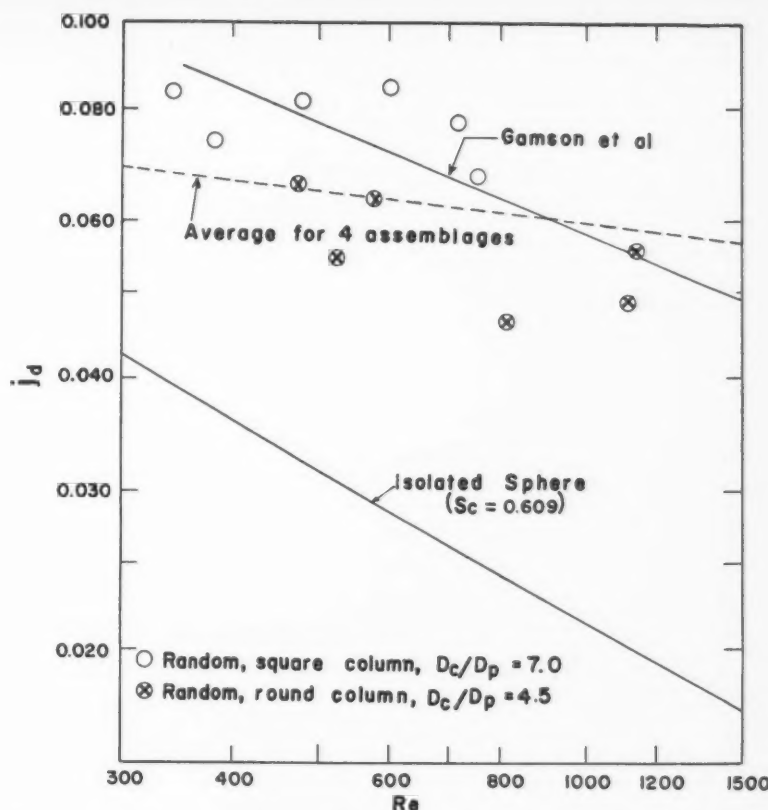


Figure 9—Stacked bed composite, random beds, and isolated sphere mass transfer compared.

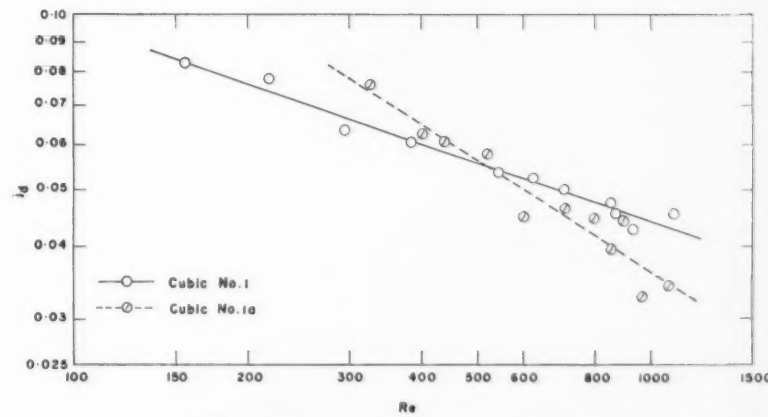


Figure 10—Effect of wall on mass transfer.

interstitial velocity V_o/ϵ in his modified moduli. The use of the Schmidt number raised to some power to modify j_a merely signifies that the given investigators employ a power for Sc other than the $\frac{1}{2}$ originally proposed by Chilton and Colburn. Its additional use in the modified Reynolds number of Ranz arises out of the form of the Frössling equation for mass transfer from an isolated sphere (87). These Schmidt number factors may be ignored in attempting

to correlate the present data, which were all at constant Sc .

Figure 11 shows the data plotted according to the method used by McCune and Wilhelm to bring their liquid-solid mass transfer data on fixed beds into line with those for a single sphere (6). No success is achieved either in reducing the scatter of the points of Figure 6 or in aligning the points about the isolated sphere line.

The method equivalent to that used

TABLE 3
DIMENSIONLESS MODULI FOR MASS TRANSFER IN RANDOMLY PACKED BEDS OF SPHERES

Investigators	Year	Modified Re	Modified j_a
McCune and Wilhelm (6)	1949	Re/ϵ	$j_a \epsilon$
Gaffney and Drew (9)	1950	Re/ϵ	$j_a Sc^{-0.09}$
Gamson (38)	1951	$Re/1-\epsilon$	$j_a/(1-\epsilon)^{0.2}$
Ergun (32)	1952	$Re/1-\epsilon$	$j_a \epsilon Sc^{1/8}$
Ranz (31)	1952	$Sc^{2/3} Re/\alpha$	$j_a \alpha Sc^{-1/3}$
Chu et al. (13, 45)	1953	$Re/1-\epsilon$	j_a

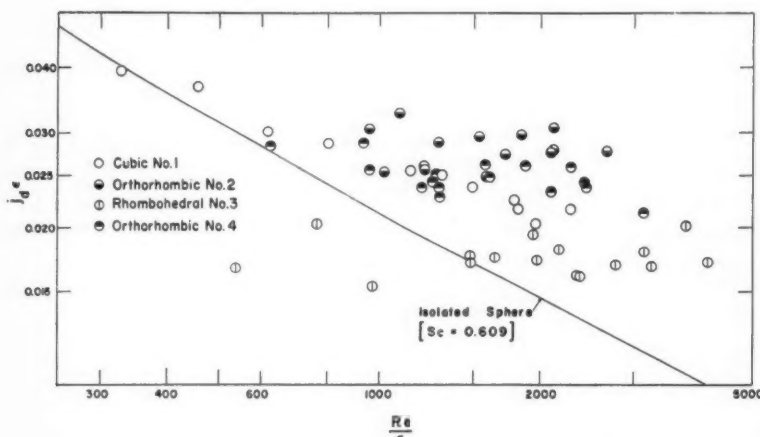


Figure 11—Correlation after McCune and Wilhelm.

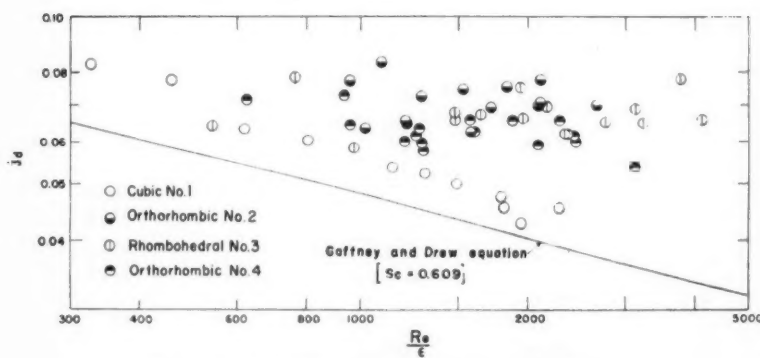


Figure 12—Correlation after Gaffney and Drew.

by Gaffney and Drew (9) to correlate liquid-solid mass transfer data in randomly packed beds of spheres is employed in Figure 12. No rectification of the data results. The straight line drawn is based on an empirical equation derived by Ergun (32) to represent the plot made by Gaffney and Drew of their own data, as well as those of McCune and Wilhelm. It misses the present data completely.

Figure 13 illustrates the application of Gamson's (38) modified moduli to the stacked bed results. The arbitrarily

empirical use of the factor $(1-\epsilon)^{0.2}$ in the denominator of the ordinate, especially after $1-\epsilon$ is already in the denominator of the abscissa, detracts from the rationality and sensitivity of this method. Little or no rectification of the data is achieved over that already present in Figure 6. Moreover, the line based on Gamson's correlation equation for fixed and fluidized beds of spheres is inadequately representative of the present data.

The combined use of interstitial

velocity and hydraulic diameter in the dimensionless groups, as proposed by Ergun (32), is the mass transfer analogue of the method developed by Blake (39), Kozeny (40), Fair and Hatch (41), Carman (42) and Ergun (43) for fluid friction in granular media. That it impairs rather than improves the correlation of the present data is apparent on comparing Figure 14 with Figure 6. In addition, the mass transfer equation derived by Ergun, equation 5b below, fails by an average factor of about 16 to predict the present data. Even if perfect mixing in the beds is assumed, an extreme possibility suggested by Ergun for gas flow through shallow beds, his line still lies at an average factor of approximately 5 above the recalculated points, which show more scatter than ever.

The modified dimensionless moduli proposed by Ranz (31), like those of McCune and Wilhelm, are designed to reduce to their corresponding unmodified forms for the case of an isolated sphere, for which $\epsilon = a = 1$. The present data are plotted according to this scheme in Figure 15, which again shows no improvement over the spread in Figure 6, but does have the virtue of approximately aligning the points about the isolated sphere line. It would seem then that for the stacked beds of this study, a is a more successful parameter than ϵ for relating the mass transfer data to those for an isolated sphere. The relevant difference between stacked and randomly packed beds for transfer processes is probably the continuous but periodic variation of fractional free area with bed height in the case of the former, as opposed to the statistical constancy of fractional free area in the case of the latter (44). A constant fractional free area is moreover equal in value to both a and ϵ . This probably accounts for the success of McCune and Wilhelm in correlating their randomly packed bed data with that for a single sphere using ϵ as parameter, despite the failure of their method in the present instance.

Finally, the equation of Chu et al. (13, 45), which has provided a generalized correlation of mass transfer in fixed and fluidized beds of granular particles, is tested in Figure 16. Here again there is no reduction in the scatter of the points, and Chu's line, like Gamson's, falls somewhat high.

It is concluded, therefore, that methods appropriate to the correlation of mass transfer data on randomly packed beds are inappropriate to stacked beds. The same conclusion

for fluid friction was arrived at by Martin (10A).

Momentum-Mass Transfer Analogy

Starting with Reynolds' original analogy (46), Ergun (82) has derived a "theoretical" relationship between momentum and mass transfer in packed beds, ignoring completely the fact that the Reynolds and derivative analogies apply only to skin friction, but not to form drag (47). Ergun's analogy may be expressed as

$$6\epsilon Sc^{n-1} j_d = 2f \frac{\epsilon^3}{1-\epsilon} \quad (5)$$

Liquid-solid data (8, 8, 9) were used to evaluate the index n as unity. The simplified relationship is then

$$j_d = \frac{1}{3} Sc^{-1/3} f \frac{\epsilon^2}{1-\epsilon} \quad (5a)$$

Combining equation 5a with his well-supported equation for fluid friction in randomly packed beds (48), Ergun finally arrived at

$$6\epsilon Sc^{1/3} j_d = \frac{150(1-\epsilon)}{Re} + 1.75 \quad (5b)$$

When equation 5b was applied to gas-solid data (4, 28, 48, 49), it failed completely to predict the experimental results by factors ranging from 5 to 30. The smallest factor in this range applied only when the extreme assumption of perfect mixing was employed for the shallow bed mass transfer data of Hurt (48).

On a purely empirical basis, Chu et al. (13, 45) have proposed "for the practical purpose of engineering design" the following approximate analogy between mass and momentum transfer in fixed and fluidized beds of granular solids:

$$j_d = \frac{1}{10} f \frac{\epsilon^3}{1-\epsilon} \quad (6)$$

Both equations 5a and 6 imply that j_d is directly proportional to f if the other terms in the equations are fixed. This is completely contradicted by the results on the two orthorhombic assemblages. These have the same void fractions, and since Sc was essentially constant for the present experiments, all the terms other than j_d and f were thus fixed. Nevertheless a four-fold increase in f from Orthorhombic No. 2 to Orthorhombic No. 4 was accompanied by no increase in j_d .

The application of equations 5a and 6 to the present assemblages at a particle Reynolds number of 1,000 is shown in Table 4. While the Ergun analogy yields values of j_d which are

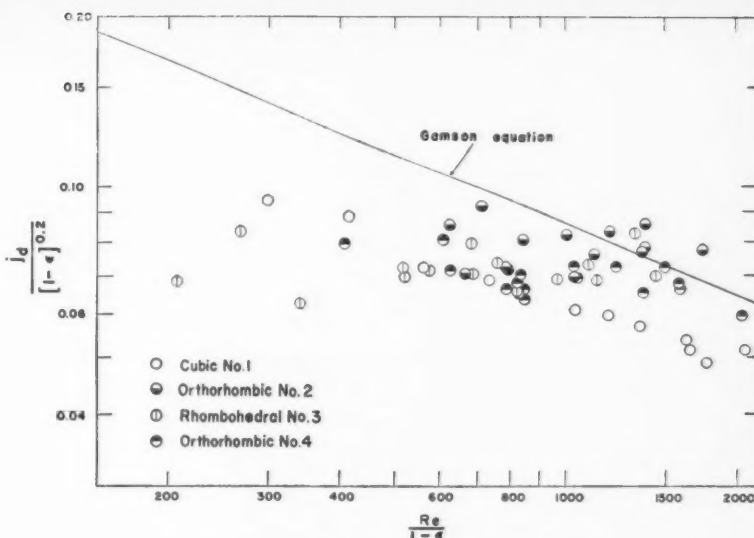


Figure 13—Correlation after Gamson.

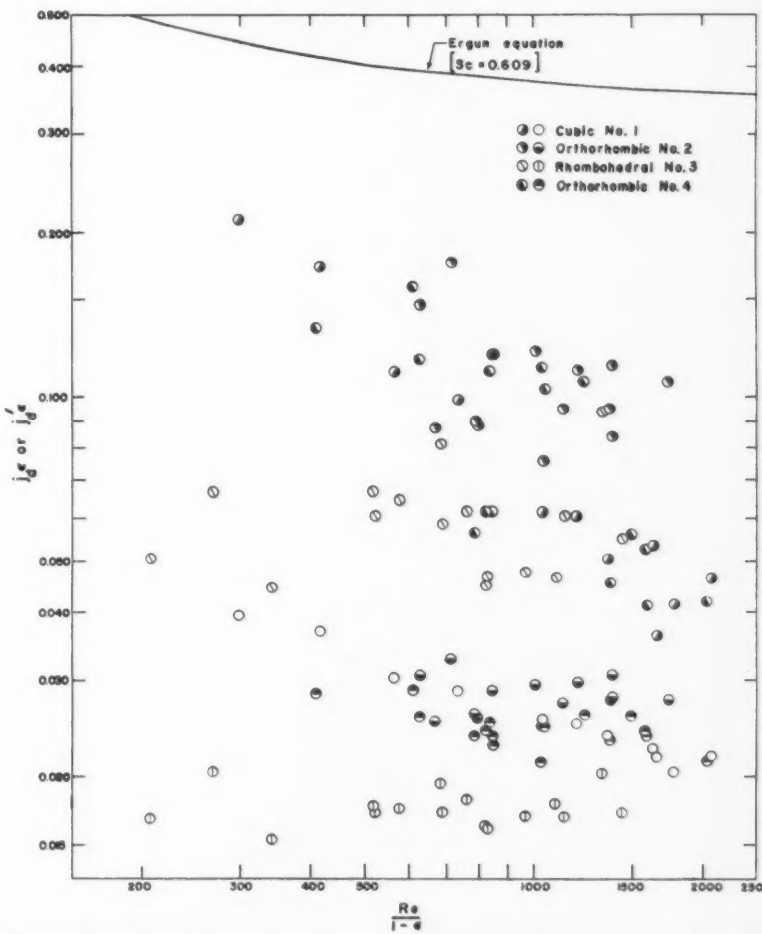


Figure 14—Correlation after Ergun (obliquely divided circles signify the assumption of perfect mixing).

TABLE 4
TEST OF MOMENTUM-MASS TRANSFER ANALOGIES AT $Re = 1000$

Packing Arrangement	f Experimental Martin et al. (19)	j_d Ergun analogy Equation (5a) $Sc = 0.609$	j_d Chu analogy Equation (6)	j_d Experimental Table 2
Cubic No. 1	1.8	0.307	0.0373	0.0439
Orthorhombic No. 2 clear passage	5.8	0.590	0.0593	0.0706
Rhombohedral No. 3	30	1.07	0.0708	0.0677
Orthorhombic No. 4	23	2.34	0.235	0.0592

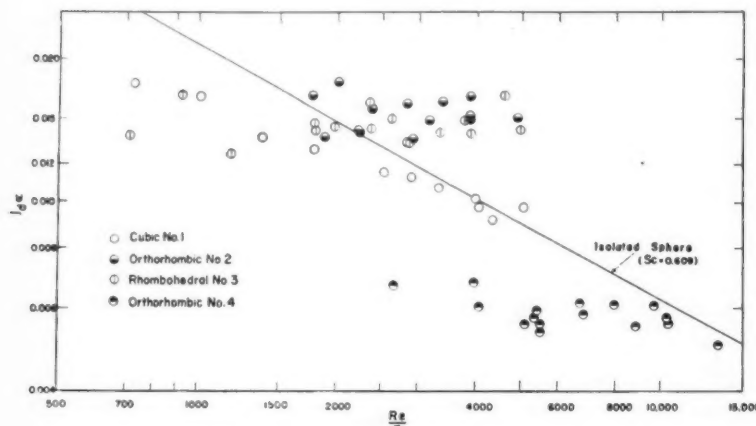


Figure 15—Correlation after Ranz.

high by factors ranging from 7 for Cubic No. 1 to 40 for Orthorhombic No. 4, the Chu analogy predicts to within 16% or less the values of j_d for the first three assemblages, though of course it still misses the j_d for No. 4 by a factor of 4.

The inapplicability of Ergun's analogy to packed beds can in part at least be explained by its failure to differentiate between skin friction and form drag, only the former of which has appreciable effect on mass and heat transfer (50). It is known that for flow past single cylinders (51), single spheres (47) and closely arrayed cylinders (52, 50), turbulent wake formation results in a much larger dissipation of energy by form resistance than by skin friction, at the higher Reynolds numbers. It would seem to follow then, that for closely arrayed or packed beds of spheres at comparable Reynolds numbers, turbulent wakes form behind the spheres, causing a large dissipation of energy (high fluid friction) without a corresponding increase in mass or heat transfer. This would also account for the fact that whereas f eventually becomes independent of Re for randomly

packed beds (7, 11, 48), j continues to fall (1-18, 28, 48, 49) right up to $Re = 60,000$, the highest particle Reynolds number at which mass or heat transfer has been studied (7, 11). The same effect again holds true for flow past isolated spheres and cylinders, as well as for flow through rough pipes (47, 50, 53). Flow through smooth pipes, by contrast, displays only skin friction and therefore both f and j continue to fall parallelwise up to the highest of measured pipe Reynolds numbers (47), as do the calculated skin friction factor (51) and experimental mass and heat transfer factors for flow normal to single cylinders (47). Exponential equations of the form of equations 3 and 4 are therefore empirically more applicable in the transitional and turbulent range of particle Reynolds number than the type similar to equation 5b.

Mixing Assumptions

The common practice of using logarithmic mean driving forces in evaluating transfer coefficients, as in equations 1 and 2 of the present study, implies the absence of any longitudinal mixing in packed beds. Ergun (82) has suggested that the

opposite extreme of perfect mixing is a better assumption for gas flow through shallow beds, which would require basing the transfer coefficients on exit driving force. However, his analysis of Hurt's data (48) in the transitional range of Reynolds number which led him to this conclusion was based on the form of equation 5b, which as indicated above, is less applicable than equation 3. A similar analysis of Hurt's data based on equation 3 leads to the opposite conclusion, as shown by the straight lines obtained by Resnick and White (49) on plotting these data as $\log j_d$ versus $\log Re$, basing j_d on logarithmic mean driving force.

Figure 17 shows the mass transfer data on Assemblage Nos. 1-4 recalculated on the assumption of perfect mixing. Regardless of the form of the functional relationship between j_d or j_d' and Re , comparison of Figure 17 with Figure 6 shows that the perfect mixing assumption results in a very much greater scatter of the points than the assumption of no axial mixing, both for the assemblages taken individually and for the combined data. This tends to support the contention that no longitudinal mixing is closer to the truth than overall perfect mixing, in the present experiments.

Recently, McHenry and Wilhelm (54) have demonstrated that their elaborate measurements of axial mixing of binary gas mixtures in a random bed of spheres can be predicted on the assumption that "perfect mixing occurs over the length represented by one particle diameter". Based upon this model it can be shown (55) that the correction factor Y which must be applied to the logarithmic mean driving potentials, as in equations 1 and 2, is given by

$$Y = \frac{1}{x} \frac{\ln R}{(R^{1/x} - 1)} \quad (7)$$

where x represents the number of perfect mixers in series and is therefore equal to L/D_p , while R is the ratio of inlet to outlet driving potentials.

For the present experiments, in which $x = 8$, and R averages 8 for water partial pressure difference and 10 for temperature difference, the corresponding values of Y are 0.88 for mass transfer and 0.86 for heat transfer. This means that the reported values of j_d and j_h should be raised by average factors of 1.14 and 1.16 respectively. It is believed that the results thus corrected would not

substantially change any of the conclusions previously drawn, especially since the individual deviations from the average correction factors are within 4% for mass transfer and 5% for heat transfer. All the points in Figures 6 and 7 would thus be raised by a practically constant factor, and the resulting best lines would lie within the previously reported standard deviations, with little change in slope.

The use of the logarithmic mean of terminal potentials is a procedure followed by practically all other investigators of steady state particle-fluid mass or heat transfer in packed beds (4, 6, 8, 9, 10, 13, 14, 15, 18, 23, 48, 49), the most notable exception being the differential heat transfer study of Denton et al. (7, 11). Thus the shallow bed results of Ganson et al. (4), partially summarized in Figure 9, would probably be subject to greater modification than the present data, due to axial mixing. The correction of such data reported in the literature by means of equation 7 is presently being initiated, in an attempt to reconcile some of the discrepancies between results of various investigations, with the point data of Denton et al. (7, 11) serving as a possible datum.

Nomenclature

- a = constant in equation (3), dimensionless.
- A = geometric surface area of spheres, sq. ft.
- b = constant in equation (4), dimensionless.
- c = concentration of diffusing component in fluid stream, lb.-mole/cu. ft.
- c^* = solubility of diffusing component in fluid stream, lb.-mole/cu. ft.
- c_p = molal heat capacity of diffusing vapor at constant pressure, B.t.u./lb.-mole ($^{\circ}$ F.).
- C_p = heat capacity of fluid stream at constant pressure, B.t.u./lb. ($^{\circ}$ F.).
- D_c = side or diameter of column, ft.
- D_p = particle diameter, ft.
- D_v = molecular diffusivity of vapor in gas, sq. ft./hr.
- f = friction factor = $\Delta P D_{pgc} / 2 L V_o \rho$, dimensionless.
- g_e = conversion factor = 4.17×10^8 (lb.) (ft.)/(hr.)² (lb.-force).
- G = superficial mass velocity = $V_o \rho$, lb./hr. (sq. ft.).
- h = particle-fluid heat transfer coefficient, B.t.u./hr. (sq. ft.) ($^{\circ}$ F.).
- H = humidity, lb. vapor/lb. dry gas.
- j = heat transfer factor, dimensionless.
- j_d = mass transfer factor = $\frac{k_a p_{ef} M_m}{G}$ (Sc)^{2/3}, dimensionless.
- j_d' = mass transfer factor evaluated on the assumption of perfect mixing in packed bed, dimensionless.
- j_h = heat transfer factor = $\frac{h}{C_p G}$ (Pr)^{2/3}, dimensionless.

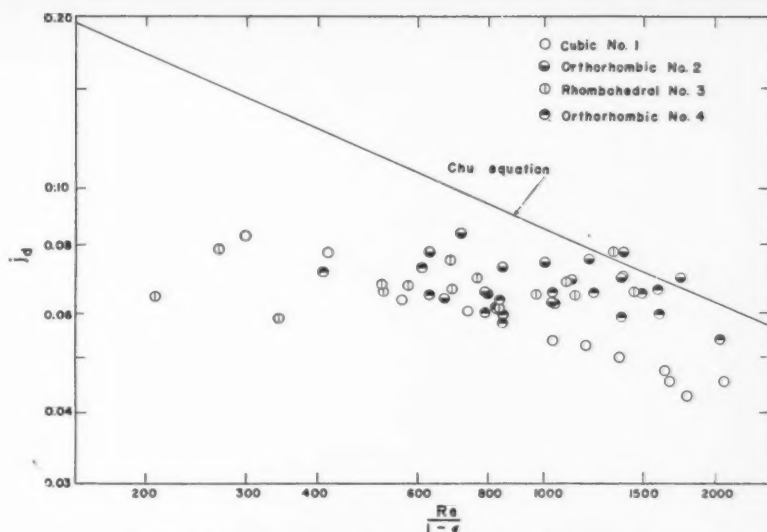


Figure 16—Correlation after Chu, Kalil and Wetteroth.

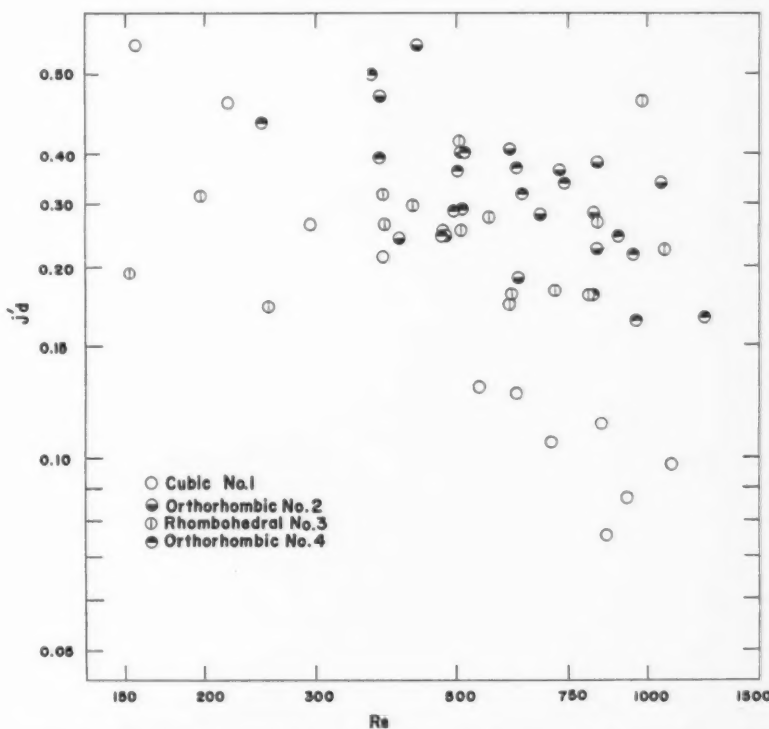


Figure 17—Results of Figure 6 recalculated on the assumption of perfect mixing.

- k = thermal conductivity of fluid stream, (B.t.u.) (ft.)/(hr.) (sq. ft.) ($^{\circ}$ F.).
- k_g = particle-fluid mass transfer coefficient, (lb.-moles vapor)/(hr.) (sq. ft.) (atm).
- L = length, height, or depth of packing, ft.
- m = constant in equation (3) = negative slope of $\log j_d$ vs. $\log Re$ curve, dimensionless.
- M_m = average molecular weight of fluid stream, lb./lb.-mole.
- M_v = molecular weight of diffusing vapor, lb./lb.-mole.
- n = constant in equation (4) = nega-
- tive slope of $\log j_h$ vs. $\log Re$ curve, dimensionless.
- N = rate of mass transfer = $w_g (H_2 - H_1) / M_v$, lb.-moles vapor/hr.
- p = partial pressure of diffusing vapor in fluid stream, atm.
- p_{ef} = mean partial pressure of non-diffusing gas in particle-fluid film, atm.
- p^* = vapor pressure of diffusing component at temperature t^* , atm.
- P = total pressure, atm.
- ΔP = frictional pressure drop, atm.
- Pr = Prandtl number = $C_p \mu / k$, dimensionless.

- q = rate of heat transfer = $w_1 C_p (t_1 - t_2) = N\lambda + NC_p (t_2 - t^*)$, B.t.u./hr.
 R = ratio of inlet to outlet transfer potentials: $(t_1 - t^*)/(t_2 - t^*)$ for heat transfer, $(c^* - c_1)/(c^* - c_2)$ or $(p^* - p_1)/(p^* - p_2)$ for mass transfer, dimensionless.
 Re = particle Reynolds number, $D_p G / \mu$, dimensionless.
 Sc = Schmidt number, $\mu / \rho D_v$, dimensionless.
 t = temperature of fluid stream, °F.
 t^* = surface temperature of spheres during constant rate period of drying, °F.
 V_o = superficial velocity of fluid, ft.²/hr. (sq. ft. empty column cross-section).
 w = weight rate of fluid flow, lb./hr.
 w_g = weight rate of non-diffusing gas flow, lb./hr.
 x = "number of perfect mixers in series" = L/D_p , dimensionless.
 Y = axial mixing correction factor to logarithmic mean of terminal driving potentials in mass or heat transfer rate equations, dimensionless.
 a = smallest fractional free area normal to major flow axis, dimensionless.
 ϵ = fractional void volume, external porosity, dimensionless.
 λ = molal latent heat of vaporization of diffusing component at temperature $t^*/B.t.u./lb.-mole$.
 μ = viscosity of fluid stream, lb/(hr.) (ft.).
 ρ = density of fluid stream, lb./cu. ft.
- (4) Gamson, B. W., Thodos, G., and Hougen, O. A., Trans. Am. Inst. Chem. Engrs., 39, 1 (1943).
(5) Johnson, F., Bentley, R., and Maurer, R., U.S. Atomic Energy Commission Rept. M.D.D.C.-990 (1945).
(6) McCune, L. K., and Wilhelm, R. H., Ind. Eng. Chem., 41, 1124 (1949).
(7) Denton, W. H., Robinson, C. H., and Tibbs, R. S., A.E.R.E. Report, H.P.C. 35 (June 1949).
(8) Hobson, M., and Thodos, G., Chem. Eng. Progress, 45, 517 (1949).
(9) Gaffney, B. J., and Drew, T. B., Ind. Eng. Chem., 42, 1120 (1950).
(10) Hobson, M., and Thodos, G., Chem. Eng. Progress, 47, 370 (1951).
(11) Denton, W. H., Proceedings of the General Discussion on Heat Transfer, Instn. Mech. Engrs. (London) and Amer. Soc. Mech. Engrs., p. 370-373 (Sept. 1951).
(12) Eichhorn, J., and White, R. R., Chem. Eng. Progress Symp. Series No. 4, 48, 11 (1952).
(13) Chu, J. C., Kalil, J., and Wetteroth, W. A., Chem. Eng. Progress, 49, 141 (1953).
(14) Dryden, C. E., Strang, D. A., and Withrow, A. E., Chem. Eng. Progress, 49, 191 (1953).
(15) Satterfield, C. N., and Resnick, H., Chem. Eng. Progress, 50, 504 (1954).
(16) Coppage, J. E., and London, A. L., Chem. Eng. Progress, 52, 57-F (1956).
(17) Glaser, M. B., and Thodos, G., "Heat and Momentum Transfer in the Flow of Gases Through Packed Beds", presented at Seattle meeting, A.I.Ch.E., June 10, 1957.
(18) Hodgins, J. W., Hoffman, T. W., and Pei, D. C., Can. J. Chem. Eng., 35, 18 (1957).
(19) Martin, J. J., McCabe, W. L., and Monrad, C. C., Chem. Eng. Progress, 47, 91 (1951).
(19A) Martin, J. J., Sc.D. Thesis, Carnegie Institute of Technology, 1948.
(20) Graton, L. C., and Fraser, H. J., J. Geol., 43, 785 (1935).
(21) Galloway, L. R., and Epstein, N., Can. J. Tech., 34, 92 (1956).
(22) Oman, A. O., and Watson, K. M., Refinery Management and Petroleum Chem. Technol., 36, R795 (1944).
(23) Wilke, C. R., and Hougen, O. A., Trans. Am. Inst. Chem. Engrs., 41, 445 (1945).
(24) Heertjes, P. M., and Ringens, W. P., Chem. Eng. Sci., 5, 226 (1956).
(25) Treybal, R. E., "Mass-Transfer Operations", p. 169, McGrawHill, New York (1955).
(26) Colburn, A. P., Trans. Am. Inst. Chem. Engrs., 29, 174 (1933).
(27) Chilton, T. H., and Colburn, A. P., Ind. Eng. Chem., 26, 1183 (1934).
(28) International Critical Tables, Vol. 5, McGraw-Hill, New York (1929).
(29) Gilliland, E. R., Ind. Eng. Chem., 26, 681 (1934).
(30) Keyes, F. G., Trans. A.S.M.E., 73, 589 (1951).
(31) Ranz, W. E., Chem. Eng. Prog., 48, 247 (1952).
(32) Ergun, S., Chem. Eng. Prog., 48, 227 (1952).
(33) Sherwood, T. K., Trans. Am. Inst. Chem. Engrs., 39, 583 (1943).
(34) Furnas, C. C., U.S. Bur. Mines Bull., No. 307 (1929).
(35) Rose, H. E., and Rizk, A. M. A., Proc. Instn. Mech. Engrs. (London), 160, 493 (1949).
(36) Somerville, G. F., B.A.Sc. Thesis, University of British Columbia, April 1957.
(37) Frössling, N., Gerlands Beitr. Geophys., 52, 170 (1938).
(38) Gamson, B. W., Chem. Eng. Progress, 47, 19 (1951).
(39) Blake, F. C., Trans. Am. Inst. Chem. Engrs., 14, 415 (1921-22).
(40) Kozeny, J., Sitzungsber. Akad. Wiss. Wien, 136, IIa, 271 (1927).
(41) Fair, G. M., and Hatch, L. P., J. Am. Water Works Assoc., 25, 1551 (1933).
(42) Carman, P. C., Trans. Inst. Chem. Engrs. (London), 15, 150 (1937); J. Soc. Chem. Ind. (London), 57, 225 (1938); 58, 1 (1939).
(43) Ergun, S., Chem. Eng. Prog., 48, 89 (1952).
(44) Pirie, J. M., Trans. Inst. Chem. Engrs. (London), 27, 253 (1949).
(45) Chu, J. C., "Fluidization", edited by D. F. Othmer, Chapter 2, Reinhold, New York (1956).
(46) Reynolds, O., Proc. Manchester Lit. Phil. Soc., 14, 7 (1874).
(47) Sherwood, T. K., Ind. Eng. Chem., 42, 2077 (1950).
(48) Hurt, M. D., Ind. Eng. Chem., 35, 522 (1943).
(49) Resnick, W., and White, R. R., Chem. Eng. Progress, 45, 377 (1949).
(50) Knudsen, J. G., and Katz, D. L., "Fluid Dynamics and Heat Transfer", Univ. of Mich. Press, Ann Arbor (1954).
(51) Goldstein, S., "Modern Developments in Fluid Mechanics", Vol. II, p. 425, Oxford Univ. Press, London (1938).
(52) Wallis, R. P., Engineering, 148, 423 (1934).
(53) Smith, J. W., and Epstein, N., A.I.Ch.E. Journal, 3, 242 (1957).
(54) McHenry, K. W., Jr., and Wilhelm, R. H., A.I.Ch.E. Journal, 3, 83 (1957).
(55) Epstein, N., Paper to be submitted for publication.

Subscripts

- 1 = packed bed entrance.
2 = packed bed exit.
l.m. = logarithmic mean.

References

- (1) Furnas, C. C., Ind. Eng. Chem., 22, 26 (1930).
(2) Furnas, C. C., U.S. Bur. Mines Bull., No. 361 (1932).
(3) Saunders, O. A., and Ford, H., J. Iron Steel Inst., 141, 291P (1940).

- (4) Gamson, B. W., Thodos, G., and Hougen, O. A., Trans. Am. Inst. Chem. Engrs., 39, 1 (1943).
(5) Johnson, F., Bentley, R., and Maurer, R., U.S. Atomic Energy Commission Rept. M.D.D.C.-990 (1945).
(6) McCune, L. K., and Wilhelm, R. H., Ind. Eng. Chem., 41, 1124 (1949).
(7) Denton, W. H., Robinson, C. H., and Tibbs, R. S., A.E.R.E. Report, H.P.C. 35 (June 1949).
(8) Hobson, M., and Thodos, G., Chem. Eng. Progress, 45, 517 (1949).
(9) Gaffney, B. J., and Drew, T. B., Ind. Eng. Chem., 42, 1120 (1950).
(10) Hobson, M., and Thodos, G., Chem. Eng. Progress, 47, 370 (1951).
(11) Denton, W. H., Proceedings of the General Discussion on Heat Transfer, Instn. Mech. Engrs. (London) and Amer. Soc. Mech. Engrs., p. 370-373 (Sept. 1951).
(12) Eichhorn, J., and White, R. R., Chem. Eng. Progress Symp. Series No. 4, 48, 11 (1952).
(13) Chu, J. C., Kalil, J., and Wetteroth, W. A., Chem. Eng. Progress, 49, 141 (1953).
(14) Dryden, C. E., Strang, D. A., and Withrow, A. E., Chem. Eng. Progress, 49, 191 (1953).
(15) Satterfield, C. N., and Resnick, H., Chem. Eng. Progress, 50, 504 (1954).
(16) Coppage, J. E., and London, A. L., Chem. Eng. Progress, 52, 57-F (1956).
(17) Glaser, M. B., and Thodos, G., "Heat and Momentum Transfer in the Flow of Gases Through Packed Beds", presented at Seattle meeting, A.I.Ch.E., June 10, 1957.
(18) Hodgins, J. W., Hoffman, T. W., and Pei, D. C., Can. J. Chem. Eng., 35, 18 (1957).
(19) Martin, J. J., McCabe, W. L., and Monrad, C. C., Chem. Eng. Progress, 47, 91 (1951).
(19A) Martin, J. J., Sc.D. Thesis, Carnegie Institute of Technology, 1948.
(20) Graton, L. C., and Fraser, H. J., J. Geol., 43, 785 (1935).
(21) Galloway, L. R., and Epstein, N., Can. J. Tech., 34, 92 (1956).
(22) Oman, A. O., and Watson, K. M., Refinery Management and Petroleum Chem. Technol., 36, R795 (1944).
(23) Wilke, C. R., and Hougen, O. A., Trans. Am. Inst. Chem. Engrs., 41, 445 (1945).
(24) Heertjes, P. M., and Ringens, W. P., Chem. Eng. Sci., 5, 226 (1956).
(25) Treybal, R. E., "Mass-Transfer Operations", p. 169, McGrawHill, New York (1955).
(26) Colburn, A. P., Trans. Am. Inst. Chem. Engrs., 29, 174 (1933).
(27) Chilton, T. H., and Colburn, A. P., Ind. Eng. Chem., 26, 1183 (1934).
(28) International Critical Tables, Vol. 5, McGraw-Hill, New York (1929).
(29) Gilliland, E. R., Ind. Eng. Chem., 26, 681 (1934).
(30) Keyes, F. G., Trans. A.S.M.E., 73, 589 (1951).
(31) Ranz, W. E., Chem. Eng. Prog., 48, 247 (1952).
(32) Ergun, S., Chem. Eng. Prog., 48, 227 (1952).
(33) Sherwood, T. K., Trans. Am. Inst. Chem. Engrs., 39, 583 (1943).
(34) Furnas, C. C., U.S. Bur. Mines Bull., No. 307 (1929).
(35) Rose, H. E., and Rizk, A. M. A., Proc. Instn. Mech. Engrs. (London), 160, 493 (1949).
(36) Somerville, G. F., B.A.Sc. Thesis, University of British Columbia, April 1957.
(37) Frössling, N., Gerlands Beitr. Geophys., 52, 170 (1938).
(38) Gamson, B. W., Chem. Eng. Progress, 47, 19 (1951).
(39) Blake, F. C., Trans. Am. Inst. Chem. Engrs., 14, 415 (1921-22).
(40) Kozeny, J., Sitzungsber. Akad. Wiss. Wien, 136, IIa, 271 (1927).
(41) Fair, G. M., and Hatch, L. P., J. Am. Water Works Assoc., 25, 1551 (1933).
(42) Carman, P. C., Trans. Inst. Chem. Engrs. (London), 15, 150 (1937); J. Soc. Chem. Ind. (London), 57, 225 (1938); 58, 1 (1939).
(43) Ergun, S., Chem. Eng. Prog., 48, 89 (1952).
(44) Pirie, J. M., Trans. Inst. Chem. Engrs. (London), 27, 253 (1949).
(45) Chu, J. C., "Fluidization", edited by D. F. Othmer, Chapter 2, Reinhold, New York (1956).
(46) Reynolds, O., Proc. Manchester Lit. Phil. Soc., 14, 7 (1874).
(47) Sherwood, T. K., Ind. Eng. Chem., 42, 2077 (1950).
(48) Hurt, M. D., Ind. Eng. Chem., 35, 522 (1943).
(49) Resnick, W., and White, R. R., Chem. Eng. Progress, 45, 377 (1949).
(50) Knudsen, J. G., and Katz, D. L., "Fluid Dynamics and Heat Transfer", Univ. of Mich. Press, Ann Arbor (1954).
(51) Goldstein, S., "Modern Developments in Fluid Mechanics", Vol. II, p. 425, Oxford Univ. Press, London (1938).
(52) Wallis, R. P., Engineering, 148, 423 (1934).
(53) Smith, J. W., and Epstein, N., A.I.Ch.E. Journal, 3, 242 (1957).
(54) McHenry, K. W., Jr., and Wilhelm, R. H., A.I.Ch.E. Journal, 3, 83 (1957).
(55) Epstein, N., Paper to be submitted for publication.

Acknowledgments

The authors are indebted to the National Research Council of Canada and to the U.B.C. President's Committee on Research for grants-in-aid of this study.

★ ★ ★

The Carbon Dioxide-Hydrogen Sulphide-Methane System

Part I: Phase Behaviour at 100°F.¹

D. B. ROBINSON² and J. A. BAILEY³

The phase behavior of the carbon dioxide-hydrogen sulphide-methane system has been studied at 100°F. and 600, 1200 and 1800 lb./in.² abs. in a glass and stainless steel equilibrium cell of variable volume. The concept of the equilibrium ratio and the activity coefficient ratio is reviewed briefly. Analysis of the vapor and liquid phases in equilibrium at the three pressures permitted a calculation of equilibrium ratios and activity coefficient ratios as a function of pressure and composition. Activity coefficient ratios indicated the liquid solutions to be non-ideal under most of the conditions investigated. The presence of hydrogen sulphide suppresses the volatility of methane and increases the volatility of carbon dioxide whereas the hydrogen sulphide behaves essentially like an ideal component up to pressures of 1000 lb./in.².

A STUDY of the behavior of systems containing more than one component over a range of temperature, pressure, and concentration is frequently of scientific and industrial interest. A comparison between actual behavior and behavior predicted for ideal solutions or by generalized correlations can be made when experimental data exist. A knowledge of equilibrium phase compositions is a prerequisite to accurate design of industrial equipment used to process multicomponent systems.

A search of the literature failed to reveal any data on the ternary system carbon dioxide-hydrogen sulphide-methane, although the binary systems have been studied. It was the purpose of this research to investigate the behavior of this system at 100°F. and at three different pressures using mixtures giving a two phase system at the chosen conditions. Measurements made under these conditions permit an estimation of the nearness to ideality of the liquid solutions, and

systems has been reported by many workers. It is possible to represent the boundary between two phases for a binary system at constant temperature as a line on a pressure-composition diagram. The configuration of this line will depend on the properties of the pure components at the chosen temperature and on the nature of the solutions they form.

The addition of a third component to a binary system adds one degree

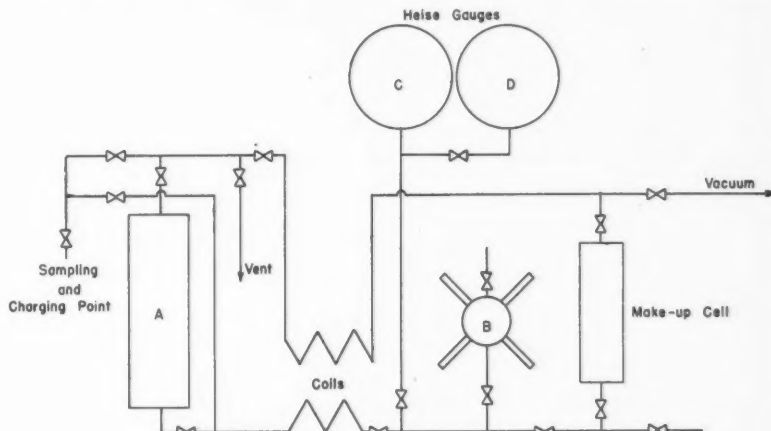


Figure 1—Schematic layout of equipment.

a determination of the equilibrium ratios for the components in the vapor and liquid phases.

THEORY

The phase behavior of single component, binary, and multi-component

of freedom. This means that the boundary between two phases is represented by a surface in three dimensions on a pressure composition diagram at a fixed temperature. It is not possible to represent graphically the variation of temperature, pressure, and composition simultaneously for a three component system. The configurations of the boundary surface depends on the nature of the pure components and the solutions they form.

¹Manuscript received September 12, 1957.

²Associate Professor of Chemical Engineering, Department of Chemical and Petroleum Engineering, University of Alberta, Edmonton, Alta.

³Fluor Corporation, Whittier, California.

Contribution from the Department of Chemical and Petroleum Engineering, University of Alberta, Presented at the 40th Annual Conference of the Chemical Institute of Canada, Vancouver, B.C., June 3-5, 1957.

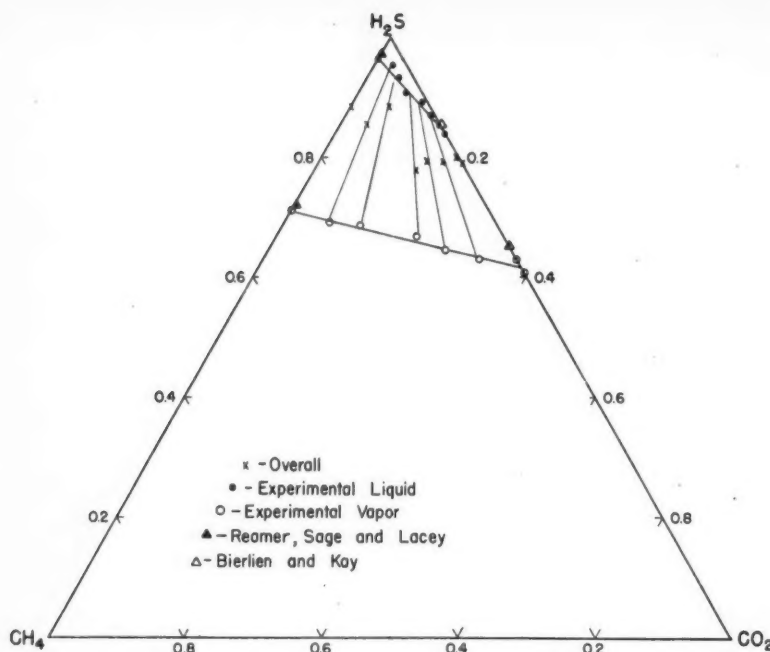


Figure 2—Phase diagram at 600 lb. per sq. in. and 100°F.

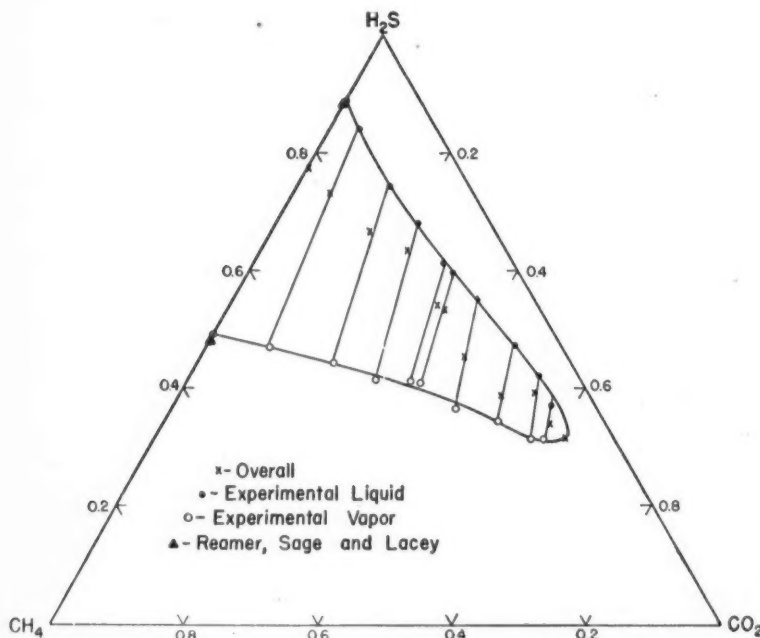


Figure 3—Phase diagram at 1200 lb. per sq. in. and 100°F.

Data have been reported by Reamer and Sage⁽¹⁾ on hydrogen sulphide, by Sweigert, Weber and Allen⁽²⁾ on carbon dioxide, and by Olds et al.⁽³⁾ on methane. Since the critical temperature for carbon dioxide and methane is below 100°F, hydrogen sulphide is the only pure component existing as a liquid under the test conditions.

Bierlien and Kay⁽⁴⁾ report data on the hydrogen sulphide-carbon dioxide system at 94 and 105°F. Reamer, Sage and Lacy⁽⁵⁾ report data on the methane-hydrogen sulphide system at 100°F. The data from these two sources were used to construct pressure composition diagrams for the binary pairs at 100°F. These diagrams were used as a guide in

selecting the conditions for testing the behavior of the three component system.

Activity Coefficient Ratios

In ideal solutions the fugacity of any component in the solution in either the liquid or vapor phase is proportional to the mole fraction of the component in the phase. This is frequently referred to as the Lewis and Randall Rule⁽⁶⁾. If conditions are such that the vapor above these solutions obeys the perfect gas law this reduces to Raoult's Law for the liquid phase and Dalton's Law for the vapor phase. Thus

$$p_i = p^* x_i \quad (1)$$

where p_i is the partial pressure of component (i) over a liquid solution of mole fraction x_i and vapor pressure p^* , and

$$p_i = y_i p \quad (2)$$

where p is the total pressure of the system and y_i is the mole fraction of component (i) in the vapor phase. If both these laws are valid

$$p^* x_i = p y_i \quad (3)$$

These ideal relationships may break down for several reasons. If the vapor does not behave like an ideal gas, the partial pressure of any component in it will not equal the pressure exerted by the component if it alone occupied the same volume at the same temperature. At pressures significantly above the vapor pressure corresponding to a given temperature for a pure material, the effective vapor pressure of the liquid may be considerably different from the saturation pressure. Abnormal intermolecular attractions or repulsions of different components in solution can also cause actual pressures to differ from those predicted from ideal laws.

The activity coefficient has been defined as a factor which allows for deviations from ideal behavior of components in solution. Thus one can say

$$p_i = \gamma'_i p^* x_i \quad (4)$$

where γ'_i is a factor which allows for all deviations from ideality. An alternative form is

$$f_v y_i = \gamma'_i f_L x_i \quad (5)$$

where pressures have been replaced by fugacities. In this equation f_v denotes the fugacity of pure component (i) as a vapor at the pressure and temperature of the system, f_L denotes the fugacity of pure component (i) as a liquid at the temper-

ture and corresponding vapor pressure of component (i) in the system, and γ_i denotes the activity coefficient ratio which includes the effect of pressure on the fugacity of the liquid and the effect of intermolecular forces.

The influence of pressure on the fugacity of the liquid can ordinarily be estimated by methods which use the general equations for fugacity and assume a constant or average specific volume of the liquid over the pressure range involved. In the system under investigation two of the components do not exist as liquids, so that the specific volume of the liquid is imaginary. Therefore, no attempt was made to correct the fugacity of the liquid for pressure.

Obtaining numerical values of f_v and f_{vL}^* for use in Equation 5 involves the determination of a relationship between fugacity, pressure, temperature, and specific volume since by definition

$$RT \ln f = vdp \quad (6)$$

at constant temperature. Upon integration for a single component from its vapor pressure to any other pressure at a fixed temperature this relationship yields

$$\ln \frac{f_v}{f_{vL}^*} = \frac{1}{RT} \int_{p^*}^{p_v} vdp \quad (7)$$

Thus, a value of the ratio f_v/f_{vL}^* can be obtained by graphically integrating a specific volume-pressure curve for any component between the working pressure and the vapor pressure at a given temperature. When combined with the experimental x and y data, this ratio can be used to calculate activity coefficient ratios by rearranging equation 5 as follows:

$$\gamma_i = \frac{y_i}{x_i} \frac{f_v}{f_{vL}^*} \quad (8)$$

Equilibrium Ratios

Equilibrium ratios are commonly used to express the ratio between the concentration of components in vapor and liquid phases in equilibrium at a fixed temperature and pressure. They are defined by the equation:

$$K_i = \frac{y_i}{x_i} \quad (9)$$

It is readily appreciated that these ratios are functions of temperature, pressure, and composition. Equation

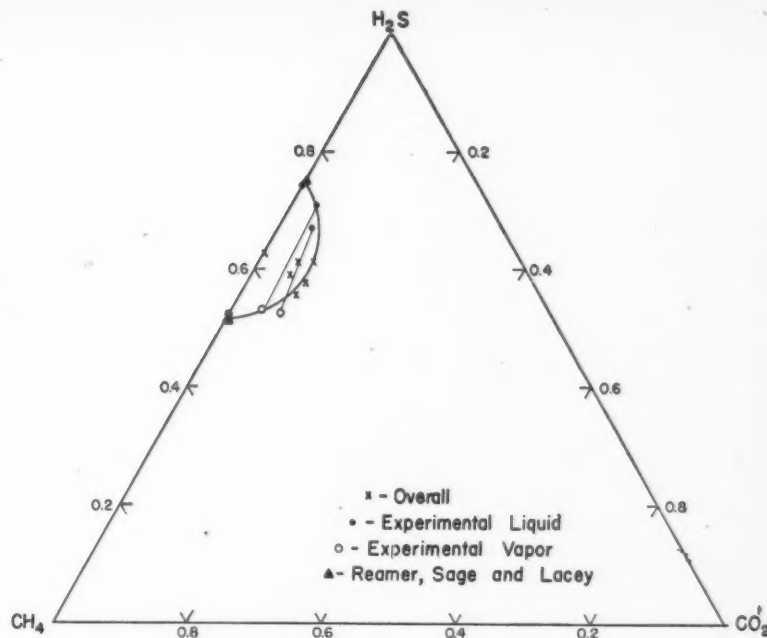


Figure 4—Phase diagram at 1800 lb. per sq. in. and 100°F.

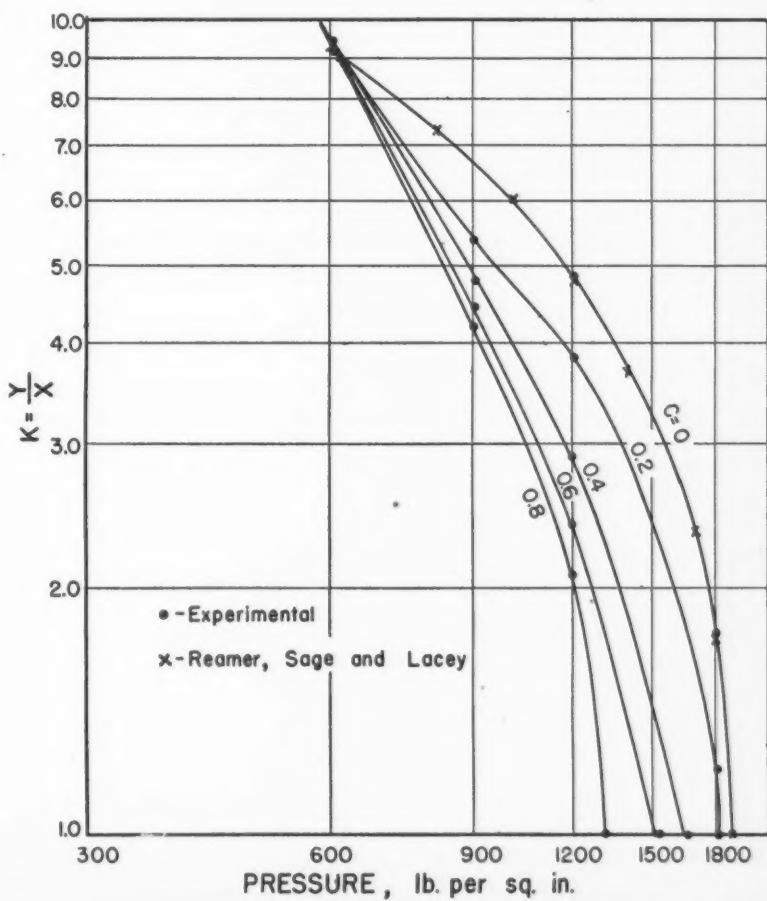


Figure 5—Equilibrium ratios for methane at 100°F.

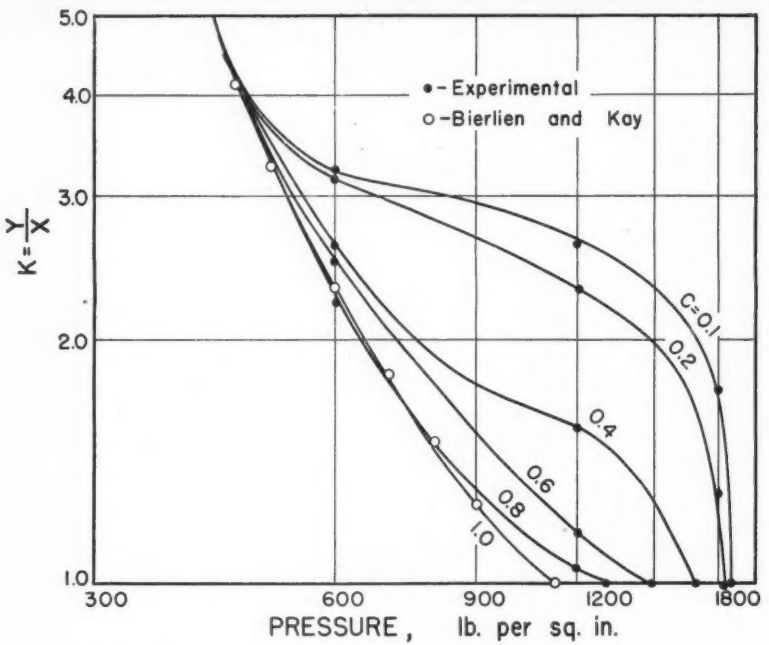


Figure 6—Equilibrium ratios for carbon dioxide at 100°F.

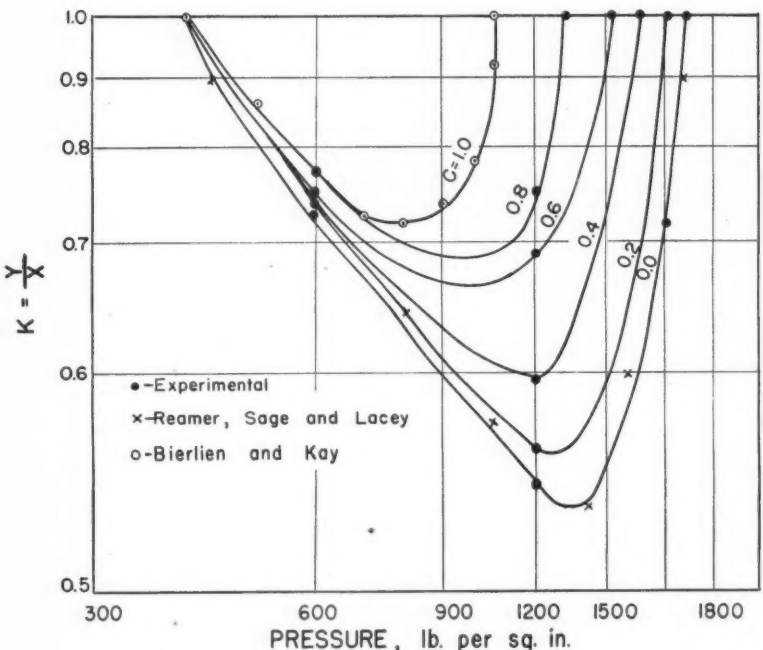


Figure 7—Equilibrium ratios for hydrogen sulphide at 100°F.

3 shows that an ideal equilibrium ratio will be given by:

$$K_i = \frac{P_i^*}{P} \quad (10)$$

Deviations from these ideal values can be expected to occur for the same reasons that activity coefficient ratios are not generally unity. In terms of

fugacity the equilibrium ratio is given by:

$$K_i = \gamma_i \frac{f_i^*}{f_i} \quad (11)$$

EXPERIMENTAL METHODS

The equipment was designed to permit experimental determinations of the variables necessary to define

the two phase boundary surface for the three component system at 100°F. A schematic layout of the equipment is illustrated in Figure 1. It consisted of a type 316 stainless steel equilibrium cell A with glass back and front sections capable of withstanding pressures of 3000 lb./in.² at 200°F. and having a volume of 110 cc. This was mounted in a constant temperature air bath on trunnions so that the whole assembly could be rocked to speed the attainment of equilibrium between phases. It was possible to observe the phases present and to measure their volumes by use of a cathetometer reading to the nearest 0.1 mm. The volume of the sample was altered known amounts by the addition or removal of mercury using the high pressure calibrated hand pump B. Pressures were measured by calibrated Heise Bourdon Tube gauges C and D covering the ranges 0-1000 and 0-5000 lb./in.². Temperatures were measured using copper-constant thermocouples and a Leeds Northrup semi-precision potentiometer. Pressures below 1000 lb./in.² were determined to ± 1 lb./in.² and above 1000 lb./in.² to ± 3 lb./in.². The temperature was constant to within ± 0.1 °F. during the runs. Auxiliary equipment necessary to add known amounts of the pure components and to take samples of the equilibrium vapor or liquid was provided. Connections throughout were made by commercial high pressure valves and tubing.

The methane used in the experiments was Phillips Petroleum Company research grade of 99.7% purity, the carbon dioxide obtained locally was 99.7% purity and the hydrogen sulphide from the Matheson Company had the following analysis: hydrogen sulphide 98.8%, methyl chloride 0.4%, methyl mercaptan 0.3%, nitrogen 0.2% and carbon dioxide 0.3%. In order to reduce the impurities admitted, the hydrogen sulphide was always removed from the liquid phase.

A series of phase compositions was determined at 100°F. for three different pressures, 600, 1200, and 1800 lb./in.² absolute. The approximate overall composition of a mixture in the two phase region at the given temperature and pressure was estimated from the known two component boundary curves at the same conditions. Known amounts of each pure component necessary to prepare the required mixture were then added to the equilibrium cell. The amount of each component added was calculated from the volume, tempera-

TABLE 1
EXPERIMENTAL VAPOR AND LIQUID COMPOSITIONS AT 100°F

Run No:	Total System			Vapor Phase			Liquid Phase		
	H ₂ S	CO ₂	CH ₄	H ₂ S	CO ₂	CH ₄	H ₂ S	CO ₂	CH ₄
PRESSURE 600 lb./in. ²									
6-1	0.796	0.204	0.0	0.608	0.392	0.0	0.840	0.160	0.0
6-2	0.792	0.143	0.065	0.660	0.222	0.118	0.810	0.170	0.020
6-3	0.776	0.152	0.072	0.667	0.206	0.127	0.905	0.069	0.026
6-4	0.882	0.053	0.060	0.684	0.115	0.201	0.937	0.044	0.019
6-5	0.790	0.159	0.051	0.644	0.259	0.097	0.891	0.101	0.008
6-6	0.804	0.196	0.0	0.630	0.370	0.0	0.815	0.185	0.0*
6-7	0.795	0.180	0.025	0.630	0.317	0.053	0.870	0.122	0.008
6-8	0.888	0.0	0.122	0.710	0.0	0.290	0.967	0.0	0.033
6-9	0.855	0.039	0.106	0.690	0.066	0.244	0.955	0.029	0.016
PRESSURE 1200 lb./in. ²									
12-1	0.775	0.0	0.255	0.490	0.0	0.510	0.891	0.0	0.109*
12-2	0.732	0.052	0.216	0.470	0.095	0.435	0.843	0.042	0.115
12-3	0.666	0.148	0.185	0.445	0.201	0.354	0.747	0.137	0.116
12-4	0.637	0.216	0.147	0.418	0.278	0.304	0.683	0.213	0.104
12-5	0.546	0.306	0.147	0.411	0.332	0.257	0.615	0.284	0.101
12-6	0.532	0.323	0.144	0.407	0.347	0.246	0.598	0.305	0.097
12-7	0.456	0.390	0.155	0.368	0.422	0.210	0.552	0.366	0.082
12-8	0.391	0.478	0.131	0.348	0.498	0.155	0.416	0.458	0.066
12-9	0.394	0.525	0.082	0.314	0.565	0.121	0.422	0.520	0.058
12-10	0.342	0.578	0.081	0.316	0.579	0.105	0.372	0.563	0.065
12-11	0.314	0.616	0.070						
Critical System Composition For 1200 lb./in. ² abs.									
PRESSURE 1800 lb./in. ²									
18-1	0.626	0.0	0.374	0.522	0.0	0.478	0.740	0.0	0.260
18-2	0.551	0.084	0.364	Single phase					
18-3	0.590	0.059	0.351	0.530	0.047	0.423	0.706	0.036	0.258
18-4	0.577	0.087	0.336	Single phase					
18-5	0.611	0.083	0.306	Single phase					
18-6	0.611	0.059	0.329	0.520	0.079	0.401	0.655	0.050	0.285

All compositions are in mole fractions.

*Calculated composition.

constant pressure addition of mercury. A sample of the liquid phase was then expanded from the cell into

the glass burette and analyzed. It was possible to calculate the liquid phase composition from the known total

TABLE 2
CALCULATED EQUILIBRIUM RATIOS AND ACTIVITY COEFFICIENT RATIOS AT 100°F

C	Vapor Composition			Liquid Composition			Equilibrium Ratio			Activity Coefficient Ratio		
	H ₂ S	CO ₂	CH ₄	H ₂ S	CO ₂	CH ₄	H ₂ S	CO ₂	CH ₄	H ₂ S	CO ₂	CH ₄
PRESSURE 600 lb./in. ²												
0.0	0.710	0.0	0.290	0.966	0.0	0.034	0.735	—	8.55	1.008	—	1.07
0.2	0.690	0.063	0.247	0.952	0.020	0.028	0.725	3.14	8.96	0.944	1.99	1.12
0.4	0.680	0.128	0.192	0.930	0.050	0.020	0.731	2.56	9.60	1.002	1.619	1.20
0.6	0.668	0.200	0.132	0.896	0.090	0.014	0.745	2.22	9.43	1.021	1.404	1.08
0.8	0.640	0.288	0.072	0.876	0.116	0.008	0.730	2.48	9.00	1.00	1.569	1.025
1.0	0.610	0.390	0.0	0.840	0.160	0.0	0.726	2.44	—	0.995	1.543	—
PRESSURE 1200 lb./in. ²												
0.0	0.490	0.0	0.510	0.895	0.0	0.105	0.548	—	4.85	1.007	—	1.10
0.2	0.468	0.105	0.427	0.842	0.046	0.112	0.556	2.28	3.81	1.022	2.26	0.866
0.4	0.439	0.225	0.336	0.735	0.148	0.117	0.597	1.52	2.87	1.097	1.50	0.652
0.6	0.402	0.360	0.235	0.585	0.315	0.100	0.688	1.14	2.38	1.283	1.13	0.541
0.8	0.325	0.540	0.135	0.435	0.500	0.065	0.747	1.08	2.08	1.373	1.07	0.473
PRESSURE 1800 lb./in. ²												
0.0	0.519	0.0	0.481	0.720	0.0	0.280	0.721	—	1.72	1.484	—	0.555
0.2	0.550	0.090	0.360	0.630	0.070	0.300	0.874	1.29	1.20	1.80	1.418	0.387

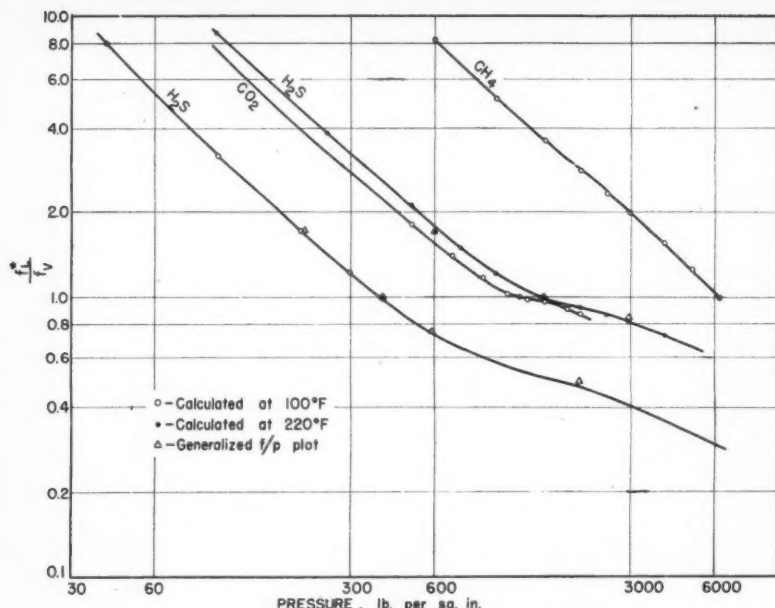


Figure 8—Fugacity ratios for ideal solutions.

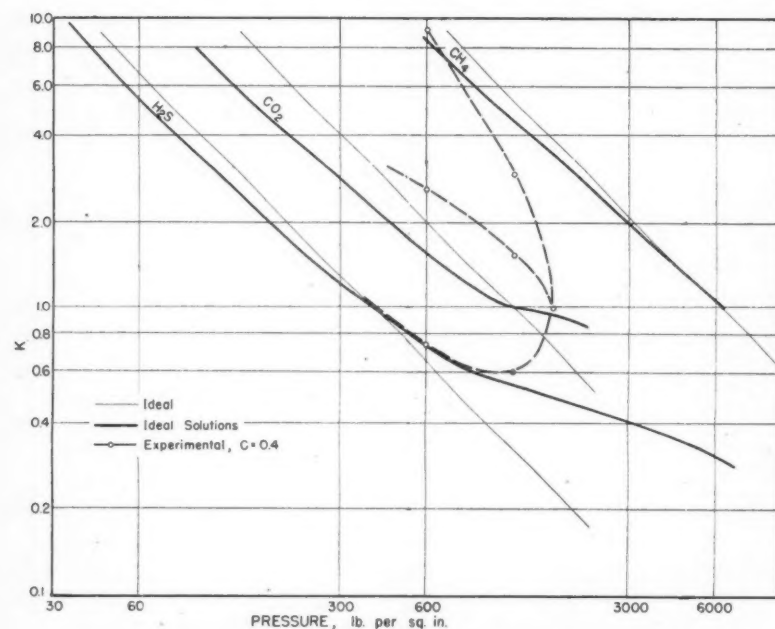


Figure 9—Experimental and theoretical 'K' values at 100°F. for C 0.4.

cell contents and the vapor phase volume and its analysis, so that a check could be obtained on the liquid phase analysis.

Similar measurements were made at each of the three pressures. At 1200 and 1800 lb/in.² the tests were terminated when the critical condition was reached.

EXPERIMENTAL RESULTS

The experimental data obtained at 600, 1200, and 1800 lb/in.² are pre-

sented in Table 1 and are indicated graphically in Figures 2, 3 and 4. The calculated liquid composition is reported in two cases where the liquid sample was spoiled during the analysis.

At 600 lb/in.² the pressure is below the critical pressure of the hydrogen sulphide-carbon dioxide and hydrogen sulphide-methane two phase region at 100°F. and the two phase region therefore extends from boundary to boundary. At 1200 lb/in.² the

pressure is above the critical pressure for the hydrogen sulphide-carbon dioxide binary but below the critical pressure for the hydrogen sulphide-methane binary. Conditions similar to this exist at 1800 lb/in.² but the two phase region has retreated towards the hydrogen sulphide-methane boundary.

The overall composition for run No. 12-11 was at or very near the composition of the ternary critical mixture at this pressure. At 1205 lb/in.² the mixture was in the single phase region. At 1203 lb/in.² there was a suggestion of two phases but they were separated by an indistinct meniscus which appeared and disappeared in the fluid made violently turbulent by the action of numerous tiny bubbles circulating through the liquid and fine droplets forming and falling from the vapor. A sudden reduction in pressure of about one pound on this system resulted in such an eruption that the whole system became opaque. This separated into two phases separated by a very flat hairline meniscus after a considerable period of time at 1200 lb/in.². No attempt was made to sample these phases. The liquid phase which was somewhat oily at 600 lb/in.² was exceptionally fluid at 1200 lb/in.².

The compositions represented by runs No. 18-2, 18-4 and 18-5 in the 1800 lb/in.² series exhibited behavior similar to that just described for run No. 12-11. They were all very close to the two-phase boundary surface. Mixtures 18-4 and 18-5 exhibited interesting color effects, becoming dark yellow and reddish orange instead of a pale straw yellow. The color reached its greatest intensity in run No. 18-5. Mixtures 18-2 and 18-4 showed retrograde condensation in the two phase region between about 1800 and 1730 lb/in.².

Data of Sage, Reamer, and Lacey (5) and interpolated data from Bierlien and Kay (4) for the binary systems are included on Figure 2, 3 and 4. Agreement for the hydrogen sulphide-methane system is good but repeated experiments with the hydrogen sulphide-carbon dioxide system indicated higher concentrations of carbon dioxide in both the liquid and vapor phases.

Equilibrium Ratios

Equilibrium ratios were calculated from the experimental x-y data shown in Table 1. The influence of composition was accounted for by using a parameter C defined as the ratio of the mole fraction carbon dioxide to

the sum of the mole fraction carbon dioxide plus methane in the vapor phase. The use of this type of parameter has been explained by Carter (6). Values of x and y at regular intervals of the parameter were read from Figures 2, 3 and 4. The calculated equilibrium ratios are shown in Table 2 and in Figures 5, 6 and 7.

Boundary curves at C equal to zero and unity representing the binary hydrogen sulphide-methane and hydrogen sulphide-carbon dioxide systems respectively were determined at pressures intermediate to those investigated from published data as indicated. No border curves exist at C equal to zero for carbon dioxide or for C equal to unity for methane since these refer to systems containing neither component.

Each curve is passed through the value $K = 1$ at the pressure corresponding to the ternary critical pressure for the given value of C . The intermediate pressures were determined from a plot of C against P using the experimental values at 600, 1200, and 1800 lb/in.² and the binary criticals at $C = 0$ and $C = 1$ from published data.

Activity Coefficient Ratios

Activity coefficient ratios were calculated according to equation 8. Values of f^*_L/f_v were obtained for each component at the three experimental pressures and 100°F. by graphical integration. A hypothetical vapor pressure for carbon dioxide was estimated as 1210 lb/in.² and for methane as 6200 lb/in.² by extrapolating a $\log p^*_1$ vs $1/T$ plot to 100°F. Vapor pressure data for carbon dioxide were taken from Perry (7) for methane from Olds et al (8), and for hydrogen sulphide from Reamer and Sage (1). Specific volume data for hydrogen sulphide vapor are empirical above 394 lb/in.³, the vapor pressure at 100°F. The f^*_L/f_v values at higher pressures were estimated by extrapolating the curve using a similar curve calculated at 220°F. ($T_R = 1.01$) and data from a generalized f/p plot (8) as a guide. These curves are shown on Figure 8.

A comparison between K values based on Dalton's and Raoult's Laws, on the ideal solution law, and on experiment is given in Figure 9 for a value of $C = 0.4$.

The calculated activity coefficient ratios are shown in Figures 10, 11 and 12. It is seen that increased pressure reduces the volatility of the more volatile component and increases the volatility of the less volatile component.

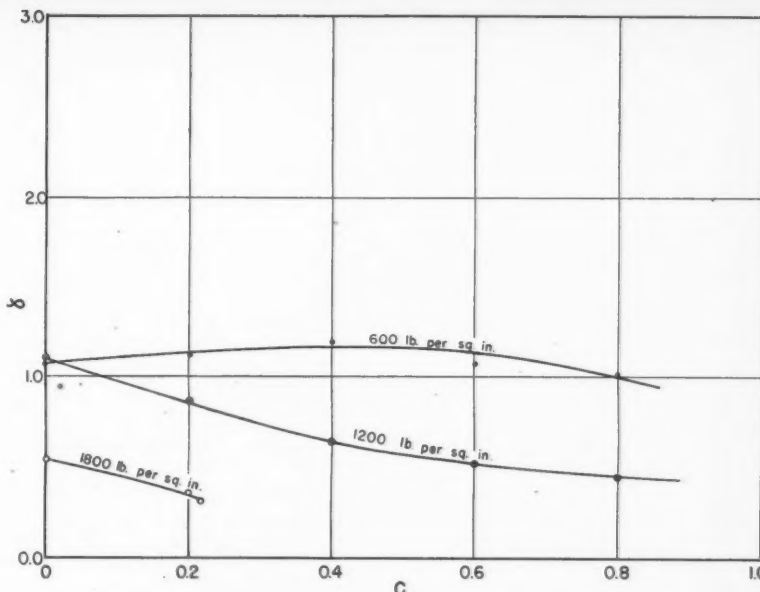


Figure 10—Activity coefficient ratios for methane at 100°F.

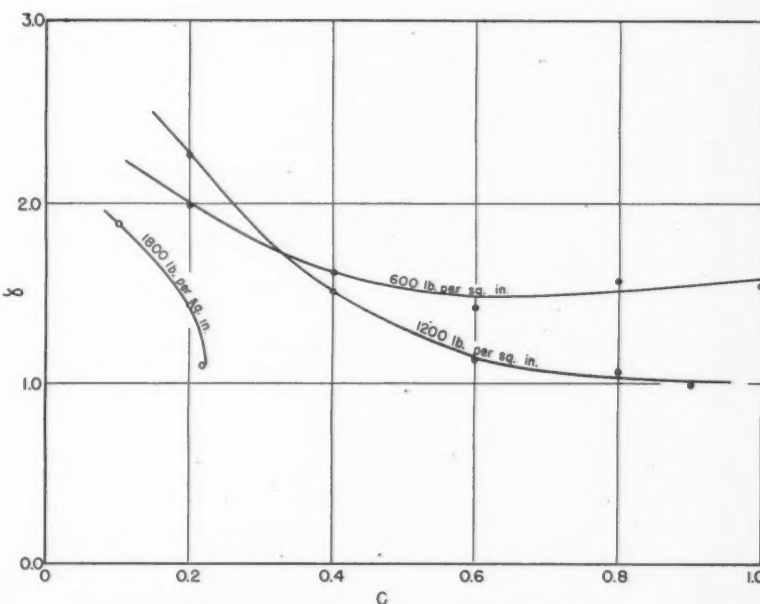


Figure 11—Activity coefficient ratios for carbon dioxide at 100°F.

Conclusions

The hydrogen sulphide-carbon dioxide-methane system forms co-existing liquid-vapor phases at 100°F. extending from 394 lb/in.², the vapor pressure of hydrogen sulphide, to 1910 lb/in.², the critical pressure of the binary hydrogen sulphide-methane system. A locus of critical points exists from the hydrogen sulphide-carbon dioxide binary at 0.27 mol fraction hydrogen sulphide and 1075 lb/in.² to the hydrogen sulphide-

methane binary at 0.60 mol fraction hydrogen sulphide and 1910 lb/in.².

The activity coefficient ratios indicate the liquid solutions to be non-ideal under most conditions investigated. The presence of the hydrogen sulphide significantly influences the behavior of the methane and carbon dioxide, reducing the volatility of the methane and increasing the volatility of the carbon dioxide at all pressures investigated. The hydrogen sulphide is essentially unaffected by the pre-

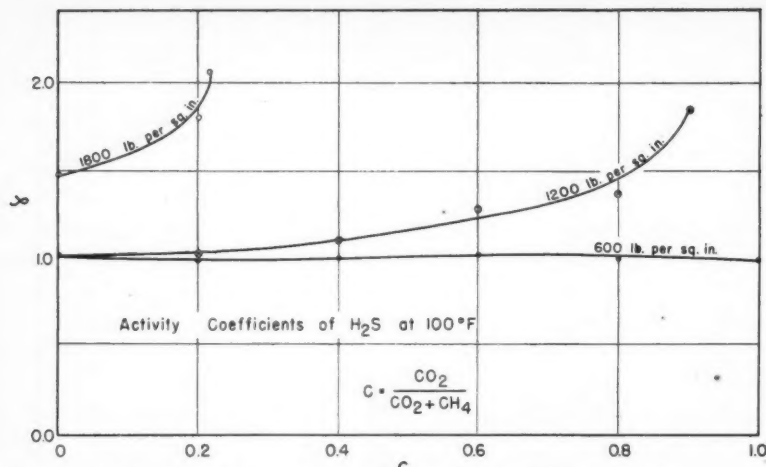


Figure 12—Activity coefficient ratios for hydrogen sulphide.

sence of the other components at pressures below about 1000 lb/in.².

Work is continuing on this system at temperatures below the critical for carbon dioxide. Some refinements have been made in the experimental and analytical techniques.

Nomenclature

C = mole fraction carbon dioxide divided by mole fraction carbon dioxide plus mole fraction methane in the vapor phase of the ternary system, dimensionless.

f = fugacity, atm.

f^*_L = fugacity of a pure component at its vapor pressure corresponding to a given temperature, atm.

f_v = fugacity of a pure component as a vapor at the pressure and temperature of the system, atm.

p = pressure, atm.

p_i = partial pressure of a component i in a mixture, atm.

p^*_i = vapor pressure of pure component i in a mixture at the temperature of the mixture, atm.

R = gas constant.

T = temperature, °R.

v = specific volume, ft.³/mole.

x_i = mole fraction of component at equilibrium in the liquid phase, dimensionless.

- y_i = mole fraction of component i at equilibrium in the vapor phase, dimensionless.
- γ = activity coefficient ratio, dimensionless.
- γ' = activity coefficient ratio for component i based on Raoult's and Dalton's Laws, dimensionless.

References

- (1) Reamer, H. H., and Sage, B. H., Ind. Eng. Chem., 42, 140 (1950).
- (2) Sweigert, R. L., Weber, P., and Allen, R. L., Ind. Eng. Chem., 38, 185 (1946).
- (3) Olds, R. H., Reamer, H. H., Sage, B. H., and Lacey, W. N., Ind. Eng. Chem., 35, 922 (1943).
- (4) Bierlien, J. A., and Kay, W. B., Ind. Eng. Chem., 45, 618 (1953).
- (5) Reamer, H. H., Sage, B. H., and Lacey, W. N., Ind. Eng. Chem., 43, 976 (1951).
- (6) Lewis, G. N., and Randall, M. "Thermodynamics and Free Energy of Chemical Substances", McGraw-Hill Book Co., Inc., New York, New York (1923).
- (7) Perry, J. H., "Chemical Engineers' Handbook", McGraw-Hill Book Company Inc., New York, New York, Third Edition, p. 254 (1950).
- (8) Hougen, O. A., and Watson, K. M., Chemical Process Principles, Part II, John Wiley and Sons Inc., New York, New York (1943).
- (9) Carter, R. T., Sage, B. H., and Lacey, W. N., Trans. A.I.M.E., 142, 70 (1941).

Acknowledgment

The financial assistance received for this work from The Consolidated Mining and Smelting Co. of Canada Limited, National Research Council of Canada and British American Oil Company is gratefully acknowledged.



Recent Developments in the Extrusion of Plastics¹

G. L. BATA²

The present state of knowledge of the operating variables affecting the extrusion of plastics is reviewed. An operating diagram of practical utility has been described and its use is recommended in connection with every-day problems in an extruding plant. The question of controlling quality is dealt with and methods for improving quality are suggested.

It took more than 2,000 years, a mass of empirical observations and trials and errors to develop the Archimedean screw of the Roman's water pump into the modern adiabatic extruder used for the processing of plastics. The first solid foundation for the quantitative picture of to-day was supplied in 1822⁽¹⁾ in the form of a set of basic differential flow equations. Many famous names established the solid theoretical grounds⁽²⁻⁴⁾ and it took the effort of half-a-dozen more authors⁽⁵⁻¹⁰⁾ until these data became applicable to a practical machine. Carley, Jepson, Mallouk, McKelvey and Strub⁽¹¹⁻¹⁷⁾ working in a team collected this information a few years ago. They established the theoretical background as it is known to-day. This valuable work triggered an enthusiastic upsurge in engineering research and development during the last couple of years. This paper summarizes the information presently available in this field.

This paper will be confined to a discussion of the operation of an extruder and die in a simplified way. The description will be centered around polyethylene resins, as they are the fastest growing plastic material adaptable to extrusion. The findings should be true, at least qualitatively, for other thermoplastic resins as well.

Theoretical Background

The essentials of an extruder are a cored, threaded shaft (screw)

rotating in a fixed cylinder (barrel) with a feed port at one end, an exit port (die) at the other. The theoretical data presented here apply—for the sake of simplicity—to a melt extruder, i.e. one handling preplasticized material, considered here to be essentially a true Newtonian liquid. However, for most practical purposes these data are applicable to an ordinary plasticizing extruder where a solid, granular feed is plasticized into a fluid. In any case, it is the melt section of the extruder, which primarily governs the performance of the machine and the resulting picture is thus a practically true one.

Considering the pressure conditions prevailing in an extruder (Figure 1)⁽¹⁸⁾ the resin flow can be resolved into a forward flow component due to the pumping action of the screw and a backward flow component due to the pressure gradient acting against this pumping action, built up by the resistance at the die.

This pumping action becomes obvious if the helical screw channel and the barrel wall are expanded into an equivalent straight channel, sliding at an angle against a plane, as on Figure 2.

The driving force may be resolved into two vector components, one acting parallel and the other perpendicular to the direction of the channel. This latter is called transverse flow and is mainly responsible for the

mixing action of the extruder, contributing nothing to the output.

The whole forward flow is created by the vector acting alongside the channel, called drag flow. This drag flow is the most important and the only positive factor contributing to the output of the machine. It may be represented as⁽¹⁸⁾

$$Q_d = \frac{\pi^2 D^2 h \sin \phi \cos \phi}{2} N = aN \quad (1)$$

where

D = diameter of screw, in.,
h = depth of channel, in.,
 ϕ = helical angle, degrees,
N = screw speed, revolutions per sec.,
 a = forward flow constant, defined by screw dimensions as above.
 Q_d = drag flow along channel, cu. in. per sec.

It may be seen in Figure 3⁽¹⁹⁾ that, the drag flow is the sole output of the extruder if there is no pressure built up due to the resistance of a die or other restrictions to the flow, like a screen pack.

In the case of an extruder and a screw of a given design its magnitude depends only on the rotational speed of the screw⁽¹⁹⁾. Should the channel depth be changed by replacing the screw with a shallower one, this discharge rate will fall proportionately in accordance with equation 1. Should the screw be changed again to one of larger diameter, but of the same channel depth, the output will vary as the diameter.

The backward flow created by the pressure built up ahead of the screw may also be divided into two additive components: the pressure flow acting backward in the channel and parallel to it and the leakage flow between the barrel wall and over the top of the screw flights, due to the clearance

¹Manuscript received August 18, 1957.

²Associate Director of Development, Resins, Carbide Chemicals Company, Division of Union Carbide Canada Limited, Montreal, Que.

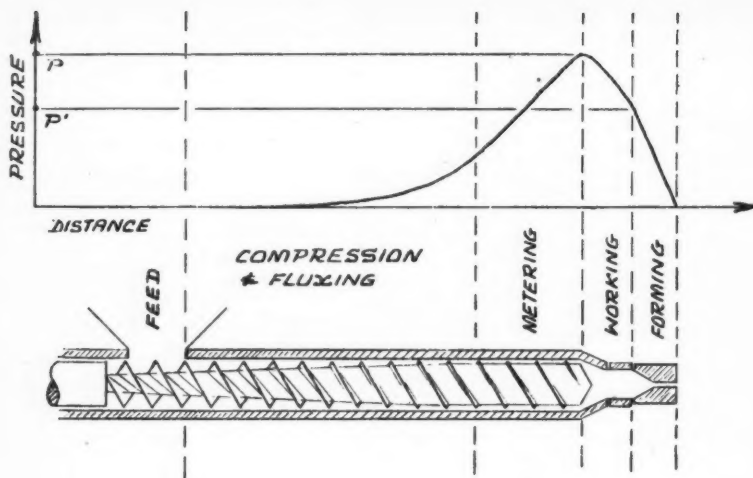


Figure 1—Pressure profile in an extruder.

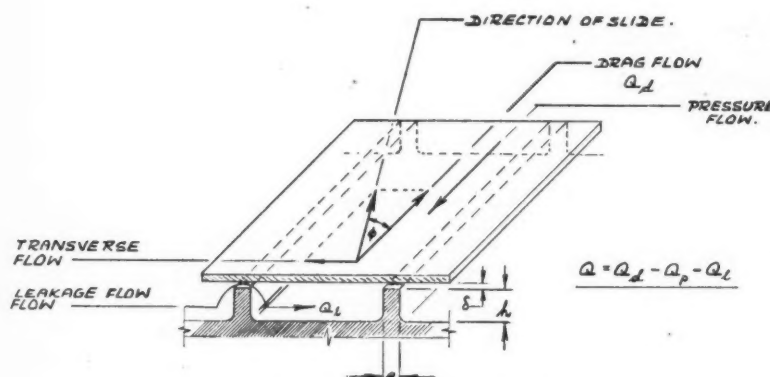


Figure 2—Flow pattern in extruder channel.

existing there. These two components may be represented as⁽¹⁸⁾

$$Q_b = \frac{\pi D h^3 P \sin^2 \phi}{12 \mu L} = \beta \frac{P}{\mu} \quad (2)$$

and

$$Q_l = \frac{\pi^2 D^2 \delta^3 P \tan \phi}{10 e \mu L} = \gamma \frac{P}{\mu} \quad (3)$$

where

Q_b = pressure flow, cu. in. per sec.,

Q_l = leakage flow, cu. in. per sec.,

P = pressure drop along screw, lbs-force per sq. in.,

μ = apparent viscosity of resin, lbs-force sec. per sq. in.,

L = effective length of screw, in.,

δ = clearance between barrel and top of flights, in.,

e = width of screw thread land, in.,

β = pressure flow constant defined by screw dimensions as above,

γ = leakage flow constant defined by screw dimensions as above.

The apparent viscosity of the resin at a given temperature has to be determined experimentally in the

extruder itself, using the equations previously given⁽²⁰⁾ at approximately the same speeds and output and pressure as those to which the equation will be applied. h has to be replaced by an experimentally determined H effective depth for an adequate practical description of the flow phenomena.

Equations 1, 2 and 3 may be summarized for the total output (Q) of the extruder in a simplified equation as

$$Q = Q_d - Q_b - Q_l \quad (4)$$

or

$$Q = \alpha N - \beta P/\mu - \gamma P/\mu \quad (5)$$

The last member of the second equation may be usually neglected in a well designed extruder if the clearance between the top of the flights and the barrel wall is very small. Equation 5 is represented by a straight line if the pressure in the extruder head (P) is plotted against the output (Q), various screw speeds

(N) giving separate lines, as in Figure 3. This is true only if N and P are mutually independent variables. It is possible, as may be seen there, to impose such a great resistance to flow that the output of the extruder falls off completely.

A characteristic output versus pressure (Q vs. P') may be established for the extruder die as well^(19, 21):

$$Q = c (P'/M) \quad (6)$$

and if there is no screen pack used and the friction drop in the die head is negligible, $P = P'$ and equation 6 may be also plotted on the same diagram of Figure 3. Theoretical formulae are available for c for various basic shapes such as circular, slit or tubular dies, but an experimentally determined viscosity has to be used in the calculations.

Making equation 6 equal to equation 5, the intersection of the two curves is the operating point of the extruder. The practical applicability of this point will be discussed later in this paper.

Based on Newton's viscosity law (shear stress equals the product of viscosity and shear rate) and considering the vectorial implications of Figures 1 and 2, the total power consumption of an extruder may be integrated into the following formula⁽¹⁵⁾,

$$Z = (\pi^2 D^3 L/h) N^2 \mu + (a/\cos^2 \phi) NP + (\pi^2 D^2 e L/\delta \tan \phi) N^2 \mu \quad (7)$$

where

Z = power required, lbs-force, in. per sec., μ = apparent viscosity, lbs-force, sec. per sq. in.

The same apparent viscosity may be used here which was previously obtained for flow equations.

These calculations have applicability for such plastics as nylon which are closer to Newtonian behaviour than polyethylene. However they are applicable to the latter too until shear rates do not vary. Modifications of equation 7 have been attempted to fit better the behaviour of non-Newtonian plastics⁽²²⁾ by the use of the power law given in equation 13. For practical purposes however it is advisable to use the graphical techniques discussed later in the section dealing with power requirements.

It is possible to calculate the energy balance of the extruder as⁽²¹⁾

$$W_s + W_h = W_m + W_w + W_r \quad (8)$$

where

W_s = energy input by screw drive (consistent units),

W_h = energy input by heaters,

W_m = energy increase in material,

W_w = energy lost to cooling water of screw,
 W_r = energy lost through radiation and convection.

W_r is the only component which cannot be measured directly, but it may be determined from Figure 4 (21) as the vertical difference between the curves W_h and $(W_m + W_w - W_s)$. Between the screw speeds where $(W_m + W_w - W_s)$ and the W_h curves intersect the N axis the heaters act only as insulators to counteract heat losses, whereas at screw speeds above the W_h intersection the heaters switch off and the machine acts as a truly adiabatic extruder. In this case all the heat energy required is obtained from the work of the screw.

The design of such high-speed, adiabatic extruders is a desirable trend, resulting in increased output at a high temperature and in some cases improved quality, not limited by the capacity of the barrel heaters and the heat sensitivity of the resin.

It has been shown (16) that a well defined relationship can be established between the performance of geometrically similar extruders, and if such variables as screw speed (N) and apparent melt viscosity (μ) are kept the same, the following equations apply:

$$Q_2 = x^3 Q_1 \quad (9)$$

$$Z_2 = x^3 Z_1 \quad (10)$$

$$P_2 = P_1 \quad (11)$$

where

$$x = D_2/D_1 = h_2/h_1 = \delta_2/\delta_1 = e_2/e_1 = L_2/L_1 \quad (12)$$

"x" may be called scale-up factor and the suffix 2 refers to the larger and suffix 1 to the smaller extruder. There is a good agreement between observed and calculated results for melt extruders.

Liquid flow may be rheologically described by the empirical Ostwald-de Waele law for non-Newtonian fluids (22, 23), as the n-th power of the shear stress in proportion to the shear rate, if shear rates do not vary too widely.

$$s^n = K (du/dy) \quad (13)$$

Applying equation 13 to an extruder slit die, it may be written as

$$(P'd/t)^n = K (Q/l d^2) \quad (14)$$

The same shear stress is expressed here in terms of pressure drop (P') through the die, die opening (d) and die land length (t). The shear rate is given in terms of extrusion output (Q), slit length (l) and die opening. The uniformity of the extruded film

may be expressed as a uniformity index (24)

$$U_i = \frac{Q_f}{Q_i} \quad (15)$$

defined as the ratio of the local extrusion rate at the far end (Q_f) and at the feed inlet point (Q_i) of the extrusion die. Carley (24, 25) expressed this uniformity index as a function of n , l , d , t and the radius (R) of the feed channel behind the die lips, thus presenting a workable principle for the rational design and operation of silt dies. The constants n and K are specific to the resin used, but are dependent on temperature. They may be easily determined experimentally in a suitable extrusion plastometer (26).

It is to be emphasized that, in the foregoing considerations, the viscosity

(μ) is considered to be greatly dependent not only on the grade and type of the resin used, but also on the temperature (T). The following equation has been presented (28) describing the temperature dependence of viscosity:

$$\mu = \mu_0 \cdot e^{B(T_0-T)} \quad (16)$$

where e is the base of the Napierian logarithms and B is the temperature "coefficient" of viscosity, expressed in reciprocal Kelvin degrees ($1/K^\circ$).

Operating an Extruder

The two aims in operating an extruder for a commercial application are: low cost and high quality—no matter what is the shape or purpose of the product.

Low cost consistent with high quality, from the point of view of the

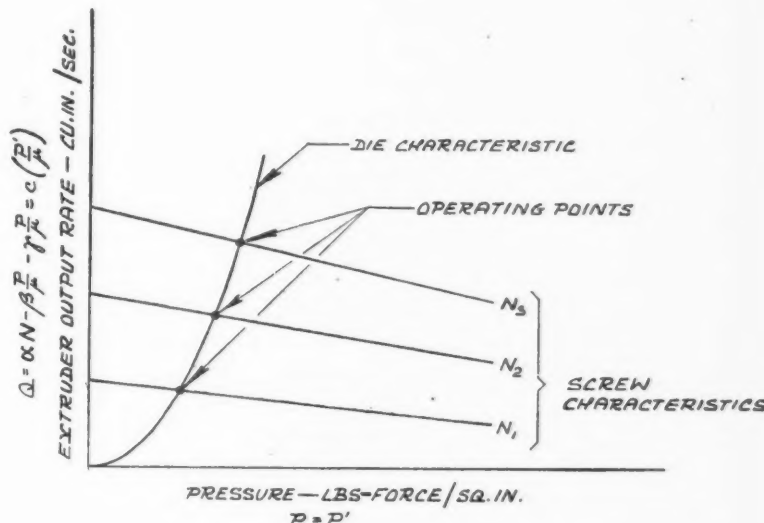


Figure 3—Extruder operating characteristics.

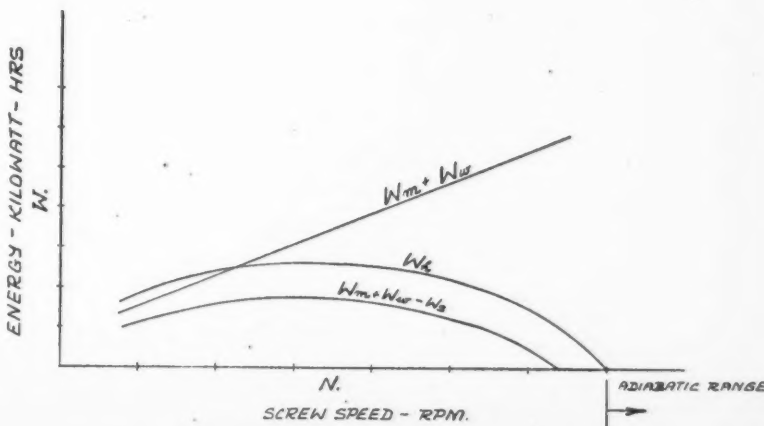


Figure 4—Energy balance of extruder.

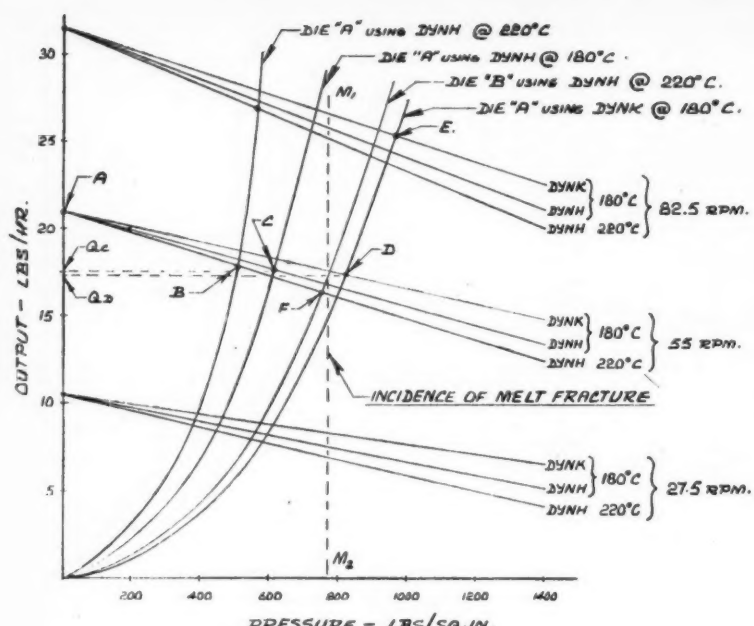


Figure 5—Extruder operating diagram.

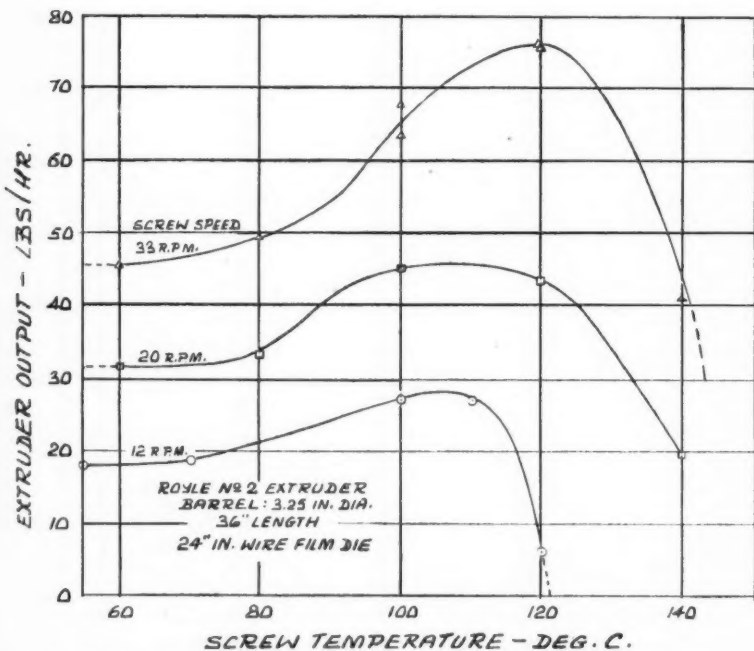


Figure 6—Effect of screw speed and temperature on extruder output.

operator, can be reached only through increased output, good power economy, minimum expenditure of labor, low maintenance cost, minimum depreciation expense and the use of raw materials of uniform quality. These conditions are very closely interconnected, but may be broken down into their basic components: output, power, product quality and

design. The first three are dealt with here as dependent on the basic variable of the process. Due to space limitations, design considerations will not be discussed though they are considered to be of outstanding importance for the maximum operational efficiency of the machine.

Chiefly the major process variables dealt with are screw speed, pressure,

stock temperature, heating and cooling and viscosity—resulting in output variations, power consumption and variations of quality.

Output. An experimentally determined diagram of output versus pressure, screw speed, resin viscosity (grade and temperature) is shown in Figure 5⁽¹⁹⁾. This graph shows the major variables in a condensed and simple form and may be prepared easily for any extruder equipped with a pressure gauge and stock thermocouples^(27, 28). A diagram of this kind is very useful in changing extruder conditions; and extrapolations may be safely made by the judicious application of the theoretical background.

Figure 5 is approximately equivalent to a diagram prepared for an $1\frac{1}{2}$ in. diameter extruder using a die "A" of $c = 1.7 \times 10^5$ and a die "B" of $c = 2.5 \times 10^5$.

Should the extruder be running without a screen pack at a screw speed of $N = 55$ r.p.m. with no die mounted on the head of the machine, its operating point will be at A irrespectively of the grade or temperature of the resin extruded. ($Q = Q_d + O + O$). If die "A" is mounted, and a DYNH-type resin of melt index of 2.0 dg/min. is used and at a stock temperature of 220°C , the operating point will shift to B and the output will drop from 21 to 18 lb./hr. By changing to a narrower die "B" at the same conditions, the output will drop further to 16.5 lb./hr. as indicated by operating point F.

During these losses of output the pressure in the extruder head increased from 0 to 500 p.s.i. due to the increasing die resistance and the output drop is explained by the resulting backward flow ($Q_p + Q_1$).

To consider the effect of stock temperature, the operating point may be changed from B to C by lowering the temperature of the resin from 220° to 180°C . This change will have very little effect on the output, but may strongly influence the quality, an aspect to be discussed later. The lowering of the stock temperature is equivalent in its effect to increasing the apparent viscosity of the resin and equations 5 and 6 may be called in to account for the changes. Similar is the effect of switching to a more viscous resin of the DYNK-type, having a melt index of 0.3 dg/min., as indicated by a change of operating point C to D. At first glance it may seem surprising that a seven times more viscous resin does not cut down the output of the extruder. The effect of the viscosity on output will be al-

most equalized by the opposing effects of equations 5 and 6; but a closer examination of Figure 5 will reveal that the pressure increase will create an additional power requirement, if the number of screw revolutions remained the same. This aspect will also be discussed later in further detail.

For optimum output and quality, the temperature of the screw is also of major importance beside the actual stock temperature itself. Figure 6 illustrates this (81) and the graph is self-explanatory. The sudden drop in output at a high screw temperature is caused by the clogging and fouling of the helical channel of the screw by prematurely fused resin close to the feed section. This clogging eventually eliminates the forward flow component (Q_a of equation 4) completely. Such a phenomenon should emphasize the need for the adequate cooling of the feed section of the barrel too.

The influence of the feed zone on the output of the extruder was discussed by Barnell and Mol (20). They emphasized the importance of dynamic coefficients of friction between the particles themselves and the wall.

Quality Considerations. The quality aspect of plastics extrusion is a rather neglected field in the technical literature. This may be due to the inherent theoretical difficulties connected with the interpretation of visco-elastic flow phenomena as related to extrudate appearance and properties.

The discussion will be limited to quality aspects which may be controlled between the hopper and the die of the extruder, to avoid the great number of possible variable combinations after the extrudate left the die.

One of the most frequent quality complaints is the roughness of the surface of the extrudate. Excluding the possibility of resin inhomogeneity and volatile content, Tordella (82) advanced the theory of "melt fracture". Melt fracture is an extrudate roughness transverse to the extrusion direction, originating at the die inlet and occurring at the above critical extrusion pressures. For the sake of simplicity Figure 5 may be considered again as an excellent guide to correct melt fracture phenomena. The line M_1M_2 should represent the incidence of melt fracture; melt fracture being more and more pronounced anywhere to the right from this line. If extrudate roughness occurs at operating point E, this deficiency may be largely eliminated by

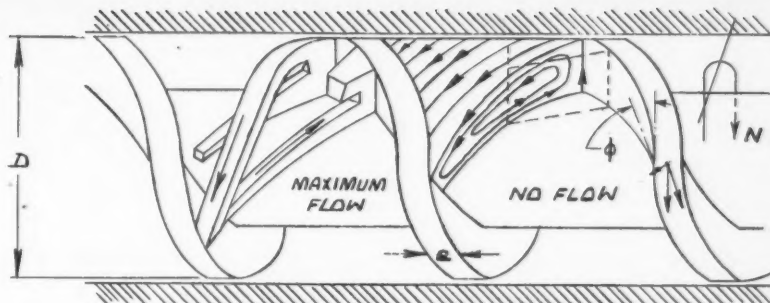


Figure 7—Sectional view of the flow pattern in an extruder.

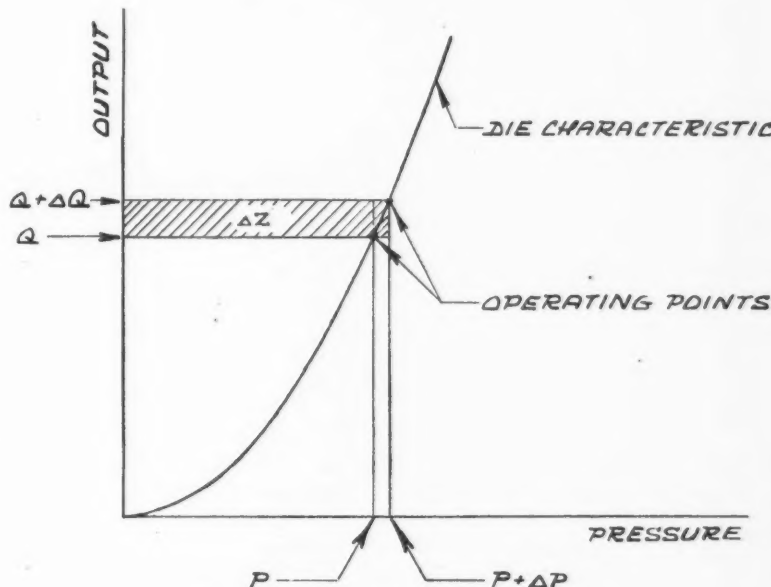


Figure 8—Changes in power requirement.

slowing down the extruder to D; or further improvement may be obtained by changing to a softer resin at C. It is not absolutely necessary to obtain improvements at the cost of output, as a change from E to G will preserve the same productivity with improved quality. When none of these changes is beneficial or feasible, a tapering of the die inlet will shift further the line M_1M_2 to the right of the chart, liberating a larger area for operation free of melt fracture. The approximate line of incidence of melt fracture could be conveniently determined for any extruder and die combination, extending Figure 5 into a more reliable extrusion guide.

Haine and Land (81) discussed various film quality considerations as dependent on extruder conditions. Such properties as gloss, haze, clarity, blocking tendency, shrinkage, tensile strength, surging and "nerviness" of the product are empirically correlated with extrusion variables.

The transverse flow in the extruder barrel, as previously mentioned in connection with equation 1, is of great importance from the viewpoint of extrudate quality.

Combined with the leakage and backward flow components, it is responsible for the mixing and homogenizing effect obtained in the extruder. This mixing effect is the result of a complicated flow pattern, represented in Figure 7 (11). Back pressure from the die and the screen pack, design variables of the screw, and the number of screw revolutions per second are the controlling factors in the mixing action. The viscosity of the resin is a complex, partly independent variable, greatly contributing to the resulting extrudate homogeneity. The individual effect of these variables may be estimated from the equations presented earlier, but a detailed analysis of these data should be the subject of a separate investigation. However, product quality is not de-



Exploded view of a slit die.

pended on this mixing effect alone, and the time spent by the resin in the extruder can not be directly correlated to quality (36).

The important problem of film gauge uniformity is discussed by Carley (24, 25) as referred to earlier. By judicious application of equations 14 and 15 and through their extension, the following steps are recommended to improve film uniformity at the die, in the given order of preference:

a) the feed channel before the die lips should be of adequately large diameter;

b) the land length of the die lips is to be varied along the length or circumference of the die to counteract friction losses along the feed channel;

c) adjustable die opening is recommended, giving a maximum attainable film uniformity of $\pm 5\%$;

d) die temperature may be varied along the slit to counteract friction losses (this step is not considered practical).

Carley gives quantitative data to guide in the use of the design and operating variables involved. These data refer to both flat and tubular slit dies. However, in the case of tubular dies, an easier solution is to completely circumvent the problem by the use of bottom-fed dies (33); these completely eliminate gauge uniformity problems arising at the die. This type of die is a definite improvement toward an optically more uniform film, as gauge variation is only the first step to introducing further variations in haze, gloss and clarity values.

Empirical data were published for the land lengths of pipe extrusion dies also (34), in order to obtain uniform wall thickness. Qualitative design considerations are also discussed in detail elsewhere (35).

Power Requirements. It has been mentioned earlier, that power requirements may be different even at the same output rate, if the pressure created in the extruder head is different due to viscosity or die resistance characteristics. Considering Figure 8, which is a generalized case of Figure 5, a change of output (ΔQ) will result from a change of pressure (ΔP). The change of power requirement (lb.-force \times in./sec.) may be expressed as the product of output change (cu.in./sec.) and the prevailing pressure (lb.-force/sq. in.)

$$\Delta Z = (P + \Delta P) \Delta Q$$

$$\lim_{\Delta P \rightarrow 0} \Delta Z = dZ - PdQ \quad (17)$$

$$Z = \int_0^Q P dQ$$

Accordingly Z may be expressed as the area between the Q -axis and the die characteristic curve, cut off by a horizontal line at the operating point.

Using a specific example taken from Figure 5, the change of the resin from the viscous DYNK (operating point D) to the less viscous DYNH (operating point C) will result in power economy at essentially the same output, because the area $ODQ_D O$ is much larger, than the area $OCQ_C O$.

The actual calculation of the integral can be avoided by either cutting out the respective areas from heavy paper and comparing their weights on a laboratory balance or by plotting the original operating diagram on finely divided graph paper and counting the number of small squares in both areas. However only differences in power requirement

should be calculated this way, as the areas do not represent power losses due to friction, etc.

Data obtained this way are accurate enough for practical operating considerations. Their main value is in their use to extrapolate to new operating conditions, if a change is being planned in the shop. Equation 7 may be used to counter-check results obtained.

References

- (1) Navier, C. L. M., Mem. Acad. Sci. (Paris) 6, (1882).
- (2) Boussinesq, M. J., Math. Pures Appl. 2nd S. 13, 377 (1868).
- (3) Poiseuille, J. L. M., Compt. Rend. 15, 1167 (1842).
- (4) Reynolds, O., Trans. Roy. Soc. A177, 157 (1886).
- (5) Rowell, H. S., Finlayson, D., Engineering 114, 606 (1922); 126, 249 (1928).
- (6) Grant, D., Walker, W., Plastics Progress (ed. Morgan, P.) Iliffe & Sons, London (1951).
- (7) Pigott, W. T., Trans. ASME 73, 947 (1951).
- (8) Rogowsky, Z., Engineering 162, 358 (1948).
- (9) Rigbi, Z., Brit. Plastics 23, 100 (1950).
- (10) Eirich, F. R., Inst. Mech. Eng. (London) Proc. 156, 62 (1947).
- (11) Carley, J. F., Strub, R. A., Ind. Eng. Chem. 45, 970 (1953).
- (12) Carley, J. F., Mallouk, R. S., McKelvey, J. M., Ind. Eng. Chem. 45, 974 (1953).
- (13) Carley, J. F., Strub, R. A., Ind. Eng. Chem. 45, 978 (1953).
- (14) McKelvey, J. M., Ind. Eng. Chem. 45, 982 (1953).
- (15) Mallouk, R. S., McKelvey, J. M., Ind. Eng. Chem. 45, 987 (1953).
- (16) Carley, J. F., McKelvey, J. M., Ind. Eng. Chem. 45, 989 (1953).
- (17) Jepson, C. H., Ind. Eng. Chem. 45, 992 (1953).
- (18) Gore, W. L., SPE Journ. 9, No. 3, 6 (1953).
- (19) Maddok, B. H., Bakelite Kabelitems 92, July 1956.
- (20) Sackett, R. D., Techn. Paper, 12th Ann. Nat. Conf. SPE, Vol. II, 265 (1956).
- (21) Gaspar, E., Ibid., Vol. II, 247 (1956).
- (22) Ostwald, W., Kolloid-Z. 36, 99 (1925).
- (23) deWaele, A., J. Oil. Col. Chem. Assoc. 4, 33 (1923).
- (24) Carley, J. F., Mod. Plastics 33, No. 12, 127 (1956).
- (25) Carley, J. F., J. Appl. Phys. 25, 1118 (1954).
- (26) Nason, H. K., J. Appl. Phys. 16, 338 (1945).
- (27) Carley, J. F., Ind. Eng. Chem. 45, 858 (1953).
- (28) Bernhardt, E. C., Techn. Paper, 11th Ann. Nat. Conf. SPE, Vol. I, 327 (1955).
- (29) Darnell, W. H., Mol, E. A. J., SPE Journ. 12, No. 4 (1956).
- (30) ASTM Test D-1238-52T.
- (31) Haine, W. A., Land, W. M., Mod. Plastics 29, February 1952.
- (32) Tordella, J. P., Techn. Paper, 12th Ann. Nat. Conf. SPE, Vol. II, 285 (1956).
- (33) Schenkel, G., Kunststoffe 46, 221 (1956).
- (34) Perkins, R. S., SPE Journ. 12, No. 8, 47 (1956).
- (35) Schenkel, G., Kunststoffe 46, 176 (1956).
- (36) Brax, H. J., Bakelite Co., Development Department, Bound Brook, N.J., private communication.
- (37) Tordella, J. P., SPE Journ. 9, No. 5, 6 (1953).
- (38) McKelvey, J. M., Bernhardt, E. C., SPE Journ. 10, No. 3, 22 (1954).

★ ★ ★

The Velocity of Fall of Circulating and Oscillating Liquid Drops Through Quiescent Liquid Phases¹

A. I. JOHNSON² and L. BRAIDA³

This paper reports studies of the rate of fall of liquid drops passing through quiescent liquid phases, with an attempt to correlate the velocity data with the circulation and oscillation of the drops.

Organic liquids with physical properties ranging in density from 1.1040 to 2.9612 gms./cc., viscosity from 0.4779 to 9.630 centipoises, and interfacial tension from 26.08 to 45.30 dynes/cm. were used as the disperse phases. Water and glycerol solution ranging in density from 0.9970 to 1.1919 gms./cc., and viscosity from 0.8937 to 27.73 centipoises were used as the continuous phases. In this way the more important physical properties affecting the fall velocity of the drops were investigated.

Drops were formed from stainless steel nozzles ranging in size from one-half inch inside diameter to hypodermic needle size below one-sixty-fourth of an inch in diameter. The circulation was studied by suspending aluminium particles in the disperse phase and photographing the drops in motion with a high speed movie camera. By this method the films could be projected in slow motion or studied by frame by frame projection.

The voluminous data was correlated by applying a continuous phase viscosity correction factor to the Hu-Kintner correlation. This curve can be used to determine the fall velocity for a drop of any size whose physical properties lie within the range investigated. A break point in the curve serves as a criterion for oscillation.

In chemical engineering there are many operations in which two phases are contacted as drops of one phase dispersed in the other. In general the two fluids have different densities so that there is relative motion between the disperse and continuous phases. Liquid-liquid extraction is one such operation for which the velocity data and the circulation and oscillation studies of this paper may be of value both for basic studies and for the design of process equipment.

Literature published in the past

deals with the extension of solid sphere data as applied to fluid spheres. Recently, the velocity of fall of organic liquids through water has been studied and a correlation obtained, this correlation being restricted in its application.

Recent investigations have indicated that circulation and oscillation are important factors influencing heat and mass transfer operation. Since there is little information on circulation and oscillation of drops, this investigation was undertaken to study factors affecting circulation and

oscillation and the fall of drops through water and liquids other than water as a first step for future research on heat and mass transfer studies.

Historical Discussion

There is considerable information available on the fall velocity of rigid spheres in fluids^(1, 2, 3). The friction factor versus Reynolds number curve for solid spheres has been well established. The motion of liquid drops through a continuous phase is more complex than that of the solid sphere, as evidenced by the fact that as yet no satisfactory correlation has been proposed to include existing data on drop motion.

Bond⁽⁴⁾, and Bond and Newton⁽⁵⁾, have shown that for small drop radii, the rate of descent of a drop is very close to the value given by Stoke's law for solid spheres. After a certain drop radius, the rate of descent deviates from Stoke's law and falls more closely to that predicted by Hadamard⁽⁶⁾, and Rybczynski⁽⁷⁾, who applied a correction taking into account viscosity and surface tension.

Hu and Kintner⁽⁸⁾, studied the fall of 10 different organic liquid drops through water and presented a correlation of their data with the Weber group, the Reynolds number, and the friction factor as correlating moduli.

Licht and Narasimhamurty⁽⁹⁾, conducted a similar study using some of the liquids employed by Hu and Kintner. A comparison of the data indicates that Licht and Narasimhamurty found higher fall velocities, the difference amounting to roughly 10%. This may be attributed to a

¹Manuscript received September 30, 1957.

²Associate Professor of Chemical Engineering, University of Toronto.

³Graduate student, Department of Chemical Engineering, University of Toronto.

Contribution from the Department of Chemical Engineering, University of Toronto. Part of this material including motion pictures of the falling drops was presented before the Chemical Engineering Division, The Chemical Institute of Canada, March, 1956.

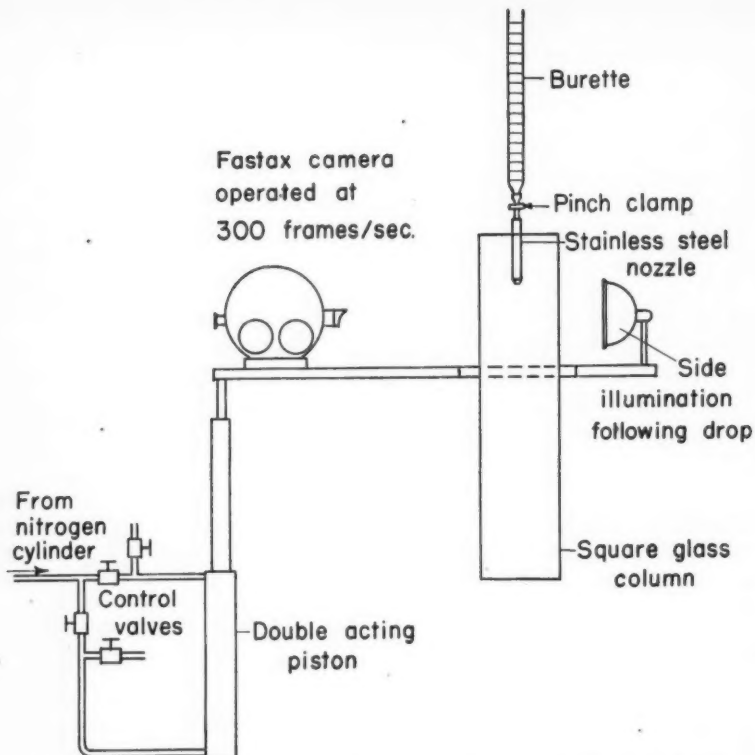


Figure 1—Apparatus for photographing circulating and oscillating drops.

difference either in methods of timing employed or in the physical properties of the liquids used. The ratio of the drag coefficient of a liquid drop to that of a rigid sphere of the same volume and density and the same fall velocity as the drop was plotted against a dimensionless group but failed to give satisfactory results. Their data was also checked against the correlation of Hughes and Gilliland⁽¹⁰⁾, in terms of a terminal velocity group, a surface tension group and a specific gravity group, but poor results were obtained. In developing their correlation Hughes and Gilliland had to assume that the density and viscosity ratios were unimportant. This is reasonably true for liquid drops falling through gases but not through liquids.

Hughes and Gilliland⁽¹⁰⁾ have published a review of drop mechanics, in which they attempt to describe the effects of acceleration, distortion, circulation and oscillation to the time-distance-velocity relationships for the drop and the continuous fluid.

Several articles on the motion of gas bubbles in liquids have been published; of these the following may be mentioned. Haberman and Morton⁽¹¹⁾, report work on drag and shape of air bubbles in water, and

several liquids over a very large range of Reynolds numbers. Garner and Hammerton⁽¹²⁾ conducted a similar study using bubbles of ethylene and carbon dioxide as well as air. Emphasis was placed on the circulation within the bubble in accordance with Hadamard's modification of Stoke's law for a fluid sphere. Peebles and Garber⁽¹³⁾ have also developed a correlation for bubble velocity in various liquids.

Garner⁽¹⁴⁾ and Garner and Skelton⁽¹⁵⁾ studied liquid mixing as affected by the internal circulation within droplets. Their belief is that circulation is largely dependent on diffusion occurring in the drop and that this takes place only above a fairly closely defined Reynolds number. Garner related the deformation of a drop to the initiation of circulation in the drop.

Spells⁽¹⁶⁾ obtained photographs of the streamlines inside drops moving through another liquid, making use of the Schlieren pattern produced by imperfectly mixed water-glycerine mixtures, a method first used by Hagerty⁽¹⁷⁾.

Savic⁽¹⁸⁾ investigated circulation as a factor influencing the heat transfer to a drop. In this connection he

obtained excellent photographs of internal circulation and calculated the time required to establish circulation when special surface effects do not interfere. He also considered the distortion of the drop suspended in a gas stream and found that the calculations agree quantitatively with experiments in a vertical wind tunnel.

Kronig and Brink⁽¹⁹⁾ presented a solution to the problem of diffusion in a moving spherical drop with fully developed circulation. The stipulation that the Reynolds number be one or less seriously limits the scope of application of their equation. Korchinski⁽²⁰⁾ showed that the Kronig-Brink theory held for Reynolds numbers greater than one.

Korchinski studied the effect of circulation on heat transfer and concluded that with circulating drops, the effective diffusivity within the drop is 2.25 times the molecular diffusivity. He also measured drop velocities and found that for Reynolds numbers below 200, circulation had no effect on the friction factor plot of bromobenzene compared to the solid sphere line. Korchinski's work avoided oscillating drops.

Recently Klee and Treybal⁽²¹⁾ have reported rise velocities of drops lighter than water. They correlated their results using dimensional analysis for the two regions below and above the peak velocities indicated on Figures 2, 3, and 6.

Correlation Methods

Fluid spheres differ from solid spheres in that the fluid can be set into motion by the viscous drag in the fluid medium outside the drops. Drops are in addition subjected to deformation because of the differences in pressure acting on various parts of the surface. These differences have been the subject of many experimental investigations and theoretical analyses.

Dimensional analysis has been used by many workers to obtain a correlation between drop velocity and the variables concerned. In this instance the following dimensional analysis was carried out giving

$$u = \phi(\mu_o, \mu_c, \rho_c, \Delta\rho, \sigma, g, D)$$

$$\frac{D u^2 \rho_c}{\sigma} =$$

$$\left(\frac{\mu_o}{\mu_c} \right)^a \left(\frac{\sigma \Delta\rho D}{\mu_c^2} \right)^b \left(\frac{\mu_c^4 g}{\Delta\rho \sigma^3} \right)^k \left(\frac{D \rho_c}{\mu_d} \right)$$

Using the drop velocity data obtained in this research, various log plots were considered in order to obtain the coefficients of a, b, h, k, but

none proved feasible. By rearranging the above, the N_p group, used by Hu and Kintner (8), was obtained: $N_p = \frac{\sigma^3 \rho_c^2}{g \mu_c \Delta \rho}$

By plotting $C_D N_{We} N_p^{0.15}$ against $\frac{N_{Re}}{N_p^{0.15}}$ all data for the organic

dispersed phase-water systems could be correlated on one line similar to the results of Hu and Kintner.

In this Hu-Kintner correlation the various terms are

$$\text{Drag coefficient: } C_D = \frac{(\rho_o - \rho_c) g^D}{\rho_c u^2}$$

$$\text{Weber number: } N_{We} = \frac{D u^2 \rho_c}{\sigma}$$

$$\text{Reynolds number: } N_{Re} = \frac{D \rho_c u}{\mu_c}$$

In all of these numbers D is the equivalent diameter, that is, the diameter of a sphere of the same volume as the drop under study. In this method of plotting data the ordinate involves the physical properties and the square of the diameter, the abscissa involves the drop velocity.

When data for organic solvent drops falling through aqueous glycerol solutions was plotted on the above Hu-Kintner plot, a correlation was not obtained as the continuous phase viscosity varied. A viscosity correction for the continuous phase was applied with the final result that experimental data was correlated by a plot of

$$\frac{C_D N_{We} N_p^{0.15}}{\left(\frac{\mu_c}{\mu_w}\right)^{0.14}} \text{ against } \frac{N_{Re}}{N_p^{0.15}}$$

Experimental Details

(a) Preliminary Photographic Study of Drop Behaviour

In order to make a comprehensive study of the behaviour of drops falling through a quiescent phase, it was necessary to photograph the drop while in motion. The apparatus used is shown in Figure 1. A 16 mm. Fastax camera, manufactured by Wolleens Optical Company, Rochester, N.Y., was mounted on a movable piston, operated by nitrogen from a pressure cylinder which could be lowered at the same rate as the falling drop. A sight wire was mounted on the base plate in order that the drop could be followed. There are two features of this camera that should be mentioned. The speed can be varied from zero to seven

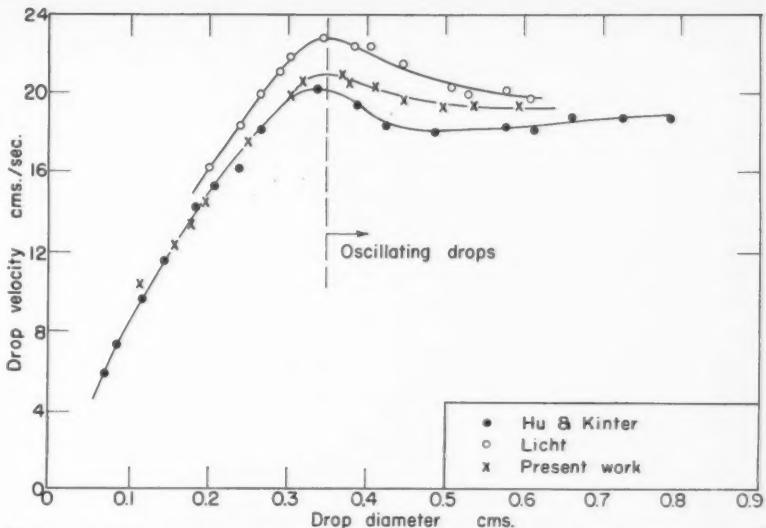


Figure 2—Fall velocities of carbon tetrachloride drops in water (25°C)—comparison of present data with previous work.

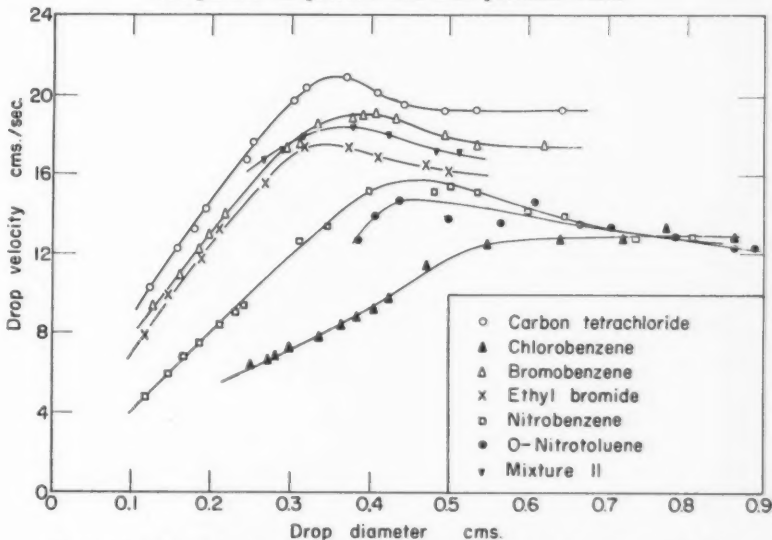


Figure 3—Fall velocities of drops of organic solvents in water (25°C).

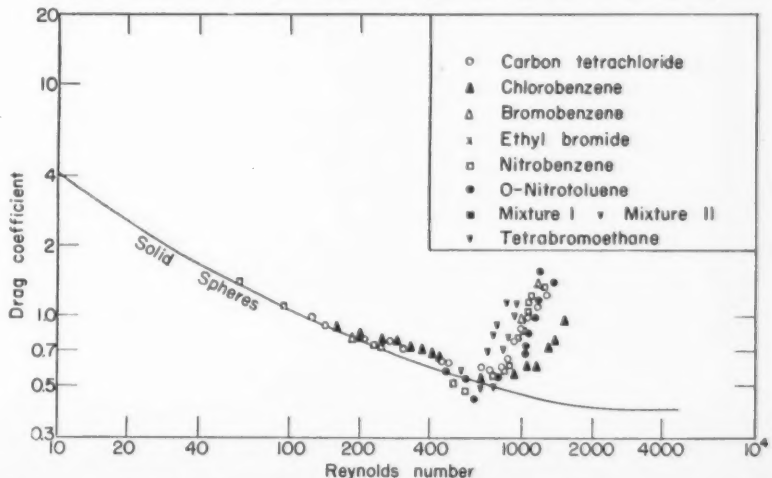


Figure 4—Drag coefficients of organic solvent drops falling through water (25°C)—comparison with solid sphere data.

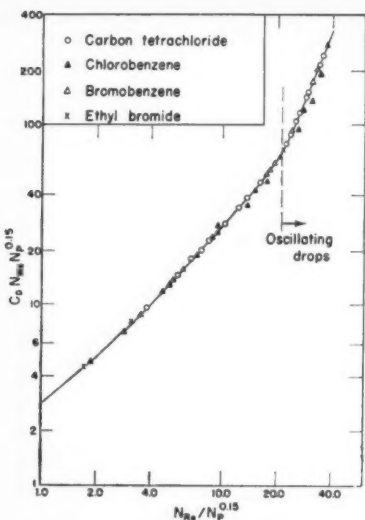


Figure 5—Application of the Hückel-Kintner plot to data of this research—organic solvent drops falling in water (25°C).

thousand pictures per second by varying the voltage. There is a built in timing light which flashes one hundred and twenty times a second. This flashing light leaves light marks on the film, and thus the velocity of fall of the drops can be determined. In this research the camera was operated at a rate of three hundred frames per second by two six volt wet cells, since the camera does not function very well on alternating current at this low voltage.

The lighting system presented a problem. The falling drop could be photographed very well, but the circulation path indicated by the reflection of light of the aluminium particles could not be seen. In the final arrangement a light was mounted on an arm extended from the camera to provide side illumination of the drop as it fell. Two other photofloods were placed at the back of the tank. Dupont 930A film was found to give the best results.

The dropping tank consisted of four pieces of plate glass cemented together to make a column four inches square. On the side of the tank farthest from the camera lens, white lines were painted every two centimeters from the three to the twenty-five centimeter mark, and every five centimeters from twenty-five to seventy-five centimeters. A piece of black paper was fastened over this so that the markings would show on the film. The velocity of all drops photographed was determined by counting the light blips between the markings on the film.

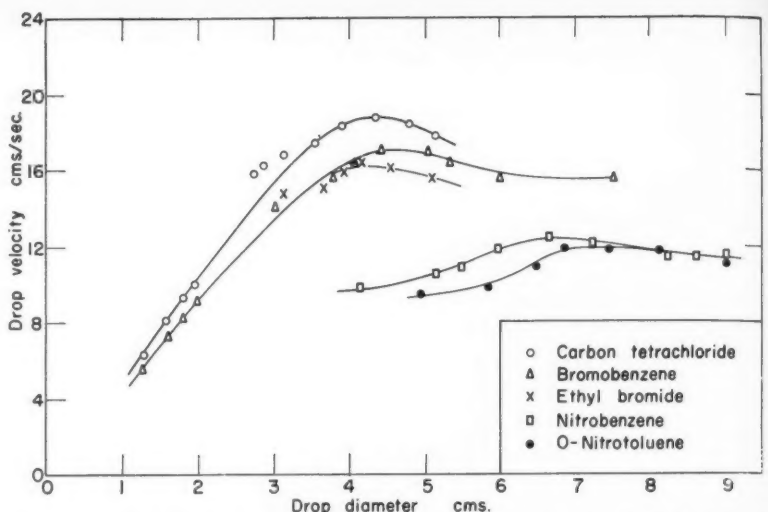


Figure 6—Fall velocities of organic solvent drops in aqueous 28.5% glycerol solution (25°C).

Since the lights caused heating of the continuous phase, the temperature was not controlled and varied between 25°C. and 29°C. The drops photographed at 25°C. were found to have practically the same velocity of fall as those obtained by stop watch measurements.

(b) Measurement of Drop Velocity

Drop velocities were measured in a second column in which the temperature of the continuous phase could be controlled. A four inch diameter glass cylinder was placed inside a six inch diameter one and made water tight by rubber gaskets and brass rods connecting two brass plates tightly together. The space between the two cylinders acted as a constant temperature jacket, the water being circulated by a pump connected to a constant temperature bath maintained constantly at 25°C. $\pm 0.2^\circ\text{C}$. Dispersed phase was metered from a jacketed burette to the nozzle through a piece of polythene tubing, the flow controlled by a screw clamp. The tips of the nozzles were placed 3.5 cms. below the top of the column and immersed in 2.5 cms. of the continuous phase. Both this column and the one in which drops were photographed were large enough to avoid wall effects.

All timing was done with a stopwatch manually operated and calibrated against 60 cycle time signals to an agreement within less than one-tenth of a second in 10 minutes. The stopwatch was started as soon as the drop left the nozzle and stopped

after the drop had passed a mark 97.5 cms. down the column. As many as 25 velocity determinations were made for a single drop size each one varying no more than two-tenths of a second, and the results averaged.

The drop volume was obtained by allowing 200 drops to fall and recording the volume of the aggregate. This was done as many times as needed to give reproducible results.

When drops were formed from the micrometer burette, a definite volume was delivered and the drop then knocked off the needle by gently tapping the instrument.

(c) Systems Used

Since density, viscosity and surface tension of the disperse phase influenced the behaviour of the drops and similarly the density and viscosity of the continuous phase, various disperse and continuous phases were investigated. The organic liquids chosen were essentially insoluble in the continuous phases. The properties of distilled water were taken from the International Critical Tables, and all apparatus used in determining the physical properties was calibrated using distilled water at 25°C. All physical property determinations were carried out at 25°C. $\pm 0.2^\circ\text{C}$. Interfacial tensions were measured by the method of Andreas⁽²¹⁾.

Tables 1, 2, and 3 summarize the physical properties of the systems used.

Carbon tetrachloride was selected first in order that comparisons might be made with previous work. It has

TABLE 1
SIGNIFICANT PHYSICAL PROPERTIES FOR ORGANIC DROPS FALLING IN WATER

Liquid	Viscosity μ_0 (cos.)	Density ρ_0 (gms/cc.)	Density Diff. $\Delta\rho$ (gms/cc.)	Interfacial Tension σ (dynes/cm.)	N_P
Carbon tetrachloride.....	0.9291	1.5857	0.5887	45.30	2.511×10^{10}
Chlorobenzene.....	0.7822	1.1040	0.1070	36.81	7.413×10^{10}
Bromobenzene.....	1.0730	1.4900	0.4930	38.12	1.786×10^{10}
Ethyl bromide.....	0.4777	1.4445	0.4475	31.09	1.067×10^{10}
Nitrobenzene.....	1.7839	1.1980	0.2010	26.08	1.403×10^{10}
O-Nitrotoluene.....	2.0658	1.1583	0.1613	26.98	1.936×10^{10}
Tetrabromoethane.....	9.3349	2.9612	1.9642	39.06	4.82×10^9
Mixture No. I*.....	2.0902	2.0511	1.0541	41.21	
Mixture No. II**.....	1.3047	1.5072	0.5102	35.63	
Carbon tetrachloride inc.***.....	4.4119	1.5883	0.5913	37.84	

*A solution of tetrabromoethane, carbon tetrachloride, and chlorobenzene.

**A solution of carbon tetrachloride and ethyl bromide.

***A solution of a commercial resin, Parlon, in carbon tetrachloride.

TABLE 2
SIGNIFICANT PHYSICAL PROPERTIES FOR ORGANIC DROPS FALLING IN
AQUEOUS 28.5% GLYCEROL

Liquid	Density ρ_0 (gms/cc.)	Density Diff. $\Delta\rho$ (gms/cc.)	Interfacial Tension σ (dynes/cm.)	N_P
Carbon tetrachloride.....	1.5857	0.5172	44.26	1.286×10^9
Chlorobenzene.....	1.1040	0.0355	30.93	6.39×10^9
Bromobenzene.....	1.4900	0.4215	34.60	7.54×10^9
Ethyl bromide.....	1.4445	0.3760	27.36	4.18×10^9
Nitrobenzene.....	1.1980	0.1295	21.61	5.98×10^9
O-Nitrotoluene.....	1.1583	0.0898	24.39	1.24×10^9
Tetrabromoethane.....	2.9612	1.8927	38.25	2.27×10^9
Mixture No. I.....	2.0511	0.9826	38.63	
Mixture No. II.....	1.5072	0.4387		
Carbon tetrachloride inc.	1.5883	0.5198		

Density of 28.5% Glycerol = 1.0685 gm/cc.

Viscosity = 1.974 cps.

TABLE 3
SIGNIFICANT PHYSICAL PROPERTIES FOR ORGANIC DROPS FALLING IN
AQUEOUS 60% GLYCEROL

Liquid	Density ρ_0 (gm/cc.)	Density Diff. $\Delta\rho$ (gm/cc.)	Interfacial Tension σ (dynes/cm.)	N_P
Carbon tetrachloride.....	1.5857	0.4346	38.29	2.88×10^8
Bromobenzene.....	1.4900	0.3389	32.13	2.17×10^8
Ethyl bromide.....	1.4445	0.2934	25.91	1.32×10^8
O-Nitrotoluene.....	1.1583	0.0072	18.75	
Tetrabromoethane.....	2.9612	1.8101	36.36	5.93×10^8
Mixture No. I.....	2.0511	0.9000	37.78	1.336×10^8
Mixture No. II.....	1.5072	0.3561	38.37	1.43×10^8
Carbon tetrachloride inc.	1.5883	0.4372	46.30	

Density 60% Glycerine = 1.1511 gms/cc.

Viscosity = 8.823 cps.

concentrations of glycerol. The first method consisted of forming the drops at a slow counting speed, one drop every three seconds. By this method the drops could be counted

accurately and the timing error was kept to a minimum. The second method consisted of forming the drops at a higher rate, thus increasing the volume slightly and the

a viscosity near that of water and a density in the middle range of the liquids selected. Other liquids were chosen accordingly so that all physical properties could be varied at one time or another. Bromobenzene has a density close to that of carbon tetrachloride, but has slightly higher viscosity and lower interfacial tension. Chlorobenzene has a lower density and interfacial tension with nearly the same viscosity as the above mentioned liquids. Liquids of intermediate densities were prepared by mixing carbon tetrachloride, tetrabromoethane and chlorobenzene; these are called mixtures I and II in the tables and on the graphs.

(d) Method of Drop Formation

Drops were first formed from a stainless steel reservoir through a stainless steel valve and thence through the nozzles. This was not suitable because aluminium particles accumulated at the valve and a constant flow could not be obtained. This method also prevented the simultaneous measurement of the drop volume.

Glass burettes were finally used for measuring the volume of drops. Polythene tubing was used to connect the nozzles to the burette. This type of tubing had been used by previous workers (22, 9), since it contains no soluble material which might alter the physical properties of the disperse phase. For drops of large volumes, a fifty milliliter burette was used and for smaller drops a micrometer pipette was obtained. This was capable of delivering accurately volumes as small as 0.002 ml.

The nozzle design was similar to that used by Hayworth and Treybal (28). Each nozzle was constructed of stainless steel carefully machined and bevelled at 45° to a sharp edge. These nozzles ranged from one-half inch inside diameter to one-sixteenth of an inch. For smaller drops hypodermic needles were used. The oblique end of the needle was removed and the tip rounded off by careful grinding on an oil stone.

The production of constant volume drops presented the greatest problem of all in the experimental work, as the rate of drop formation at the nozzle greatly influenced the drop volume and velocity of fall of the drops specially when continuous phases of over thirty per cent glycerol in water were used. Two drop formation procedures were adopted. The first one of these was used for all continuous phases, while the second was used only for higher

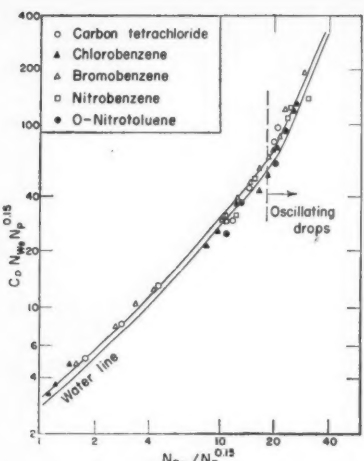


Figure 7—Application of the Hu-Kintner plot to data of this research—organic solvent drops falling in aqueous 28.5% glycerol (25°C).

velocity of the drop considerably. This rate depended on the system being used. Thus for concentrations of glycerol above 30%, there will be two sets of data.

The two phases were not mutually saturated with one another before the determinations, since the mutual solubilities were in all cases very low. No difference in results were obtained by using a continuous phase that had been allowed to stand in the column for a few days.

Observations on Drop Motion

Because a discussion of oscillation, circulation and drop behaviour of all systems observed would be too lengthy, only a few general comments will be made.

The frequency and manner of oscillation depends on the drop diameter, drop velocity and physical properties of the systems. A small drop with a high velocity will oscillate more quickly than a large drop with less velocity. A drop of tetrabromoethane of 0.395 cm. diameter and velocity of 25.57 cms./sec. will oscillate quickly so that the change in shape can hardly be seen. In the case of a drop of chlorobenzene of diameter 1.086 cms. and velocity of 12.56 cms./sec. the oscillations are very slow and the distortion very erratic.

When oscillation ceases, distortion is present and circulation is fully developed. As the drop diameter and drop velocity decrease, the extent of circulation inside the drop varies considerably, this again depends on the physical properties of the two phases. For some drops circulation was observed to be fully developed for a short distance whereupon the

circulation path moved towards the forward stagnation point giving rise to what might be termed one-half and one-quarter circulation. For still smaller drop diameters, there was only a little motion near the forward stagnation point and in some cases no circulation present at all.

The exact explanation for the decay of circulation is not yet fully established, as the flow patterns around the drop would have to be investigated. It might be suggested that there is a separation point with liquid spheres much like that found with solid spheres and that the induced circulation is greater at the

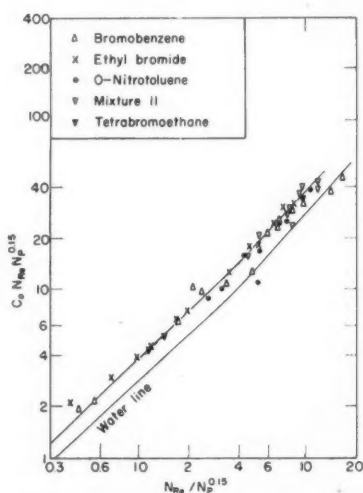


Figure 8—Application of the Hu-Kintner plot to data of this research—organic solvent drops falling in aqueous 60% glycerol (25°C).

forward end of the drop.

If the rate of formation at the nozzle was increased, the drops were found to have an additional velocity of circulation. If the drop diameter and velocity are sufficiently great, the drop will propel itself or swim down through the continuous phase giving rise to an increased velocity of fall and velocity of circulation even though the drop diameter is the same and circulation fully developed. This occurred in continuous phases having a concentration of glycerine greater than 30%.

Discussion of Graphs

Organic Liquids Falling in Water

Figure 2 illustrates velocity of fall data for carbon tetrachloride drops in water and shows that the data obtained lie between the results reported by previous workers. This difference is probably due to the timing methods employed and is small. The fall velocities of liquid drops increase

linearly with diameter, reach a maximum, and fall off asymptotically to some constant value. This behaviour of liquid drops is different than that of rigid spheres.

Figure 3 indicates similar curves for other liquids falling through water.

The peak velocity in each case occurs at a drop diameter where oscillation was observed to begin both visually and by photographic studies. The velocity plot for tetrabromoethane is not shown as it is beyond the scope of the graph. Chlorobenzene is the lowest curve since it has the lowest density. (See Table 1 for physical properties.) The upper curves are those liquids with greater density differences and higher surface tensions. From the curves it appears that the effect of density on the fall velocity is greater than the effect of surface tension. Viscosity of the disperse phase does not appear to have any discernable effect on the fall velocity at least over the viscosity ranges of the dispersed phase used. This is evidenced by the proximity of the bromobenzene and ethyl bromide curves. The difference in viscosity of the two liquids is considerably greater than the difference in interfacial tension and density.

The general form of the $\log C_D$ vs. $\log N_{Re}$ curve is shown as Figure 4. At low Reynolds numbers C_D values fall rather closely to the curve for solid spheres. The slight deviation from the solid sphere line can be explained by the distortion of the drops. Further increase in drop size

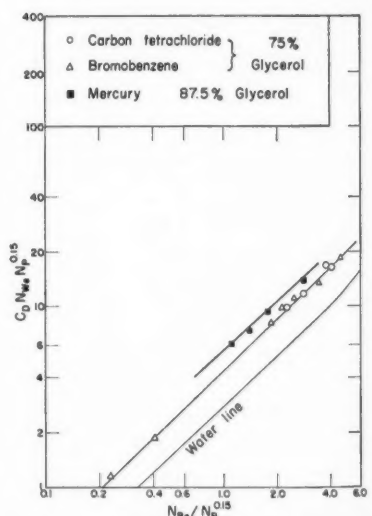


Figure 9—Application of the Hu-Kintner plot to data of this research—organic solvents drops falling through aqueous 75% glycerol solution (25°C). Some of Korchinski's mercury drop data are also shown.

brings about a zig-zag motion and oscillation and deformation are present. The oscillation induced by the peak velocity causes a sharp increase in the value of C_D , thus causing a sharp rise in the $\log f_a$ vs. $\log Re$ curve. After this abrupt rise, deformation of the drops becomes more and more severe and the oscillation progressively erratic. There is some crossing of the curves but all have the same general pattern, the more dense liquids lying to the right while the lighter liquids such as chlorobenzene are on the left.

The Hu-Kintner plot of $C_D \cdot N_{We} \cdot N_p^{0.15}$ against $N_{Re} \cdot N_p^{0.15}$ for this data is shown in Figure 5. A definite break occurs at a value of $N_{Re}/N_p^{0.15} = 22$. Again this point occurs at the same conditions discussed above, that is, all drops above this break oscillate.

Organic Liquids Falling in 28.5% Glycerol

The behaviour of drops in 28.5% glycerol is similar to their behaviour in water and velocity data is shown in Figure 6. The velocity increases linearly with drop diameter until the peak velocity is reached. After this point the velocity again decreases. Since the continuous phase viscosity has been increased the oscillations are not as erratic and deformation is quite pronounced. The curves in this region are considerably smoother than the same curves when water is used as the continuous phase. Chlorobenzene is not shown on this plot as the values are beyond the scope of the graph. As before, the upper curves are those liquids which have greater density differences, while the lower ones are liquids such as o-nitrotoluene and bromobenzene with low density differences. All data were plotted on the $C_D \cdot N_{We} \cdot N_p^{0.15}$ vs. $N_{Re} \cdot N_p^{0.15}$ graph and a mean line drawn through the points. This is shown in Figure 7. The line shows a definite break in the same region as the organic-water plot. Above this value all drops oscillate. By applying a continuous phase viscosity correction resulting in a plot of

$$(C_D \cdot N_{We} \cdot N_p^{0.15}) / (\mu_c / \mu_w)^{0.14} \text{ vs. } N_{Re} \cdot N_p^{0.15}$$

the data can be made to fall on the water line. By this method a correlation for any system can be obtained.

Organic Liquids Falling in 60% Glycerol

With the more viscous continuous phase some difficulty was encountered in obtaining reproducible results. With carbon tetrachloride and the more dense liquids fall velocity data

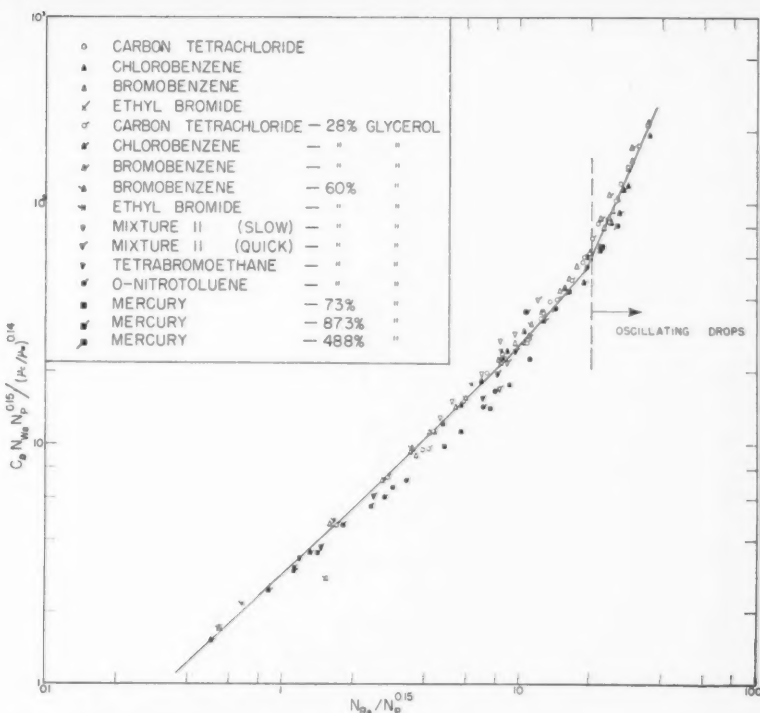


Figure 10—Modified Hu-Kintner plot for data of this research—organic solvent and mercury drops falling in water and in aqueous glycerol solutions.

for small drops knocked off the micrometer pipette were not consistent with velocity data for drops formed from the other nozzles. Accordingly carbon tetrachloride data are not shown on the graphs.

As indicated on Figure 8 data for other organic solvents were consistent.

As would be expected there are no values at the upper end of the $\log C_D \cdot N_{We} \cdot N_p^{0.15}$ vs. $\log N_{Re} \cdot N_p^{0.15}$ plot since there is no oscillation of drops. The data is considerably scattered in the upper regions of the graph, some point lying to the right of the water line. A mean line was drawn by eye through all points. Again by applying the viscosity correction indicated above the data coincided reasonably well with the water line.

Organic Liquids Falling in 75% Glycerol

In order to study the correlation still further 75% glycerol was used as the continuous phase. Similar results were obtained and are shown in Figure 9.

Korchinski's data (25) was also used in checking the correlation. The only system that could be correlated using the viscosity correction was mercury - 87.3% glycerol. Corrections to sys-

tems mercury - 43%, 48.8%, 97.8% glycerol were either above or below the water reference line. Since Korchinski did not report the densities and viscosities of the continuous phases the reported results had to be interpolated to obtain an average value of densities and viscosities of the glycerol used. This could probably give rise to some error. The more serious limitation of his data was that sufficient points were not investigated for each phase. Korchinski drew a smooth curve through all his data on a Hu-Kintner plot, having insufficient data to detect the parallel curves found in this research.

Modified Hu-Kintner Correlation

It has been pointed out that the data in Figures 7, 8, and 9 could be brought down to the water line by dividing the ordinates by $(\mu_c / \mu_w)^{0.14}$. Using alternate points obtained in this research, Figure 10 was drawn to illustrate this modification of the Hu-Kintner plot. The area in which drops were observed to oscillate is also shown. The transition point between oscillating and non oscillating drops is the same as the criterion Hu and Kintner proposed for the peak velocity on curves such as Figure 2.

With a large number of points plotted, it is more difficult to observe the break in the correlation when

oscillation begins. However this region appears to be above

$$\frac{N_{Re}}{N_P^{0.15}} = 20.$$

Concluding Remarks

In this paper new fall velocity data for organic liquid drops falling in water and in aqueous glycerol solutions has been presented. The velocity data were accompanied by visual and photographic studies of circulation and oscillation of the drops.

The Hu-Kintner plot has been used to correlate the data. A correction for the viscosity of the continuous phase has been introduced as a divisor for the $C_D N_{W_0} N_P^{0.15}$ group proposed by Hu and Kintner.

The correlating curve has been separated into a region of oscillating drops and one of non oscillating drops. There appears to be a break in the curve at the transition in drop behaviour. This corresponds to the point of peak velocity reported by Hu and Kintner.

Nomenclature

C_D	= Drag coefficient (dimensionless).
D	= Diameter (cms.).

g	= Acceleration due to gravity (cms./sec. ²).
m	= Mass of a solid sphere (gms.).
$N_P = \frac{\sigma^3 \rho_c^2}{g \mu_c \Delta \rho}$	= Physical property group proposed by Hu and Kintner.
$N_{Re} = \frac{D \rho g}{\mu_c}$	= Reynolds number.
$N_{We} = \frac{DU^2 \rho_c}{\sigma}$	= Weber number.
t	= Time (sec.).
T	= Temperature (°C.).
u	= Velocity of fall (cms./sec.).
ρ_o, ρ_c	= Densities of dispersed and continuous phases respectively (gms./cm ³).
$\Delta \rho$	= Density difference of system (gms./cm ³).
μ_o, μ_c	= Viscosities of dispersed and continuous phases (gms.)/(cm. sec.).
μ_w	= Viscosity of water.
σ	= Interfacial tension (dynes/cm).
a, h, k	= Constants.

References

- (1) Lapple, C. E., and Associates, Fluid and Particle Mechanics, First Edition, University of Delaware, Newark, Delaware.
- (2) Lapple, C. E., and Shepard, C. B., Ind. Eng. Chem., 32, 605 (1940).
- (3) Reynolds, O., Phil. Trans., 174, 935 (1883).
- (4) Bond, W. N., Phil. Mag. Ser. 7, V5 889 (1927).
- (5) Bond, W. N., and Newton, D. A., Phil. Mag. Ser. 7, V5 794 (1928).
- (6) Hadamard, Academie des Sciences, Comptes Rendus 152, 1735 (1911).

- (7) Rybczynsky, D. P., Bull. Acad. Ser. Cracow, 403 (1911). Referred to in Lamb's Hydrodynamics.
- (8) Hu, S., and Kintner, R. C., A.I.Ch.E. Journal 1, 42 (1955).
- (9) Licht, W., and Narasimhamurty, G. S. R., A.I.Ch.E. Journal 1, 368 (1955).
- (10) Hughes, R. R., and Gilliland, E. R., Chem. Eng. Prog., 48, 497 (1952).
- (11) Haberman, W. L., and Morton, R. K., David W. Taylor Model Basin Report No. 802, Sept. (1953), Washington 7, D.C.
- (12) Garner, F. H., and Hammerton, D., Trans. Inst. Chem. Eng., 3, 1 (1953).
- (13) Peebles, F. N., and Garber, H. J., Chem. Eng. Prog., 49, 88 (1953).
- (14) Garner, F. H., Trans. Inst. Chem. Engrs., 88 (1950).
- (15) Garner, F. H., and Skelland, A. P. H., Ind. Eng. Chem., 46, 1225 (1954).
- (16) Spells, K. E., Proc. Phys. Soc., 64B, 541 (1952).
- (17) Savic, P., Report No. MT 22, National Research Council, Ottawa.
- (18) Hughes, R. R., and Gilliland, E. R., Chem. Eng. Prog., 48, 497 (1952).
- (19) Hughes, R. R., and Gilliland, E. R., Chem. Eng. Prog., Symposium Series (1955).
- (20) Klee, A. J., and Treybal, R. E., A.I.Ch.E. Journal, 6, No. 3 (1956).
- (21) Andreas, J. M., Hauser, E. A., and Tucker, W. B., J. Phys. Chem., 42, 1001 (1938).
- (22) Korchinski, I. J. O., Ph.D. Thesis, University of Toronto (1956). Also Calderbank, P. H., and Korchinski, I. J. O., Chem. Eng. Sci., 6, No. 2, 65 (1956).
- (23) Hayworth, C. B., and Treybal, R. E., Ind. Eng. Chem., 42, 1174 (1950).

Acknowledgment

Leno Braida wishes to express his sincere appreciation to the Shell Oil Company for financial assistance received in the form of a scholarship.



Principles of Aeration as Applied to Waste Treatment¹

W. WESLEY ECKENFELDER, Jr.²

Aeration systems for bio-oxidation of industrial wastes can be designed employing well-known chemical engineering principles. The system is designed to transfer oxygen at the same rate it is being consumed in the respiration process at a specified dissolved oxygen level. The oxygen requirements of the system are established from relationships between the BOD removed in the process and the aeration tank solids. To supply these requirements, aeration equipment is designed from previously derived sulphite oxidation studies. Factors are applied to these data to correct for waste characteristics which will influence the oxygen transfer rate.

Economic comparisons of various aeration equipment for specific applications can be made employing this procedure.

In aeration processes, mass transfer by diffusion occurs from gas to liquid (absorption) or from liquid to gas (stripping) until a dynamic equilibrium is established. Mass transfer occurs through laminar films at the gas and liquid interfaces and through the turbulent body of fluid such that molecular and eddy diffusion processes will exist in series. Each of these diffusional resistances will vary with fluid turbulence.

It is assumed that a dynamic equilibrium is established at the interface (e.g. for each molecule which diffuses from gas to liquid one diffuses from liquid to gas). Since no concentration buildup will occur at the interface itself, the diffusional resistances may be considered in series and the controlling rate will be that which offers the greatest resistance to diffusion. It can be established from theoretical considerations that in the absorption or stripping of slightly soluble gases, such as oxygen and carbon dioxide in water, the greatest resistance occurs in the liquid film.

In those systems in which the

liquid resistance will control the rate of transfer (i.e. oxygen transfer in the activated sludge process) the quantity of gas transferred per unit time is:

$$dw/dt = k_{LA} (C_s - C_L) \quad (1)$$

Equation 1 re-expressed in concentration units becomes:

$$1/v dw/dt = dc/dt = k_{LA} A/V (C_s - C_L) \quad (2)$$

where $k_{LA}/V = k_{LA}$

Due to difficulties in measuring interfacial areas and surface renewal rates in bubble aeration the overall coefficient k_{LA} is experimentally determined to define the aeration process. k_{LA} is a function of bubble size and interfacial area, volume of liquid under aeration, time of contact of air with liquid, tank depth, agitation intensity and other physical and chemical variables characteristic of the system.

In bio-oxidation processes, oxygen dissolved in the liquid further diffuses into the microbial cell where it is consumed in the respiration process (1, 2). To account for this oxygen

consumption Equation 2 must be modified:

$$dc/dt = k_{LA} (C_s - C_L) - k_s S_a \quad (3)$$

Normal biological waste treatment plant operation approaches a steady state condition where the dissolved oxygen level in the aeration tanks is maintained substantially constant and Equation 3 may be expressed:

$$k_{LA} (C_s - C_L) = k_s S_a \quad (4)$$

In sewage and waste aeration k_{LA} will be influenced by several variables which must be considered for process design and operation. For a given application, k_{LA} will increase with increasing air rate owing to an increase in interfacial area and fluid turbulence. In most diffusion equipment, k_{LA} is related to gas rate by the exponential function

$$k_{LA} = C G^n \quad (5)$$

The gas exponent n for most commercial diffusion devices varies from 0.6-0.9 (3). Some of the sparger type aerators have exhibited an exponent of 1.0-1.1 over the operating range of the equipment.

The percentage of oxygen absorption will increase with increased liquid submergence, approximately 6-12% per foot of rise through the tank liquid (4). Increasing temperature will increase k_{LA} due to an increase in the diffusivity of oxygen in water and a reduction in viscosity. k_{LA} may be converted from one temperature to another by the relationship:

$$\frac{k_{LA}}{(T_1)} = \frac{k_{LA}}{(T_2)} \sqrt{\frac{T_1}{T_2} \times \frac{\mu_2}{\mu_1}} \quad (6)$$

k_{LA} at 10°C. will be 86% and at 30°C. 114% of the rate at 20°C.

In the presence of organic substances and surface active agents (3, 6) the transfer rate of oxygen will be

¹Manuscript received October 10, 1957.

²Associate Professor Civil Engineering, Manhattan College, New York 71, N.Y.

Contribution from Manhattan College, New York, N.Y.

This paper was presented at the Third Ontario Industrial Waste Conference, Honey Harbour, Ont., June 10-14, 1956.

the
time

Biochemical Steady State

In evalua-
tions
steady
 $k_{L,a}$
Equa-
mined
proc-

The
solved
proac-
ration
desir-
at 1
oxygen
conta-
tion
utiliz-
are
scribed
cedu-

accor-

Aera-

The
aerat-
able:

(a)
sion
plates
diox-
in a p-
and
tubes
perm-
an ac-
flexi-
tank.
these
is im-
ture.

(b)
on air
or jet

(c)
entra-
sludge
comp-
pump
turbo-
air is
eter
sparg-
is br-
of the
the
liqui-
utiliz-
plied
neg-
This
inter-
typi-
Figu-

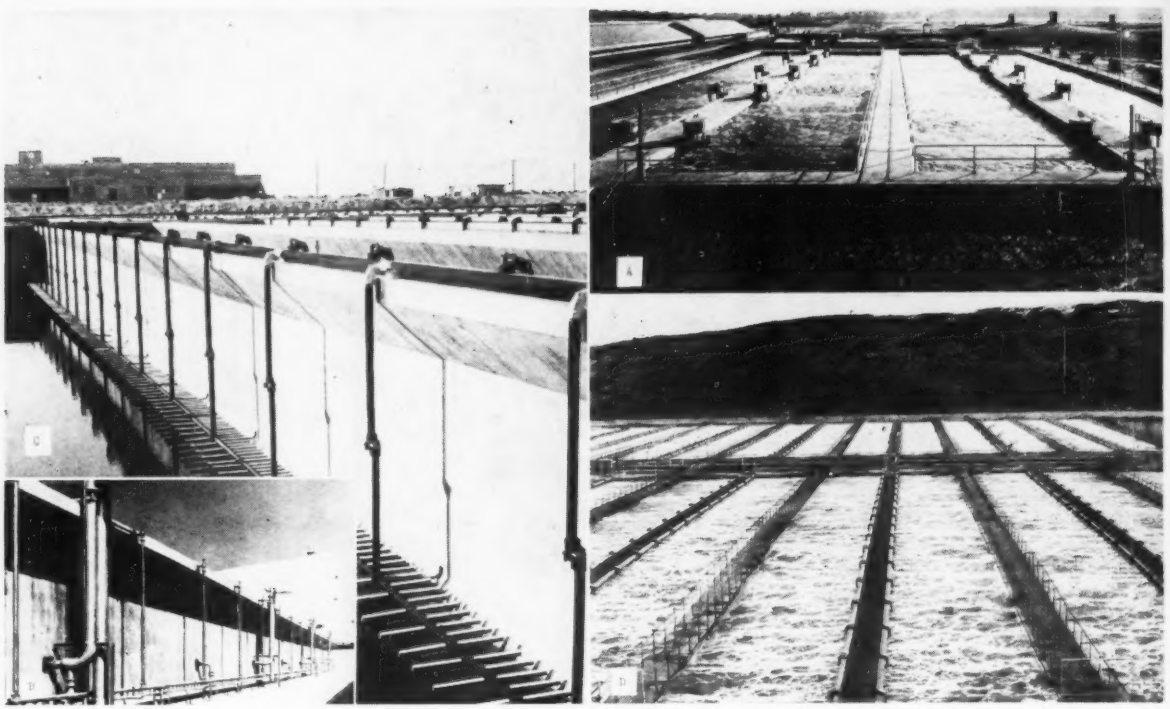


Figure 1

(A) Impingement aeration equipment

(Courtesy of Walker Process Equipment Company)

(B) Impingement aeration equipment—tank assembly

(Courtesy of Walker Process Equipment Company)

(C) Swing diffusion equipment—tank assembly

(Courtesy of Chicago Pump Company)

(D) Swing diffusion equipment in sewage aeration

(Courtesy of Chicago Pump Company)

altered from that in water. In the presence of surface active agents, an adsorbed layer forms a barrier to diffusion at the air-liquid interface. The bubble size will also be changed, thus influencing the A/V ratio. Most substances commonly encountered in sewage and wastes reduce the transfer rate. As these substances are destroyed by bio-oxidation, the rate will approach that of water. Some typical transfer rates in various industrial wastes are shown in Table 1.

Measurement of $K_{L,a}$

Overall transfer coefficients can be determined by one of several procedures. These include the sulphite oxidation test, non-steady state transfer in deaerated water and steady and non-steady state transfer in sludge-liquid systems.

In the presence of copper or cobalt salts which act as catalysts, the reaction between sulphite ion and oxygen or air proceeds rapidly and irreversibly to completion in aqueous solution. The rate of the chemical reaction is considerably more rapid than the absorption of oxygen.

Water or waste is prepared, O₂N in sulphite ion and 10⁻³ molar in

cupric ion (cobalt may be substituted for copper). Air is applied at predetermined rates and samples withdrawn at periodic time intervals (3-20 minutes) depending on the air flow and absorption rate. The rate of absorption is measured by determining the difference between the unoxidized sulphite ion concentration before and after aeration. An aliquot sample, depending on the unoxidized sulphite ion concentration, is pipetted into each of two flasks containing 50 ml. of 0.1N iodine solution. During the transfer, the tip of the pipette should be held close to the surface of the iodine solution to avoid aeration. The unoxidized sulphite ion is then determined by a back titration with standard thiosulphate solution to a starch indicator endpoint. To minimize sulphite oxidation during transfer, the pipettes should be rinsed with distilled water and flushed with nitrogen from 2-3 minutes prior to sampling.

Results are expressed as p.p.m. O₂ absorbed per hour which is $k_{L,a}C_s$.

Non-Steady State Aeration

Overall transfer coefficients may be determined by non-steady state aera-

tion under standard conditions, in which the transfer rate is computed from the change in oxygen concentration of the sample under aeration.

The dissolved oxygen present in the sample is stripped with a nitrogen purge. Air is then diffused into the sample at a specified rate and the dissolved oxygen concentration measured at selected time intervals until the sample is approximately 90% saturated.

The transfer plot may be obtained over a 12 minute aeration period, applying metered air to a liter graduate of sample through an Aloxite diffuser. The dissolved oxygen content may be measured either with a polarograph or by chemical methods.

If the oxygen transfer characteristics of aeration equipment in large tanks is to be evaluated, the use of nitrogen to deaerate the water is impractical. In these cases sodium sulphite with a cobalt catalyst may be used to deaerate followed by aeration under non-steady state conditions.

The non-steady state absorption of oxygen follows the exponential function shown in Equation 2. $k_{L,a}$ is computed from the slope of a plot of

the saturation deficit ($C_s - C_L$) vs. time of aeration.

Biological Oxidation Systems—Steady and Non-Steady State

In many cases it is desirable to evaluate $k_{L,a}$ under operating conditions in bio-oxidation systems. If steady state conditions are maintained, $k_{L,a}$ can be directly computed from Equation 4. $k_{L,a}$ may also be determined employing a non-steady state procedure.

The air is turned off and the dissolved oxygen level permitted to approach zero through microbial respiration. Air is then admitted at the desired rate and samples withdrawn at 1 minute intervals for dissolved oxygen measurement. Sampling is continued until a steady state condition is approached. The oxygen utilization rate and saturation value are determined as previously described. $k_{L,a}$ is determined by a procedure of successive approximation, according to Equation 3.

Aeration Equipment

There are three basic types of aeration devices commercially available:

(a) Porous media type orifice diffusion units. Common types are (1) plates or tubes constructed of silicon dioxide or aluminium oxide grains held in a porous mass with a ceramic binder and (2) Saran or Nylon wrapped tubes or bags. These units may be permanently placed in the bottom of an aeration tank or suspended from flexible joints along the sidewall of a tank. When air is diffused through these units, a helical or screw motion is imparted to the sludge-liquid mixture.

(b) Units employing a mechanical or air shear such as the impingement or jet aerator.

(c) Mechanical aerators which entrain atmospheric oxygen into the sludge by surface agitation or disperse compressed air by a shearing and pumping action employing a rotating turbine or agitator. In the latter unit, air is discharged from a large diameter orifice in the form of a pipe or sparge ring beneath the agitator and is broken up by the shearing action of the high speed rotating blades of the agitator moving through the liquid. For systems of low oxygen utilization rate, oxygen may be supplied by air self-induced from the negative head produced by the rotor. This eliminates the necessity for external blowers or compressors. Some typical aeration devices are shown in Figure 1.

TABLE I.
OXYGEN ABSORPTION CAPACITY OF SOME TYPICAL INDUSTRIAL WASTES

Waste or Substance	Air Flow cu. ft./min./1000 cu. ft. of aeration capacity	Temp. °C.	$k_{L,a}$ waste $k_{L,a}$ water
Sewage... after oxidation.....	10 10	17.0 17.0	0.82 0.98
Kraft Mill Waste..... after oxidation.....	90 90	36.5 37.0	0.70 0.79
Pulp Mill Waste..... after oxidation.....	20 20	24.0 24.0	0.70 0.95
Synthetic Fibre Waste..... after oxidation.....	90 90	20.0 20.0	2.34 1.34

Aeration Performance

Standard porous diffuser units are designed to deliver 4-8 cu. ft./min. per tube. The performance of aeration equipment is generally specified in terms of percent absorption efficiency at a specified temperature. Absorption efficiency is defined as the lbs of oxygen absorbed divided by the lbs of oxygen supplied to the system. The absorption efficiency varies with the porosity of the tube or plate. The absorption efficiency for a porosity 60 Aloxite tube in sulphite solution was found to vary from 13.5% at 4 cu. ft./min. to 12.1% at 8 cu. ft./min. at 20°C. and 13.5 ft. submergence. The Chicago Pump Co. has reported an absorption efficiency of 9.7% in sewage aeration at an air flow of 4 cu. ft./min. per tube and a dissolved oxygen content of 0.8 p.p.m. (20°C.). An absorption efficiency of 8.7% was found by the author on activated sludge aeration at an average air flow of 6.4 cu. ft./min. The tubes are placed in the aeration tank 2 feet above the floor with a minimum and maximum spacing of 6 inches and 2 feet respectively. A minimum air flow of 3 cu. ft./min. per lineal foot of tank must be maintained.

The open orifice nozzle type unit is designed to deliver 8-16 cu. ft./min. per unit at a spacing of 12-30 inches. Sulphite tests of this unit have shown a range of absorption efficiency of 6.2% at 4 to 9.8% at 16 cu. ft./min. (13.5 ft. submergence). In sewage activated sludge, an efficiency of 7.5% (zero dissolved oxygen) at an air flow of 25 cu. ft./min. per unit was obtained. An efficiency of 8% was found at an air flow of 15 cu. ft./min. per unit. Recent performance studies of this equipment in paper mill waste oxidation showed a range in absorption efficiency of 8 to 11 percent over an air flow range of 4.5 to 24.7 cu. ft./min. per unit at 40°C.

The impingement aerator employs a water stream which is air lifted from the aeration tanks acting as a shearing device for air bubbles discharged from a large orifice mounted on leaders at 15-24 inch centres. The absorption efficiency in sulphite solution varied from 15.2% at 4 to 11.5% at 12 cu. ft./min. per unit. In Kraft mill waste activated sludge treatment the absorption efficiency was 9.4% at 11.4 cu. ft./min. per unit. After one year's operation, the use of defoamers and unit clogging reduced the overall absorption efficiency to 4.0%.

The jet aerator pumps liquid from the aeration tanks through a piping manifold. The unit aspirates and disperses atmospheric air or air from a blower within the ejector's capacity. 18.3-20% absorption in sulphite solution has been reported. Over a liquid pumping range of 34-44 U.S. gal./min., 0.66-1.0 lb. O₂/hr. can be absorbed in sulphite solution. Experiments on pharmaceutical waste oxidation found a transfer efficiency of 25%.

The turbine aerator finds principal application in the treatment of high BOD industrial wastes. While the absorption limit of most diffused aeration units is 150 lb. O₂/day/1000 cu. ft., mechanical aerators can disperse as much as 600 lb. O₂/day/1000 cu. ft. Oxygen absorption in the turbine aerator will be a function of the air flow rate and the power input to the rotating agitator. Absorption efficiencies as high as 30% have been reported in some applications.

Aeration Design

(a) **Oxygen Uptake Rate.** The oxygen uptake rate in the aeration system will vary as the sludge passes through various growth stages. The rate can be generally considered in two phases; active respiration which occurs in the presence of nutrients and is characteristic of a growing

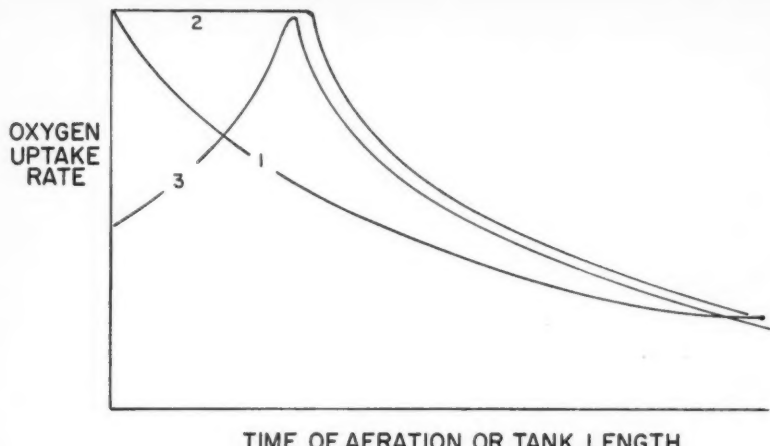


Figure 2—Oxygen utilization curves through aeration tank length.

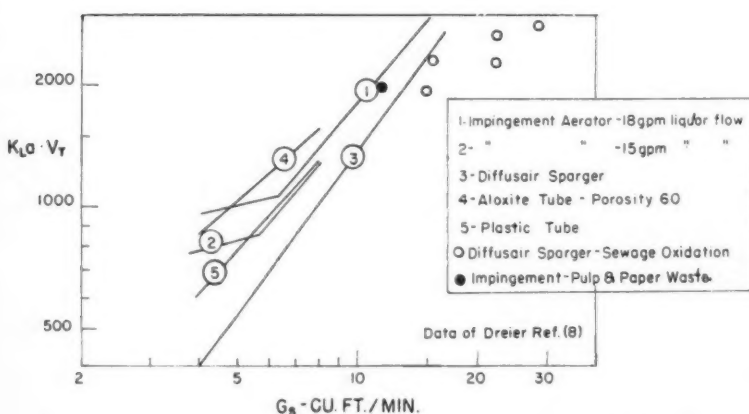


Figure 3—Performance curves of commercial aeration equipment.

sludge and endogenous respiration which is the autoxidation of cellular tissue. The endogenous respiration rate is 5-10% of the active respiration rate.

The total oxygen requirements can be related to the BOD removed through the relationship.

$lb. O_2/day = a lb. BOD \text{ removed}/day + b lb. MLVSS$ (7)

(MLVSS is the volatile suspended solids in the aeration tanks)

In the long rectangular aeration tanks used in conventional activated sludge practice, the sludge-liquid mixture is rolled down the tank length with a spiral motion imparted by the air and as the BOD in the inlet waste undergoes oxidation and synthesis, the oxygen utilization rate decreases, approaching the endogenous level at the end of the aeration basins.

Depending on the concentration of sludge employed and the BOD of the waste, the uptake rate curve through the aeration tanks may follow one of

three patterns (Figure 2). Curve 1 would be representative of a low BOD waste, such as sewage, in which there is little or no sludge growth. Likewise curve 3 indicates conditions when the concentration of BOD is high and the sludge solids low, rapid sludge growth results in an increasing uptake rate until the available BOD is consumed. When the sludge solids are high, there is only a slight increase in solids through growth and the average uptake rate approximates Curve 2.

A variable utilization rate will usually not be found when square or circular tanks are employed. The homogenizing effect of the agitation and aeration will tend to equalize the utilization rate at the mean level.

In order to take economic advantage of the decreasing utilization rate through the aeration tanks, tapered aeration can be employed. k_{La} can be adjusted to meet the necessary demand, by reducing the number of individual aeration assemblies along

the tank length or the air rate can be regulated at each point in the aerator by appropriate valving. In deriving a tapered aeration design, the variation of k_{La} with oxidation must be considered. The value of k_{La} relative to water, a , will increase with oxidation.

(b) Oxygen Saturation. Oxygen saturation will be influenced by partial pressure, temperature and the presence of dissolved and other solids. At atmospheric pressure and room temperature in wastes, saturation will vary usually from 90-95% of water.

Since air is usually released at a 12-15 foot depth in waste oxidation practice, its partial pressure is influenced by the increased pressure of the entering air. As the air bubbles rise through the tank, oxygen is absorbed, reducing the oxygen concentration in the gas phase. The effect of these factors must be considered in deriving a mean saturation value, as follows:

$$C_s = \frac{C_w C^*}{C^*} \left(\frac{P_b}{29.4} + \frac{O_t}{42} \right) \quad (8)$$

C_s is the oxygen saturation value corresponding to the average partial pressure of oxygen in the gas stream entering and leaving the aerator. C_w is the oxygen saturation value in the waste at atmospheric pressure. C^* is the oxygen saturation value in pure water at atmospheric pressure and water vapour saturation. P_b is the absolute pressure in pounds per square inch at the depth of air release. O_t is the percent concentration of oxygen in the air leaving the tank. The effect of water vapor pressure is neglected in Equation 8. While the mean gradient for rising air bubbles is defined by Equation 8, the gradient for surface aeration will be defined by C_s at atmospheric conditions and the gradient during interface formation by the partial pressure at the diffuser outlet. For practical purposes, it is assumed these factors produce a compensatory effect.

(c) Oxygen Transfer. It may be assumed that the quantity of oxygen transferred per unit time by an air diffusion unit within the critical area of air dispersion is a function of depth, temperature, gas flow and waste characteristics. The transfer characteristics of diffusion units at specified depths may be related by the absorption number

$$\frac{k_{La} V_T}{G_a^n}$$

Performance data, derived from sulphite oxidation at 20°C. for several common diffusion devices, are shown

in Figure 3. Data from sewage and pulp and paper waste oxidation are also shown to illustrate the deviation from the sulphite curves. In Figure 3 the solid lines represent data obtained by Dreier⁽⁸⁾ in sulphite solution at a submergence depth of 13.5 feet and a temperature of 20°C. The gpm liquor flow specified is U.S. gal./min.

In diffused aeration systems $k_{L,a}$ may be varied by (a) unit spacing selection; (b) diffuser permeability or other variable selection which defines bubble size; (c) air flow. In turbine aerators $k_{L,a}$ may be varied by either the impellor speed or the air flow.

Design Procedure

1. Oxygen saturation at process operating temperature and pressure is computed from Equation 8.

2. The minimum operating dissolved oxygen level should be maintained between 0.5 and 1.0 p.p.m. to insure aerobic action. At dissolved oxygen levels less than approximately 0.5 p.p.m. the respiration rate of the sludge is retarded and the BOD removal efficiency impaired.

3. The unit oxygen uptake rate for the various BOD removal levels is estimated from an experimental plot or computed from Equation 7.

4. The oxygen demand distribution will be a function of time of aeration. This may be obtained by a laboratory or pilot plant study. The actual demand distribution in the aeration tanks will depend on the hydraulic characteristics of the particular tanks as designed and will approximate one of the curves shown in Figure 2.

5. $k_{L,a}$ for each section of the system can be computed from Equation 4.

6. Aerator performance in sulphite solution at 20°C. and 13 foot submergence depth can be obtained from Figure 3 or from data similarly derived. The operating $k_{L,a}$, derived from Equation 5, must be corrected for temperature if the operating temperature deviates from 20°C. and for the oxygen transfer coefficient, α , of the specific waste.

7. From Figure 3 (or similar plot) the unit air flow-volume factor to transfer the required oxygen is selected.

8. After selecting a tank width and an air flow per unit, the unit spacing is computed.

9. This should establish the design for the most severe operating conditions. Under less severe conditions

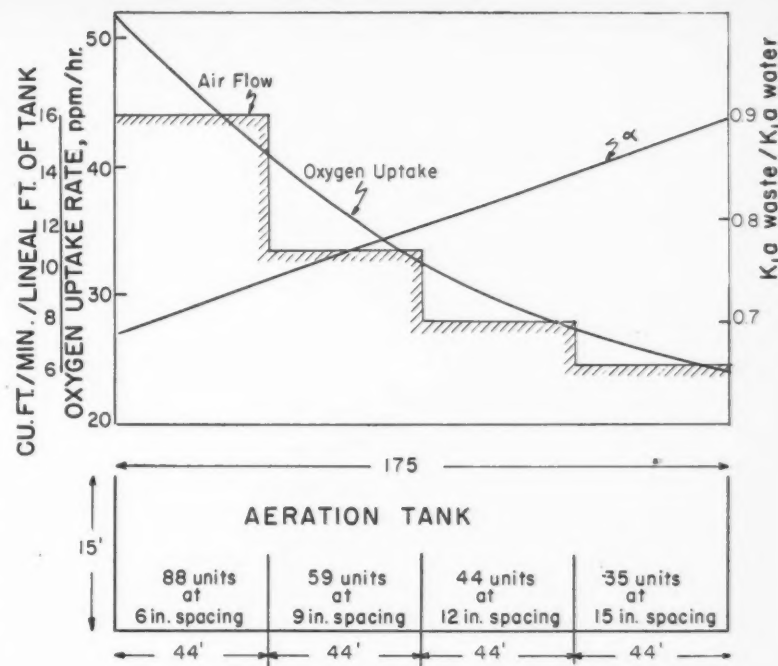


Figure 4—Aeration design chart.

(winter operation, lower BOD loadings, etc.), the reduced required air flow can be computed in a similar manner.

The design procedure may be illustrated by the following example:

Example:

An aeration tank is to be designed for the biological oxidation of an industrial waste. The BOD removal and oxygen utilization rate characteristics have been established from pilot plant studies. The relationship between BOD removal and oxygen utilization, Equation 7, was found to be:

$$\text{lbs } O_2/\text{day} = 0.55 \text{ lbs BOD removed/day} + 0.08 \text{ lbs MLVSS}$$

If under maximum operating conditions 4,160 lbs of BOD will be removed in an aeration tank of 400,000 U.S. gal. capacity, compute the aeration equipment spacing to meet this requirement, assuming 2,500 p.p.m. MLVSS.

(a) Oxygen Requirements

The average oxygen requirement in the tank is:

$$\begin{aligned} \text{lbs. } O_2/\text{day} &= 0.55(4,160) + \\ &\quad 0.08(2,500)(8.34)0.4 \\ &= 2,290 + 662 \\ &= 2,952 \text{ lbs. } O_2/\text{day} \end{aligned}$$

The average oxygen uptake rate is:

$$r_t = \frac{2952}{24 \times 0.4 \times 8.34} = 36.8 \text{ ppm/hr}$$

The distribution of oxygen utiliza-

tion is defined by curve 1, Figure 2. The uptake rate can be expressed as a ratio to the mean uptake rate in the tank (computed from Equation 7). It is convenient to consider the distribution as average values for each quarter section of the tank.

Tank Length %	Ratio to Mean	Uptake rate; p.p.m./hr.
0-25	1.3	1.3 . 36.8 = 47.9
25-50	1.0	1.0 . 36.8 = 36.8
50-75	0.8	0.8 . 36.8 = 29.5
75-100	0.7	0.7 . 36.8 = 25.8

(b) Calculation of Required α

$$\alpha \text{ for raw waste} = 0.60$$

$$\alpha \text{ for effluent} = 0.90$$

If the return sludge recycle is 30 percent of the waste flow the average α at the inlet end of the tank is $0.7 \times 6.0 + 0.3 \times 0.9 = 0.69$

If the increase in α through the aeration tank is linear, the mean in the first quarter of the tank is 0.72.

(c) Aeration Tank Dimensions

The total tank volume is 400,000 U.S. gal. (53,300 cu. ft.). Assuming a depth of 15 ft. and a width of 20 ft., the length is 175 ft. (44 ft./quarter).

(d) Oxygen Saturation

Operating temperature = 30°C., $f = 0.95$. Assuming transfer efficiency

is 8%, submergence on diffusers = 13 ft.

$$C_s = fC^* \left(\frac{P_b}{29.4} + \frac{O_t}{42} \right) =$$

$$0.95 \times 7.63 \left(\frac{20.3}{29.4} + \frac{19.6}{42} \right) = 8.4 \text{ p.p.m.}$$

(e) Required $k_{L,a}$ —first quarter

Employing an operating dissolved oxygen level of 1.0 p.p.m.

$$k_{L,a} \text{ at } 30^\circ\text{C.} = \frac{r_r}{(C_s - C_L)} = \frac{47.9}{(8.4 - 1.0)} = 6.47$$

$$k_{L,a} \text{ at } 20^\circ\text{C.} = k_{L,a} (30^\circ\text{C.}) \sqrt{\frac{T_1}{T_2} \frac{\mu_2}{\mu_1}} = 6.47 \times 0.88 = 5.7$$

correcting for α

$$k_{L,a} = 5.7 / 0.72 = 7.92$$

(f) Diffuser Spacing

The operating data for a particular diffuser in water at 20°C. and 13 ft. submergence is as follows:

Air flow, cu. ft./min./unit	$k_{L,a} \times V_t$
4	610
5	800
6	975
7	1160
8	1350

Designing for 8 cu. ft./min./unit

$$k_{L,a} \cdot V_t = 1350$$

$$V_t = 1350 / 7.92 = 170 \text{ cu. ft.}$$

$$\text{unit spacing} = \frac{170}{15 \times 20} = 0.565 \text{ ft. or } 6.8 \text{ in.}$$

use average spacing of 6 inches

The other sections of tank may be computed in similar fashion. If the computed spacing is beyond design limits, the unit depth and width must be adjusted to bring the unit spacing within the specification. The complete design is shown in Figure 4.

It should be noted that in many cases the nature of the waste changes day by day and the physical condition of the air dispersion device is altered by incrustation, etc. In these cases the performance characteristics of the air dispersed should be based on a statistical analysis of transfer rates under varying operating conditions.

Conclusions

An aeration design procedure is presented for activated sludge units treating industrial wastes. Considerable work remains to be done to more firmly establish the aeration characteristics of various diffusion devices in water and to establish the nature and magnitude of deviations in transfer rate when these devices are employed in industrial waste treatment.

Nomenclature

$k_{L,a}$ = absorption coefficient, p.p.m./hr./p.p.m. concentration gradient

C_s = oxygen saturation in waste, p.p.m., corresponding to the average partial pressure of oxygen in the aeration tanks

C_L = dissolved oxygen concentration in waste, p.p.m.

a = fraction of BOD removed which is oxidized

b = endogenous respiration, % per day

T = absolute temperature

μ = viscosity, cp.

f = ratio of oxygen saturation in waste to oxygen saturation in pure water

P_b = pressure at diffuser discharge, lb./sq. in. abs.

O_t = oxygen concentration of air leaving aeration tanks, %

G_a = air flow to diffuser unit, std. cu. ft./min.

V_t = volume of aeration tank occupied by one diffusion unit, cu. ft.

α = ratio of $k_{L,a}$ in waste to $k_{L,a}$ in pure water

r_r = oxygen uptake rate, p.p.m./hr.

References

- (1) Gaden, E. L. Jr., Ph.D. Thesis, Columbia Univ. (1949).
- (2) Eckenfelder, W. W. Jr., *Sew. and Ind. Wastes Jour.*, 24, 10, 1221, Oct. (1952).
- (3) Eckenfelder, W. W. Jr., *Chem. Eng. Prog.*, 52, 7, 286 (1956).
- (4) Kountz, R. R., Proc. 9th Ind. Waste Conf., Purdue Univ. (1954).
- (5) Eckenfelder, W. W., Raymond, L. W., and Lauria, D. T., *Sew. and Ind. Wastes*, 28, 11, 1357, Nov. (1956).
- (6) Holroyd, A., *Water and San. Eng. (Brit.)*, 3, 301 (1952).
- (7) Eckenfelder, W. W., and O'Connor, D. J., Proc. 9th Ind. Waste Conf., Purdue Univ. (1954).
- (8) Dreier, D., *Biological Treatment of Sewage and Industrial Wastes*, p. 222, Reinhold Pub. Corp., New York, 1956.



